INTERMOLECULAR INTERACTION IN AND BETWEEN MOLECULES AND SUBSTRATES RELEVANT TO BIO-MEMS

Thesis submitted in fulfillment of the

requirements for the degree of

Doctor of Philosophy

in Physics

By

Jonathan Lalnunsiama

To

Department of Physics
Mizoram University, Aizawl
Mizoram, India

JUNE 2012

INTERMOLECULAR INTERACTION IN AND BETWEEN MOLECULES AND SUBSTRATES RELEVANT TO BIO-MEMS

Thesis submitted in fulfillment of the

requirements for the degree of

Doctor of Philosophy

in Physics

By

Jonathan Lalnunsiama

Registration No and Date: MZU/Ph. D/ 327/10.06.2010

To

Department of Physics
Mizoram University, Aizawl
Mizoram, India

June 2012

Dr V Madhurima
Associate Professor
Department of Physics
Room No 208
Email:madhurima.v@gmail.com

MIZORAM UNIVERSITY

AIZAWL 796 009 MIZORAM
Phones : 0389 - 2330435, - 2330522
FAX : 0389 - 2330522

MZU-1/P-14/03/PHY/Ph.D./ Dated: 12th June, 2012

Certificate

This is to certify that the thesis entitled ''Intermolecular interaction in and between molecules and substrates relevant to Bio-MEMS' submitted by Jonathan Lalnunsiama, registration: MZU/Ph.D/327 of 10.06.2010 for the degree of Doctor of Philosophy of the Mizoram University, Aizawl, contains the record of original investigations carried out by him under my supervision. He has been duly registered and the thesis presented is worthy of being considered for the award of the Ph. D. degree. This work has not been submitted for any degree of any other university.

(V.Madhurima)

Supervisor

Declaration of the Candidate

Mizoram University
Aizawl: Mizoram
Department of Physics

I, Jonathan Lalnunsiama, a Ph.D scholar in Physics Department, Mizoram University, Aizawl, do hereby solemnly declare that the subject matter of this thesis is the record of the work done by me. I have genuinely worked on my Ph. D. thesis under the supervision of Dr.V.Madhurima, Department of Physics, and Mizoram University. This thesis is being submitted to Mizoram University for the degree of Doctor of Philosophy in Physics. This work has not been submitted to any other University or Institute for any other degree.

The title of the thesis is 'Intermolecular interaction in and between molecules and substrates relevant to biomems'. I also declare that this investigations relate to authentic research works undertaken by me.

(Dr. V.Madurima)
Supervisor
Department of Physics,
Mizoram University,
Aizawl, Mizoram

(Jonathan Lalnunsiama)
Candidate

Dated: 12th June, 2012

Acknowledgement

In the preparation of this thesis, I have profound gratitude to my supervisor Dr.V. Madhurima. Her permission to tap her outstanding intellectual reservoir and her patience in guiding me throughout my research is precious and valuable to me. While working on my thesis, she gave a whole set of encouragement, advise and inspiration that compels me to work efficiently

I sincerely acknowledge UGC for research fellowship, DST India, NRB for research equipment and main office staff of Mizoram University for their valuable support and help.

I acknowledge all the teaching faculty of the Department of Physics, Mizoram University, Aizawl for their support during the course of this Ph. D. work. My heartfelt thanks go especially to Dr. R.K Thapa Dean school of physical science, Dr. R. C. Tiwari HODs, Dr. Zaithanzauva Pachuau, Dr. Hranghmingthanga, Dr. S. Rai,Dr. B. Lalremruata and Dr. Lalthakimi Zadeng their support during the course of my Msc and PhD. My thanks are to all the non-teaching staff: Mr.V.Mala, Mr. Mawitea, Mr. Kapa, Mrs. Malawmpuii, Mr. Tluanga, Mr. Taia and Mrs Rosie.

I thanks my research mate Debarun Dhar Purkayastha for his valuable contribution in my work.

I acknowledge Dr. Muthukumaran Dept. Chemistry Mizoram University for his endless support, Prof. K.Kannan, Department of chemistry Guru Gobind Singh Indraprastha University Delhi for suggesting the Ubiquitin problem, Dr.K.C.James Raju University of Hyderabad for AlO and Tio_2 substrates, Prof. A.Subrahmanyam IIT Madras for ITO substrate, Dr. Sudesha Lahiri Bhattacharya Dept. of Biotechnology Mizoram University for BSA sample, Dr N.Senthil Kumar and Dr.J.Bhattacharya Dept. of Biotechnology Mizoram University for their fruitful discussion.

I give thanks to my colleagues Dr. Sandip, Dr. Madhav Prasad Ghimire, Dr.Rosanglian, Lalnunpuia, Dibya Prakash Rai, Amit Shankar, Ricky Lalhmangaihzuala, Lalrintluanga Sailo,Lalrinthara Pachuau,T.Malsawtluanga,Hari, Sanjay,Lawrence,Aldrin, Pau and Lalrosanga for their insightful discussion, sharing their valuable ideas during the whole period of the study. I also thank Dhanoj, Dipendra, Lawmkima, Laltanpuia and Lalramnghaka for all the support and fruitful discussions while they did their MSc.

Acknowledgement

The people who deserve special acknowledgement are my family. They serve as a backbone to my academic career and are also responsible for what I have become today. My parents, K. Dingliana Sailo and Ch. Lalhmingthangi in the first place are the person who laid the foundation stone of my academic career and took full responsibility in maintaining the aspect of education in my life. They are the ones who provided me with love and good academic environment at home. My grandparents Ch. Lalkhuma (L) and_Sainguri sailo (L), my uncle and aunt C. Lalbiakthanga and C. Lalthanpari are the one who encouraged and inspired me and gave me moral support. To my brother and sisters Lalawmpuii Sailo, Lalremruata Sailo, Lalhmangaihzuali Sailo and Lalnunthari Sailo thanks for being supportive and caring.

I would like to thank all those people who pray for me and who give advice me and encouragement. At the same time, I expressed my apology that I could not name them personally. It is my prayer that may God be with all my benefactors and repay them for what they did to me.

I devote my entire acknowledgement to God who provided me with good health and golden opportunity from every angle to do my research.

Dated: 9th June, 2012

Department of Physics,

Mizoram University, Aizawl. **(JONATHAN LALNUNSIAMA)**

CONTENTS

List of Figures

LIST OF TABLES

I would like to dedicate my thesis to my grandmother Sainguri Sailo (L) who passed away on 4th February, 2010 . She is the source of my inspiration and the stream of morality that guides my academic path. Though her flesh returned to the earth, yet she lives inside my heart through her words.

I shall meet her again
in the heavenly abode
to depart no more…

Synopsis

INTERMOLECULAR INTERACTIONS IN AND BETWEEN MOLECULES AND SUBSTRATES RELEVANT TO BIO-MEMS

(Synopsis of the proposed research for the Ph.D. degree under Mizoram University)

Name of the Scholar	**:**	**Mr. Jonathan Lalnunsiama**
Name of the Supervisor	**:**	**Dr. V Madhurima**
Date of Admission	**:**	**2nd September, 2009**
Date of Approval by BOS	**:**	**30th April, 2010**
Date of Approval by School Board	**:**	**10th June, 2010**
Registration No.	**:**	**MZU/Ph.D/337 of 10.06.2010**
Date of completion of Pre-Ph.D	**:**	**10th March 2010.**

Course work

Department of Physics

School of Physical Sciences

Mizoram University,

Tanhril, Aizawl

INTERMOLECULAR INTERACTIONS IN AND BETWEEN MOLECULES AND SUBSTRATES RELEVANT TO BIO-MEMS

INTRODUCTION

Although physico-chemical characterization of biological systems is a well established field of research, there are many aspects that are yet to be fully understood. With the present day proliferation of micro and nano scale bio-devices, also called bio-MEMS in general, the need for characterization of biological systems for properties relevant to bio-MEMS is important.

MEMS (Micro Electro Mechanical Systems) is a general name given to micron sized electronic devices capable of performing more than one kind of a task, such as electrical and mechanical. MEMS could include functions such as optical, chemical, magnetic etc. In the present work any molecule that is of significance to bio-MEMS will be called a bio-molecule and molecules which are not themselves bio-molecules but can be used to understand the interactions in them will be referred to as bio-relevant molecules.

There are two main kinds of bio-MEMS; those where the molecules are static and the others where the bio-fluid flows. bio-MEMS used for DNA analysis is an example of the former and an insulin pump is an example of the later. Abolfathi has given a brief introduction to bioMEMS [Abolfathi (2006)]. In this work we consider only the former kind, i.e., micro-fluidics is not considered here.

Structure of molecules at the liquid/solid interface is important in understanding wetting, adhesion, biocompatibility, nucleation, boundary conditions for fluid flow and permeability of small molecules. The study of intra and inter molecular interactions in bio-molecules is well established. The typical routes of study are dielectric spectroscopy, infrared spectroscopy, nuclear magnetic resonance (NMR) and X-ray diffraction. Given the complex nature of bonding and the specific nature of interactions involved with each solvent, these intra and intermolecular interactions are still available for study.

One of the key features in the performance of bio-MEMS is the interaction of biological molecules with the substrates used to make the devices. In order to understand these interactions two distinct interactions need to be studied. One is the interaction between the bio-molecules themselves and the other is the interaction of these molecules with MEMS substrates. The interaction of bio-molecules and bio-relevant molecules with specific substrates is not known. However these interactions play a key role in device performance since excessive sticking of the molecules to the MEMS substrate leads not only to what is called stiction (sticking of the micro scale cantilevers etc to the substrate) but also to non-availability of the molecule for specific cause intended. On the other hand excessive rolling of the bio-molecule over the substrate is also not desirable. Sessile drops are used even in microfluidic devices for actual chemical analysis.

With these research problems in mind the intermolecular interactions in bio-molecules and bio-relevant molecules and their interactions with MEMS substrates is taken up for study.

SCOPE OF THE PRESENT STUDY

Extensive studies have been performed for the dielectric, spectroscopic and conformational analysis of amino acids. Not much is known about the interaction of these molecules with substrates such as quartz, glass, ITO etc. These interactions are important in the performance of micro bio-devices such as bio-MEMS. The present work attempts to understand interactions in bio and bio relevant molecules and their interactions with MEMS related substrates.

REVIEW OF LITERATURE

A brief review of available literature for the present studies is presented. Structure of amino acids and proteins has been the subject of interest for many researchers. The usual methods for the determination of structure are NMR [Wishart *et al*., (1992); Sakakibara *et al*., (2009)], FTIR [Goormaghtigh *et al*., (2009); Severcan *et al*., (2001)], X-Ray diffraction [Diaz-Moreno *et al*., (2006)] and computational methods. Since the literature on this subject is large and not the prime focus of present work, it is not discussed any further.

The development of micro-electro-mechanical Systems (MEMS) technology and its integration into complex systems for biological applications has generated a new field of study, called bioMEMS. MEMS technology brought the idea for building two dimensional (2D) or three dimensional (3D) structures, with micrometer-scale precision, using different materials with differing chemical or physical properties such as polymers, metals and dielectrics. The complexity of MEMS technology correlates with the requirements from biomedical applications, resulting in a large range of bioMEMS applications, from biosensors, immune-isolation devices, micro-needles or injectable micromodules up to pacemakers and cardiology devices.

Hydrogen bonds in liquids and between liquids and substrates play an important role in the fabrication of bio-MEMS. The spectroscopic studies of free OH stretching bands in liquid alcohols taking into account the concomitant effect of both rotational isomerism and hydrogen bonding by Palombo *et al.*, (2006). Large changes in contact angle values as a function of alcohol concentration were observed at small alcohol concentrations by B. Janczuk *et al*., (1985). The static permittivity, relaxation time and Kirkwood correlation factor decrease with increase concentration of butyl methacrylate in alcohol was found by Sivagurunathan *et al*., (2007) by study dielectric of butyl methacrylate-alcohol mixtures by time-domain reflectometry.

Hydrogen bonds were studied from a theoretical point of view, among others, by Kollman and Allen (1972), through computations by Makarewicz (2008), from spectroscopic experiments by Tuttle *et al*., (2004) and also from statistical analysis of the data available on hydrogen bonds in literature as seen from the works of Sarma and Desiraju (1986) and Desiraju, (1991,1996). The present research work concentrates on computational and experimental methods. Literature available on computational studies of hydrogen bonds include studies using semi empirical Hartree-Fock methods [Rios and Rodrigues (1992), Madhurima and Jonathan (2010)], ab intio Hartree-Fock methods [Nagy and Erhardt (2008)], Density Functional Theory (DFT) [Sim *et al*., (1992)] and Monte Carlo methods [Georg *et al*., (2005)] among others. The present study will use semi empirical and ab initio hartree-fock methods.

Contact angle can be used to study intermolecular hydrogen bonded systems. Intermolecular hydrogen bonds increase the surface tension in any given liquid and consequently reflect as a change in the contact angle of the liquid with a substrate. Experimental results for the temperature dependence of the contact angle of liquids on non-polar solids have been presented by Schonhorn (1966). Hua Hu *et al*., (2002) have investigated experimentally the evaporation of a sessile droplet with a pinned contact line by analytic theory and by computation using the finite element method (FEM).

Contact angle of amino acids on polymeric substrates has been studied by Bayramoglu (2005). Changes in wetting and energetic properties of glass caused by deposition of different lipid layer. Initial spreading kinetic of high-viscosity droplets on anisotropic surface was studies by Bliznuk *et al*., (2010). Due to evaporation of drop the contact angle is altered. Evaporation of water droplet on polymer surface studies were performed by Jung-Hoon Kim (2007). Droplet evaporation study applied to DNA chip manufacturing has been studied by Dugas *et al*., (2005). Experimental and computational studies of self-assembly of trimethylamine oxide (TMAO) at hydrophobic interfaces and its effect on protein adsorption: has been studied by Gaurav Anand *et al*., (2010).

The use of attenuated total reflection (ATR) for the study of IR spectra of proteins on substrates is dealt with in the review article by Chittur (1998). Protein and membrane fouling were studied using FTIR by Delaunay *et al*., (2008). Determination of protein structure in aqueous media using FTIR spectroscopy has been dealt by Haris and Severcan (1999). Use of ATR measurements to determine the secondary structure of proteins has been discussed by Goormaghthig *et al*., (2009). The anomaly between the spectrum of aqueous proteins by ATR and transmission method has been attributed to dispersion effects.

OBJECTIVES

Study the intermolecular interactions between small molecules that can throw light on the interactions in bio molecules such as amino acids. The objective of the present work is to

- Study bio-relevant molecules such as simple liquids that possess the functional groups that are available in the bio molecules. Examples are acids and amines.
- Study of bio-molecules will include simple amino acids and proteins.
- Study of the interactions of small molecules and bio molecules with solid substrates that are relevant to MEMS. The substrates intended for studies are glass, quartz, glass coated with Indium Tin Oxide (ITO) and silicon, since they are used in bio-MEMS.
- The studies will include FTIR studies, contact angle studies and computational conformational analysis.

EXPERIMENTAL METHODOLOGY

The present work will involve experimental and computational techniques. The experimental methods to be undertaken are contact angle measurements and FTIR spectroscopy. Computational method will involve determination of the minimum energy conformer of the molecules using a method such as Hartree-Fock or density functional theory (DFT). A brief introduction to each of the methods is presented here.

FTIR Spectroscopy

Visible light does not penetrate biological tissues beyond about 1 cm, since it is strongly absorbed by the tissues. Water, a strong absorber of light has an absorption peak at about 900 nm. However these tissues and molecules show characteristic absorption spectra in the Near -IR and IR frequency regions.

Absorption of infrared radiation by any material arises primarily from molecular vibrations. The frequency of vibration (and hence the absorption intensity) is dependent on the molecular interaction and hence infrared spectroscopy is among the sensitive tools for the study of weak molecular interactions. It has the added advantage of being non-destructive. The spectral line positions and shapes are sensitive to local solid effects such as stress, strain and defects; this

can complicate the interpretation of spectra and also be useful to study the effect of defects etc. IR spectroscopy is hence a function of the chemical bond in the specific context.

In this experiment the intensity of a probe IR beam after interaction with the sample is measured. This intensity (in the absorption or transmittance or reflectance mode) is a function of the molecular interactions that exist in the system. Measurements are made in the range of 400-4000 cm^{-1}. The ratio of the intensity before and after the light interacts with the sample is determined. The plot of this ratio versus frequency is the infrared spectrum**.** In the Fourier Transform Infra Red (FTIR) spectrometer, a Michelson interferometer is made use of to ensure that beams of all frequencies traverse the same optical path. In this method the signal-to-noise ratios are better by orders of magnitude and they also have a better resolution.

For an IR beam of intensity I_o passing through a material, if I_t is the intensity of the transmitted beam, the transmittance at a given frequency ω (T_ω) is defined as

$$T_\mu = \left(\frac{I_t}{I_o} \right)_\mu \qquad ...(1)$$

If the measurement is made in the reflectance mode the reflection (R_ω) coefficient is similarly

$$R_\mu = \left(\frac{I_r}{I_o} \right)_\mu \qquad ...(2)$$

Where I_r is the reflected intensity.

In the absorption mode the Beer-Lambert law has to be invoked. The absorption coefficient A_ω is given by

$$A_\mu = -\log T_\mu = £_\mu (bc) \qquad ...(3)$$

Where ε_ω is the absorption coefficient of the material at the given frequency, b is the sample thickness and c is the concentration of chemical bonds responsible for the absorption.

Beer-Lambert law can be used to quantify the IR spectra, to the first approximation. For quantitative analysis it is better to use the system in the absorption mode and for qualitative

analysis, it is better to use in the reflectance mode. The reflectance mode is important for the study of surface layers on substrates.

In typical IR spectra three characteristics are commonly examined: peak position, integrated peak intensity and peak width. Each bond that is IR sensitive (subject to the appropriate quantum mechanical selection rules) has a specific peak position. The peak position is sensitive to the local chemical environment and the shift in the peak position is characteristic of the local interactions. In organic materials, C-H bonds have stretching modes around 3200cm^{-1} and C = 0 around 1700 cm^{-1}. In solids and liquids, peak width is a function of the homogeneity of the chemical bonding.

For many applications, quantitative band shape analysis is difficult to apply. Bands may be numerous or may overlap; the optical transmission properties of the film or host matrix may distort features, and features may be indistinct. If one can prepare samples of known properties and collect the FTIR spectra, then it is possible to produce a calibration matrix that can be used to assist in predicting these properties in unknown samples.

Attenuated total reflection

In the ATR mode the IR beam is transmitted into a special crystal such as ZnSe. This crystal can sustain surface modes and the sample is kept flush with the crystal. The reflection spectrum is recorded. This technique is especially useful for samples mounted on opaque substrates. The present study will use a FTIR spectrometer with ATR facilities in the range of 400-4000 cm^{-1}.

Surface contact goniometry

Surface contact Goniometer is an instrument which is used for studying the contact angle between the liquid and the substrate. From this we can determine the surface tension and adhesive energy which are important parameters governing the nature of the material. These parameters can be determined from the Drop shape analysis. It is a convenient way to measure

contact angles and thereby determine surface energy. The principal assumptions of this analysis are as follows.

- The drop is assumed to be symmetric about a central vertical axis. This means that it is irrelevant from which direction the drop is viewed.
- The drop is not in motion in the sense that viscosity and inertia play a role in determining its shape, i.e., interfacial tension and gravity are the only forces shaping the drop.

Contact angles are measured by fitting a mathematical expression to the shape of the drop and then calculating the slope of the tangent to the drop at the liquid-solid-vapor (LSV) interface line. Detail result for FTIR and Goniometer will be included in the final thesis.

Computational methodology

Experimental analysis is insufficient to draw a conclusion in order to attain a good result we have to include computational analysis for the same to get a clear picture. In our work we used Gaussian 03 software. The dielectric properties of a polar material depend on the magnitude of the dipole moment of the molecules, which, in turn, is a function of the conformation of the molecule. Experimental dielectric spectroscopy of liquids does help in the determination of the dipole moment of the system. The dipole moment thus determined from experiments is a time average over the various possible conformations. Thus tangible conclusions cannot be drawn about the exact molecular conformation. But at the micro and nano scales, such as those involved in MEMS, precise knowledge of the molecular conformation is important. The magnitude of the dipole moment thus determined can be compared with the experimental value to understand the contribution of solvation effects. The present work presents the results of conformational analysis of some alcohols and phenols and their binary systems based on the Hartree-Fock formalism. Since this formalism invokes the Born-Oppenhiemer approximation, only the electronic wave function and not the complete wave function of electrons and nuclei, is considered. The multi electron Schrodinger wave equation is given by

$$\left[-\frac{1}{2}\sum_i \vec{\nabla}_i^2 - \sum_{A,i}\frac{Z_A}{\vec{r}_{Ai}} + \sum_{A>B}\frac{Z_A Z_B}{R_{AB}} + \sum_{i>j}\frac{1}{\vec{r}_{ij}}\right]\Psi\left(\vec{r};R\right) = E\Psi\left(\vec{r};R\right) \qquad ...(4)$$

where the symbols have the usual meanings. The capital suffixes denote the nuclei and the lower case suffixes refer to the electrons. E(R) gives the potential energy surface, from which the equilibrium geometry and other physical parameters such as vibrational frequencies can be determined. $\nu(r;R)$, the electronic wave function, is contains information pertinent to the molecular polarizabilities, the dipole moment and higher multipole moments of the system. Here the relativistic effects are not considered. The equations are solved in a Self Consistent manner

The cost of HF calculations scales as the fourth power of the number of basis functions used to describe the system [Madhurima., (2006)] due to the number of two-electron integrals necessary for describing the Fock matrix. Semi empirical methods reduce the computational cost by reducing the number of such integrals by assuming the Zero Differential Overlap (ZDO) which neglects all products of basis functions depending on the same electron coordinates when located on different atoms [Mukherji., (2004)]. The output conformation of the semi-empirical studies at STO-3G basis is given as the starting geometry for the ab initio calculations performed with the 6-31 G(d) basis set. Here 6 Gaussian functions are used to describe the core region, 3 for the outer valence region and 1 for the inner valence region. Further, polarized functions are added to atoms other than hydrogen. The excess energy of the binary system indicates the strength of the hydrogen bond formed.

TENTATIVE CHAPTERIZATION OF THESIS

The provisional organization of the thesis is as follows.

- Chapter 1 will contain an introduction to the various interactions being studied.
- Chapter 2 will discuss in detail the experimental and computational methodology employed for the present work.
- Chapter 3 will contain the research findings on the small molecule systems such as alcohol, amines etc, their binary systems and their interactions with solid substrates.
- Chapter 4 will contain the findings on bio molecules such as amino acids and proteins and their interactions with solid substrates.
- Chapter 5 will expound the results with a detailed discussion and summarize the outcome of the work.

REFERENCES

Abolfathi, N., 2006. Bio-MEMS, Hydrophobic length scales http://www.nano.ir/papers/isi /A%20BioMEMS.pdf.

Bayramoglu, G., Emine, Y. and Arica M. Y., 2005. Adsorption of serum albumin and γ globulin from single and binary mixture and characterization of pHEMA-based affinity membrane surface by contact angle measurements. *Bio. Chem. Engg. J.,* **26**: 12–21.

Bliznyuk, O., Jansen H. P., Kooij, E.S. and Poelsema, B., 2010. Initial spreading kinetics of high-viscosity droplets on anisotropic surfaces solid state. *Langmuir* Article ASAP.

Chittur, K. K., 1998. FTIR/ATR for protein adsorption to biomaterial surfaces *Biomat*., **19**: 357-369.

Delaunay, D., Rabiller-Baudry, M., José M., Gozalvez-Zafrilla, Balannec ,B., Frappart, M. and Paugam, L., 2008. Mapping of protein fouling by FTIR-ATR as experimental tool to study membrane fouling and fluid velocity profile in various geometries and validation by CFD simulation *Chem. Engg. Proc*: *Process Intensification*.,**47**: 1106-1117.

Desiraju, G. R., 1991. The C-H---O hydrogen bond in crystals. What is it? *Acc. Chem. Res.,* **24**: 270-276.

Desiraju, G. R., 1996. The C-H---O hydrogen bond. Structural implications and supramolecular design. *Acc. Chem. Res***., 29**: 441- 449.

Dıaz-Moreno, I., Dıaz-Quintana, A., Gloria, S., Mairs T., Miguel A. De la Rosaa. and Dıaz-Moreno, S., 2006. Detecting transient protein–protein interactions by X-ray absorption spectroscopy: The cytochrome c6-photosystem I complex *FEBS Letters* **580**: 3023–3028

Dugas, V., Broutin, J. and Souteyrand, E., 2005. Droplet evaporation study applied to DNA chipmanufacturing. *Langmuir.,* **21**: 9130-9136.

Gaurav, A., Sumanth, N., Jamadagni., Shekhar, G. and Georges,B., 2010. Self-assembly of TMAO at hydrophobic interfaces and its effect on protein adsorption: Insights from experiments and simulations http://pubs.acs.org/doi/abs/10.1021/la100363m *of Langmuir*, Articles ASAP.

Georg, H. C., Coutinhok, K. and Canuto, S., 2005. Asequential Monte Carlo quantum mechanics study of hydrogen bond interaction and the solvatochromic shift of the n-pi transition of acrolein in water. *J. Chem. Phy.*, **123**: 124307 (8 pages).

Goormaghtigh, E., Regis, G., Benard, A., Goldsztein, A. and Raussens, V., 2009. Protein secondary structure content in solution, films and tissues: Redundancy and complementarity of the information content in circular dichroism, transmission and ATR FTIR spectra *Biochimica et Biophysica Acta* **1794**: 1332–1343.

Haris, P. I. and Severcan, F., 1999. FTIR spectroscopic characterization of protein structure in aqueous and non-aqueous media *J. Mol. Cat. B: Enzymatic.*, **7**: 207-221.

Hua Hu. and Ronald G. Larson., 2002. Evaporation of a Sessile Droplet on a Substrate. *J. Phys. Chem. B.*, **106 (6)**: 1334–1344.

Janczuk, B., Chibowski. E. and Wojcik. W., 1985. The influence of *n*-alcohols on the wettability of hydrophobic solids. *Powder Technol.*, **45**:1–6.

Jung-Hoon, Kim., Sung, I., Ahn, Jae Hyun Kim. and Wang-Cheol Zin., 2007. Evaporation of water droplets on polymer surfaces. *Langmuir* ., **2**: 6163-6169.

Kollman, P., Allen, L., 1972. The theory of hydrogen bond *Chem. Rev.,* **72**: 283-303.

Madhurima, V. and James R, K, C., 2006. A procedure to understand the properties of residual process liquids in MEMS *Proceedings of ISSS 2006 National Conference on Smart Materials Structures and Systems December1&2,* Hyderabad, India.

Madhurima, V. and Jonathan, L., 2010. Simulation of interaction in 1,4 dioxane-water system *Proc. of NSPTS-15* Pages c.3-1 to c.3-2.

Makarewicz, J., 2008. Ab initio intermolecular potential energy surfaces of the water-rare gas atom complexes. *J. Chem. Phys*., **129(18):** 184310 (1-10).

Mukherjee, S., Kalyanasis, S. and Roy, D., 2004. Solvation dynamics of 4-aminophthalimide in dioxane–water mixture *Chem. Phys. Lett.*, **384**: 128-133.

Nagy, P. I. and Erhardt, P, W., (2008). Ab initio study of hydrogen bond formation between aliphatic and phenolic hydroxyl groups and selected amino acid side chains *J. Phy . Chem.*,**112**: 4342-4354.

Palombo, F., Marco, P., Paola ,S., Assunta,M. and Rosario Sergio Cataliotti. A., 2006. Spectroscopic studies of the 'free' OH stretching bands in liquid alcohols *J. Mol. Liq.*,**125:** 139-146

Rios, M. A. and Rodriguez, J., 1992. Semi empirical study of compounds with OH-O intermolecular hydrogen bond. *J. Comp. Chem.*, ***7***: 860-866.

Sakakibara, D., Sasaki, A., Ikeya, T., Hamatsu, J., Hanashima, T., Mishima, M., Yoshimasu, M., Hayashi, N., Mikawa, T., Wälchli, M., Brian O. Smith., Shirakawa, M., and Güntert, P., and Ito, Y., 2009 Protein structure determination in living cells by in-cell NMR spectroscopy *Nature*., **458**: 07814-07818.

Sarma, J. A. R. P., Desiraju, G. R., 1986. The role of Cl---Cl and C-H—O interactions in the crystal engineering of 4-Å short-axis structures. *Acc. Chem. Res.*, **19**: 222-228.

Savage, P. E., 1999. Organic chemical reactions in supercritical water *Chem. Rev.*, **99*:*** 603-621.

Schonhorn, H., 1968. Temperature dependence of surface tension for polytetrafluorethylene (supercooled liquid) estimated from contact angles *Polymer*., **9**: 71-74.

Schonhorn, H., 1966. Dependence of Contact Angles on Temperature :Polar Liquids on Polypropylene *J. Phys. Chem.*, **70 (12):** 4086–4087.

Severcan, M., Severcan, F. and Haris, P.I., 2001. Estimation of protein secondary structure from FTIR spectra using neural networks *J. Mol. Struc***., 565-566**: 383-387.

Sim, F., St.Amant, A., Papai, I. and Salahub, D. R., 1992. Gaussian density functional calculations on hydrogen bonded systems *J. Am. Chem.Soc*., **114:** 4391-4400.

Tuttle, T., Kroker, E., Wu, A. and Gremer, D., 2004. Investigations of the NMR spin-spin coupling constants across the hydrogen bonds on ubiquitin:- the nature of hydrogen bond as reflected by the coupling mechanisms. *J. Am. Chem.Soc*., **126:** 5093-5107.

Van de Weert, M., Haris, P I., Hennink, W, E. and Crommelin, D. J. A., 2001. Fourier Transform Infrared Spectrometric Analysis of Protein Conformation: Effect of Sampling Method and Stress Factors. *Analy. Biochem.*, **297**: 160–169.

Wishart D.S, Sykes B.D and Richards F.M., 1992. The chemical shift index: a fast and simple method for the assignment of protein secondary structure through NMR spectroscopy. *Biochem.*, **31:** 1947-1651.

CHAPTER- 1

Introduction

Chapter - 1

Introduction

1.1 Intermolecular interactions

The knowledge of intermolecular forces is required for the understanding of chemical complexes such as clathrates, hydrogen-bonded networks, biological molecules such as DNA, RNA etc. Molecular forces are broadly classified into (a) intramolecular forces and (b) intermolecular forces. Intramolecular forces are those that help in the formation of a molecule and are usually a few orders of magnitude larger than intermolecular forces, such as, hydrogen bonds. For example the energy required to break an O-H bond in water is 222kcal/mol as compared to 9kcal/mol of the intermolecular hydrogen bonds. The present work concerns with intermolecular forces and hence no further reference will be made to intra-molecular forces.

Typical intermolecular forces that are encountered are (a) London dispersion forces (b) Debye forces (c) Keesom forces and (d) Hydrogen bonds. The former three are collectively known as van der Waals forces.

London dispersion forces are interactions between instantaneous dipole and induced dipoles. Debye forces are forces of interaction between a permanent dipole and the corresponding induced dipole while Keesom forces arise from interactions between two permanent dipoles. Understanding of van der Waal's forces is of particular interest in bio-mimicry (Autumn *et al.*, 2002).

Hydrogen bonds are stronger than van der Waals bonds and more directional too. They are the characteristic interactions of biomolecules that are also seen in non-biological systems. A brief introduction to hydrogen bonds is presented below.

1.2 Hydrogen Bonds

Although the term hydrogen bond has been in use for over a century, a clear definition is yet to be made and being discussed (Arunan *et al*., 2011). Usually, hydrogen bonds are thought of as interactions of the X-Y---H-Z kind with bond energies between 0.5 to 40 kcal/mol (Novakovskaya, 2012). This definition takes into account the basic fact that in hydrogen bonds, one hydrogen atom is bound to two other atoms. This unique property of hydrogen to bridge between two atoms (intramolecular bonds) or two molecules (intermolecular bonds) gives rise to the associative properties of hydrogen bonded liquids. There are a number of definitions of hydrogen bond, but most of them acknowledge the importance of the presence of a highly electronegative Y atom. The presence of a highly electronegative Z gives rise to (usually) a strong hydrogen bond while a weakly electronegative Z atom can lead to a weak hydrogen bond where the boundaries between hydrogen bond and van der Waals bond are blurred.

There have been many other definitions of hydrogen bonds based on (a) the physical forces involved (b) hydrogen donors and acceptors (c) hydrogen bond distances and hence energies etc. The various methods employed to study hydrogen bonds includes measurement of physical properties such as density, boiling point etc., spectroscopic techniques such as NMR, FTIR, neutron diffraction, Raman etc., computational and theoretical methods.

The significance of weak intermolecular interactions such as hydrogen bonds is when intermolecular interactions dominate over other effects in a system. Hydrogen bonds contribute to the anomalous properties of water (Stokely *et al.*, 2010), partially to the stabilization of the secondary, tertiary and quaternary structures of proteins, to the structures of polymers, to control molecular aggregates (Gallant *et al.*, 1991) and to

adhesion (Tareste *et al.,* 2007) among many other phenomena.

Various reviews, monographs and textbooks on hydrogen bonds are available (Forlani, 2007; Hirsch, 2003; Jacobsen and Brasch, 1965; Guardia *et al.,* 2005).

1.3 Hydrogen Bonds in Biological Systems

Depending on the strength of interactions the distance between nearest neighbors in biological systems is between 1.5 to 3.5 A. Hence hydrogen bonds in these systems fall broadly into this range of bond lengths. The importance of hydrogen bonds in biological systems stems from the fact that bio molecules are either hydrogen bonded or, like in the case of lipids, react biologically through a hydrogen bonding interaction (Sharkhel *et al.,* 2004). Self assembly of bio molecules also depends on hydrogen bonds (Lin and Mao, 2011).

The importance of hydrogen bonds in biological systems arises from the fact that these bonds have relatively small strength. Most biological processes require rapid reactions occurring close to 10^{-9}s. Hydrogen bonds allow fast association and dissociation so that many combinations of interactions can be checked before the correct association of molecules. It is understood that the specificity of biological systems comes from the trial and error of different sterically complimentary interactions between two molecules, until the best interaction is found.

Some of the early accounts of hydrogen bonds are by Latimer and Rodebush (1920), Bernal and Megaw (1935), Huggins (1936 and 1942) and the book on chemical bonding by Pauling (1939). This was followed by studies indicating the importance of hydrogen bonding in the α and β structures of protein (1951) and in base pairing in DNA helix (Watson and Crick, 1953).

Hydrogen bonds are responsible for the structure of proteins and also for the stability of complex biological molecules such as DNA. Proteins have many physiological functions and constitute mainly of C, H, O and N along with other elements. All proteins are made of 20 basic building blocks called amino acids. Proteins are characterized by their primary secondary and tertiary structures. The primary structure of protein is defined by the sequence of amino acids connected by peptide bonds. Two strands of the primary structure are often interlinked through hydrogen bonds to give rise to the secondary structure, which is usually in the form of coils or pleats. The alpha helix and beta strands are different ways of saturation of the hydrogen bond donors and acceptors in the peptide backbone. The three dimensional structure of protein is called the tertiary structure and is usually globular in shape and hydrogen bonds are among the factors that stabilize the tertiary structures of proteins. Quaternary structure of proteins refers to a larger collection of proteins.

When studying the molecular interactions in large molecules such as proteins, it is an accepted convention to study small molecules with similar interactions as prototypes of the larger molecules (Zhang *et al.,* 2008). The hydrogen bonds in proteins and amino acids can be understood by studying the hydrogen bonds in binary mixtures of liquids, which exhibit similar bonds. Hence the study of intermolecular interactions in proteins can be done through the study of proteins, amino acids and binary liquids that exhibit similar hydrogen bonds.

1.4 Bonding and Bio-MEMS

Interaction of biomolecules with substrates is of current interest with far reaching implications. For example, the interaction of proteins with substrates has applications in nanotechnology, biomaterials and biotechnology (Grey, 2004). Studies show that proteins undergo conformal changes when they come into contact with a surface, both at the solid-liquid and the liquid-vapour interfaces. The conformation in retained more on charge neutral hydrophilic surfaces than on hydrophobic surfaces. In similar environment of protein tertiary structure, depending on the influence of amino acids residue in protein (interaction of different amino acid with protein), the twenty amino acids residues have been divided in to nine groups (Saha *et al.,* 2005); [Glycine, Serine,Threonine], [Alanine,Valine], [Proline, Phenylalanine, Tyrosine, Tryptophan], [Histidine], [Cysteine], [Methionine, Leucine, Isoleucine], [Aspartic acid, Glutamic acid], [Asparagine, Glutamine] and [Arginine, Lysine].Those classifications are useful for residue characterization like size, hydrophobicity, aliphatic or aromatic or conformational flexibility of the side chain etc. Adhesion bonding technology for bio-MEMS has been designed for the bonding of glass/photoresist (SU8) structures to glass cover plates for the fabrication of micro-fluidic devices with integrated 3D-micro-electrode arrays, based on the preparation of ultra-thin adhesive layers between precision machined cylinders and roll-to-surface print transfer onto micro-machined substrates (Kentsch *et al.,* 2006). Bio-MEMS include various forms like lab-on-a-chip, microarray chips, microfluidic chips, or μTAS (micro Total Analysis System), drug delivery components and enable miniaturized instruments on chips. Their sizes vary from a few millimetres on edge to 1mm in thickness. Most of these devices require only a tiny volume a few «*l* of sample liquid for performing synthetic, analytical and detection

analysis.

1.5 Present study

The present work consists of both computational and experimental studies. Using Gaussian-03 software and by applying Hartree-Fock method, computational studies were performed to determine the most stable conformer of the molecules The experimental studies undertaken are contact angle measurements, FTIR spectroscopy and dielectric studies using RLC meter and Abbe refractometer. A brief introduction to each of the methods is presented in chapter 2. Substrates relevant to uses in bio-MEMS devices like glass, stabilize mica, nylocast, silicon, epoxy FR4, acrylic, fiber reinforce plastic (FRP), polypropylene, aluminium oxide (Al_2O_3), polyurethene, teflon, indium tin oxide (ITO) and hylam are chosen for the present study. The choice of liquids taken for study is based on the type of interaction seen in biomolecules. Liquids chosen are Alcohols (methanol, ethanol, isopropanol, butanol, hexanol and octanol), aniline and acetone. Binary mixture of aniline-alcohols or acetone-alcohol form the prototype of hydrogen bonds of the N-H--O and C=O--H kinds formation in biomolecules and a parallel studied on amino acid namely aspartic acid, cystein, glutamic acid, phenylalanine, histidine, tyrosine, methionine, arginine, proline, valine, threonine, lysine, leucine, isoleucine, tryptophan, alanine, serine and glycine and protein (ubiquitin and bovine serum albumin) has been taken up. Since amino acids and proteins are well soluble in water, their saturated solutions in water are made to contact with different substrates. By using a modified spin coater technique as discussed in chapter 2, biomolecules are coated on the glass substrate. The literature survey corresponding to the various systems are presented at the corresponding places in the next few chapters

1.6 Arrangement of thesis

Organization of thesis is based on the systematic studies of hydrogen bond of the type N-H--O and C=O--H from the organic binary liquid to biomolecules. The second chapter of the thesis consists of details of computational and experimental techniques used for the present study and their application to study of intermolecular interactions is discussed in detail. The third chapter consists of results and discussion on small organic molecules like alcohols, aniline and acetone, their binary mixture and how these systems interact with different solid substrates. The interactions occurring in small molecules are prototypes for those in larger bio molecules. The fourth chapter details the contact angle studies of various bio-molecules such as amino acids and proteins. The interactions between amino acids and protein, amino acid with substrates, amino acids with test liquid (static/dynamic) and amino acids coated layer by layer on glass substrates are presented in the chapter. The fifth and final chapter consists of the overall summary and discussion of the entire work with a few possible areas of further research being identified.

CHAPTER- 2

Experimental Details

Chapter 2

Experimental Details

Details of computational and experimental techniques used for the present research are discussed in this chapter. The computational methods used are based on the Hartree-Fock formalism. The experimental methods used are (a) dielectric measurements at RF (b) refractive index measurement (c) FTIR spectroscopy and (d) contact angle measurement. Guggenheim's method (Guggenheim, 1951) was used to determine the experimental dipole moment from the dielectric parameters.

2.1 Computational Methods

2.1.1 Introduction

Computational methods were used to determine the following (a) the conformation of single molecules of the liquids of choice (b) the conformation of binary combinations of the liquid molecules in the 1:1 ratio to inspect the actual site of interaction(s) between the two molecules (c) solvation of a molecular dipole by a solvent, by treating the solvent to be a dielectric continuum, according to Onsager's model (Onsager, 1936). Each of these is discussed below in detail. Gaussian-03 software was used for all these computations on a HP Workstation.

The motivation for computational studies is the difficulty in obtaining molecular conformations from experiments. Since computations come with inherent errors, the results of the dipole moment obtained are compared with experimental results for cross-checking. Although IR spectra can be determined from the same studies, it was not done

in the present case since the IR spectral frequencies obtained from computations are known to contain systematic errors and need to be scaled based on experimental data. Since the present studies aim at looking only at the shift in peak frequency, detailed computational studies for this were not taken up.

The Self Consistent Field-Hartree Fock (SCF-HF) method was used for all the computations. In this method the solutions to the time independent Schrodinger equation of the molecule is obtained in a self-consistent fashion. Here the molecular orbits are taken to constitute of a linear combination of atomic orbits (MO-LCAO). The orbits are expanded in terms of basis set of choice. Specific electron-electron interactions are not taken into account but are treated on an average and the calculations are done within a mean-field framework.

The main drawback of the Hartree-Fock method is that the wave function is defined for a single conformation. Energy is minimized to obtain the most stable conformation by varying molecular parameters such as bond length and bond angle. This usually gives only local minima on the potential map. Many initial conformers have to be taken up for study in order to obtain the global minima. Hence the procedure becomes tedious, especially when dealing with large molecules.

2.1.2 Hartree Fock Method

The Hartree-Fock (Jensen, 1999; Atkin *et al.*, 1997; Strich, 1993) method is an approximate method to determine the ground state wave function and the ground state energy of a many-body quantum mechanical system. In this method it is assumed that the exact N-body wave function can be replaced by a single Slater determinant for a fermionic system. The solution wave function is determined by using the variational

method. Calculations can be performed for closed-shell systems with all shells doubly occupied (Restricted Hartree Fock - RHF) or for open shell systems where some of the shells are singly occupied (Unrestricted Hartree-Fock - UHF). Only RHF has been used for the present study.

The time-independant Schrodinger equation is employed for describing the electron distribution and is given by

$$H\cdot = E\cdot \qquad \text{... (1)}$$

In the above equation, H is the Hamiltonian operator and E the energy operator and $\cdot$ their corresponding wave function.

The many body Hamiltonian of an electronic system is given by

$$H_{Tot} = T_n + T_e + V_{ne} + V_{ee} + V_{nn} \qquad \text{... (2)}$$

where, T_n =Kinetic energy of the nucleus

T_e = Kinetic energy of the nucleus

V_{ne} =Potential energy between electron and nucleus

V_{ee} = Potential energy between electrons

V_{nn} = Potential energy between nuclei

$$or, \qquad H_{Tot} = T_n + H_e + H_{mp}$$

$$H_e = T_e + V_{ne} + V_{ee} + V_{nn}$$

$$H_{mp} = -\frac{1}{2M_{Tot}}\left(\sum_{i=1}^{N}\nabla_i\right)^2$$

Here, H_e is the electronic Hamiltonian operator and H_{mp} is called the mass-polarization (M_{Tot} is the total mass of all the nuclei and the sum is over all electrons).

The time independent Schrodinger equation with the nuclear position (R) and electron coordinates (r) is given by

$$H_e(R)\cdot{}_i(R,r) = E_i(R)\cdot{}_i(R,r), \quad i = 1,2,3....\infty \qquad \text{... (3)}$$

The total exact wave function can be written as an expansion in the complete set of electronic functions, with the expansion coefficient being a function of nuclear coordinate.

$$\cdot{}_{Tot}(R,r) = \sum_{i=1}^{\infty} \cdot{}_{ni}(R)\cdot{}_i(R,r) \qquad \text{... (4)}$$

Substituting the value of eqn. (4) in eqn. (1), we get

$$\sum_{i=1}^{\infty}\left(T_n + H_e + H_{mp}\right)\cdot{}_{ni}(R)\cdot{}_i(R,r) = E_{Tot}\sum_{i=1}^{\infty}\cdot{}_{ni}(R)\cdot{}_i(R,r) \qquad \text{... (5)}$$

The nuclear kinetic energy is essentially a differential operator, and we may write it as,

$$T_n = \sum_a -\frac{1}{2M_a}\nabla_a^2 = \nabla_n^2$$

$$\nabla a = \left(\frac{\partial}{\partial X_a}, \frac{\partial}{\partial Y_a}, \frac{\partial}{\partial Z_a}\right)$$

$$\nabla_a^2 = \left(\frac{\partial^2}{\partial X_a^2} + \frac{\partial^2}{\partial Y_a^2} + \frac{\partial^2}{\partial Z_a^2}\right)$$

Where the mass dependence, sign, and summation is implicitly included in the ∇_n^2, ecpanding eqn. (5) we get.

$$\sum_{i=1}^{\infty}\left\{\cdot_i(\nabla_n^2\cdot_{ni})+2(\nabla_n\cdot_i)(\nabla_n\cdot_{ni})+\cdot_{ni}(\nabla_n^2\cdot_i)+\cdot_{ni}E_i\cdot_i+\cdot_{ni}H_{mp}\cdot_i\right\}=E_{Tot}\sum_{i=1}^{\infty}\cdot_{ni}\cdot_i \quad \text{... (6)}$$

Applying the orthonormality condition and bra-ket notation, eqn. (6) can be written as

$$\nabla_n^2\cdot_{ni}+E_j\cdot_{ni}+\sum_{i=1}^{\infty}\left\{2\left\langle\cdot_j\left|\nabla_n\right|\cdot_i\right\rangle\left\langle\nabla_n\cdot_{ni}\right\rangle+\left\langle\cdot_j\left|\nabla_n^2\right|\cdot_i\right\rangle\cdot_{ni}+\left\langle\cdot_j\left|H_{mp}\right|\cdot_i\right\rangle\cdot_{ni}\right\}=E_{Tot}\cdot_{nj}\ldots \quad (7)$$

Applying the adiabatic approximation where the form of the total wave function is restricted to one electron surface ($i \neq j$ in eqn.7 are neglected, only the terms with *i=j* survive). Except for the spatially degenerate wave functions, the diagonal first order non-adiabatic coupling element is zero.

$$\left(\nabla_n^2+E_j+\left\langle\cdot_j\left|\nabla_n^2\right|\cdot_j\right\rangle+\left\langle\cdot_j\left|H_{mp}\right|\cdot_j\right\rangle\right)\cdot_{nj}=E_{Tot}\cdot_{nj} \quad \text{... (8)}$$

Discarding the mass polarization, since it depends on the nuclear masses and its contribution to the energy is very small. Reintroducing the kinetic energy operator we have

$$\left(T_n+E_j(R)+U(R)\right)\cdot_{nj}(R)=E_{Tot}\cdot_{nj}(R) \quad \text{... (9)}$$

where, $U(R)$ is known as the diagonal correction of the nuclear masses.

In the Born-Oppenheimer (BO) approximation the motion of nucleus is neglected for the separation of electronic and nuclear motion and the diagonal correction is neglected. The resultant Schrodinger equation takes the form given in eqn.10, where the electronic energy plays the role of a potential energy.

$$\begin{aligned}\left(T_n + E_j(R)\right)\cdot\ _{nj}(R) &= E_{Tot}\cdot\ _{nj}(R)\\ \left(T_n + V_j(R)\right)\cdot\ _{nj}(R) &= E_{Tot}\cdot\ _{nj}(R)\end{aligned} \quad \text{... (10)}$$

The nuclei move on a potential energy surface (PES) in Born-Oppenheimer approximation which is a solution to the electron Schrodinger equation. The potential energy surface is independent of nuclear mass when two or more energetically electronic Schrodinger equation comes close, the Born-Oppenheimer approximation breaks down.

Since the Schrodinger equation still does not include electron-electron quantum mechanical correlations and it does not treat electron as fermions. Slater determinant has to be taken in to account. A single Slater determinant can be written as a sum of permutation over the diagonal of the determinant, where the diagonal product is denoted as $\prod$ and the determinant wave function is represent by ¤

$$¤ = A\left[¤(1)¤(2).....¤_N(N)\right] = A\prod \quad \text{... (11)}$$

$$\text{Where, } A = \frac{1}{\sqrt{N!}}\sum_{p=0}^{N-1}(-1)^p P = \frac{1}{\sqrt{N!}}\left[1 - \sum_{ij} P_{ij} + \sum_{ij} P_{ijk} - ...\right]$$

The first operator is the identity, while P_{ij} generates all possible permutation of two electron coordinates and P_{ijk} for three electron coordinates etc. The antisymetrizing operator *A* commutes with *H*, and *A* acting twice is same as *A* acting once multiply by the square root of *N* factorial.

$$\begin{aligned}AH &= HA\\ AA &= \sqrt{N!}A\end{aligned} \quad \text{... (12)}$$

Now consider the Hamiltonian operator. The nuclear-nuclear repulsion does not depend on electron coordinates and is a constant for a given nuclear geometry. The nuclear-electron attraction is a sum of terms, each depending only on one electron coordinate, which is same for electron kinetic energy. The electron-electron repulsion depends on two electron coordinates.

$$
\begin{aligned}
H_e &= T_e + V_{ne} + V_{ee} + V_{nn} \\
T_e &= -\sum_i^N \frac{1}{2}\nabla_i^2 \\
V_{ne} &= -\sum_i^N \sum_a \frac{Z_a}{|R_a - r_i|} \\
V_{ee} &= \sum_i^N \sum_{j>i}^N \frac{1}{|r_i - r_j|} \\
V_{nn} &= \sum_a \sum_{b>a} \frac{Z_a Z_b}{|R_a - R_b|}
\end{aligned}
\qquad \text{... (13)}
$$

Base on the number of electron indices, the operators for the above equation are

$$
\begin{aligned}
h_i &= -\frac{1}{2}\nabla_i^2 \; - \sum_a \frac{Z_a}{|R_a - r_i|} \\
g_{ij} &= \frac{1}{|r_i - r_j|} \\
H_e &= \sum_{i=1}^N h_i + \sum_{i=1}^N \sum_{j>i}^N g_{ij} + V_{nn}
\end{aligned}
\qquad \text{... (14)}
$$

The one electron operator h_i, describes the motion of electron *i* in the field of all the nuclei, and g_{ij} is a two electron operator giving the electron-electron repulsion. We note that the zero point of the energy corresponds to the particles being at rest (T_e = 0) and infinitely removed from each other (V_{ne} - $V_{ee} = V_m = 0$).

The energy may be written in terms of the permutation operator as (using eqn. (11) and egn. (12)

$$\begin{aligned} E &= \langle ¤ | H | ¤ \rangle \\ &= \langle A\Pi | H | A\Pi \rangle \\ &= \sqrt{N!}\langle \Pi | H | A\Pi \rangle \\ &= \sum_p (-1)^p \langle \Pi | H | P\Pi \rangle \end{aligned} \quad \text{... (15)}$$

The nuclear repulsion operator does not depend on electron coordinates and can immediately be integrated to yield a constant.

$$\langle ¤ | V_{nn} | ¤ \rangle = V_{nn} \langle ¤ | ¤ \rangle = V_{nn} \quad \text{... (16)}$$

For the one-electron operator only the identity operator can give a non-zero contribution. For coordinate 1 this yields

$$\begin{aligned} \langle \Pi | h_1 | \Pi \rangle &= \langle ¤_1(1)¤_2(2)...¤_N(N) | h_1 | ¤_1(1)¤(2)...¤_N(N) \rangle \\ &= \langle ¤_1(1) | h_1 | ¤_1(1) \rangle \langle ¤_2(2) | ¤_2(2) \rangle .....\langle ¤_N(N) | ¤_N(N) \rangle \\ &= h_1 \end{aligned} \quad \text{... (17)}$$

as all the MOs $¤_1$ are normalized. All matrix elements involving a permutation operator give zero.

$$\begin{aligned} \langle \Pi | h_1 | P_{12}\Pi \rangle &= \langle ¤_1(1)¤_2(2)...¤_N(N) | h_1 | ¤_1(1)¤(2)...¤_N(N) \rangle \\ &= \langle ¤_1(1) | h_1 | ¤_2(1) \rangle \langle ¤_2(2) | ¤_1(2) \rangle .....\langle ¤_N(N) | ¤_N(N) \rangle \end{aligned} \quad \text{... (18)}$$

This is zero as the integral over electron 2 is an overlap of two different MOs, which are orthogonal. For the two electron operator, only the identity and P_{ij} operators can give a non-zero contribution. A three electron permutation will again give at least one overlap integral between two different MOs, which will be zero. The term arising from the identity operator is

$$\begin{aligned}\langle \Pi | g_{12} | \Pi \rangle &= \langle ¤_1(1)¤_2(2)...¤_N(N) | g_{12} | ¤_1(1)¤(2)...¤_N(N) \rangle \\ &= \langle ¤_1(1)¤_2(2) | g_{12} | ¤_1(1)¤_2(2) \rangle .... \langle ¤_N(N) | ¤_N(N) \rangle \\ &= \langle ¤_1(1)¤_2(2) | g_{12} | ¤_1(1)¤_2(2) \rangle = J_{12}\end{aligned} \quad \text{... (19)}$$

and is called a Coulomb integral. It represents a classical repulsion between two charge distributions described by $¤_1^2(1)$ and $¤_2^2(2)$ .The term arising from the P_{ij} operator is

$$\begin{aligned}\langle \Pi | g_{12} | P_{12} \Pi \rangle &= \langle ¤_1(1)¤_2(2)...¤_N(N) | g_{12} | ¤_1(1)¤(2)...¤_N(N) \rangle \\ &= \langle ¤_1(1)¤_2(2) | g_{12} | ¤_1(1)¤_2(2) \rangle .... \langle ¤_N(N) | ¤_N(N) \rangle \\ &= \langle ¤_1(1)¤_2(2) | g_{12} | ¤_2(1)¤_1(2) \rangle = K_{12}\end{aligned} \quad \text{... (20)}$$

and is called an exchange integral, which has no classical analogy. Note that the order of the MOs in the *J* and *K* matrix elements is according to the electron indices. The energy can thus be written as

$$E = \sum_{i=1}^{N} h_i + \frac{1}{2}\sum_{i=1}^{N}\sum_{j=1}^{N}(J_{ij} - K_{ij}) + V_{nn} \quad \text{... (21)}$$

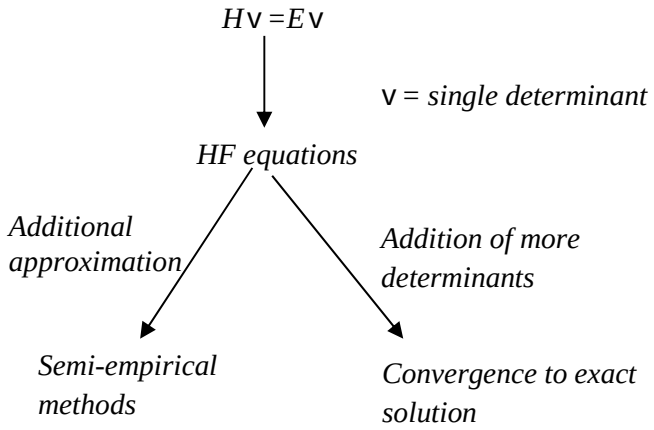

Figure 2.1: Hartree-Fock method

2.1.3 Self consistent field (SCF) technique

Self consistent field technique begins with a set of approximate orbitals (basis set) for all of the electrons in the system, where it selects one electron as a starting geometry. The potential energy of the system in which the electron moves is calculated by freezing the distribution of all the other electrons, by treating their averaged distribution as a single centro-symmetric source of potential. It calculates the selected electron in Schrodinger equation to get a new and more accurate orbital for that electron and repeats the procedure for all the other electrons in the system. A single cycle is complete once each electron has been evaluated. The process is started again with the first electron evaluated, using the newly calculated orbital as the starting point. It continue this process through the iteration (repeating, or cycling) process until the calculations does not change the values of the orbital and declare the calculation to be done, as the orbital are now considered to be self-consistent.

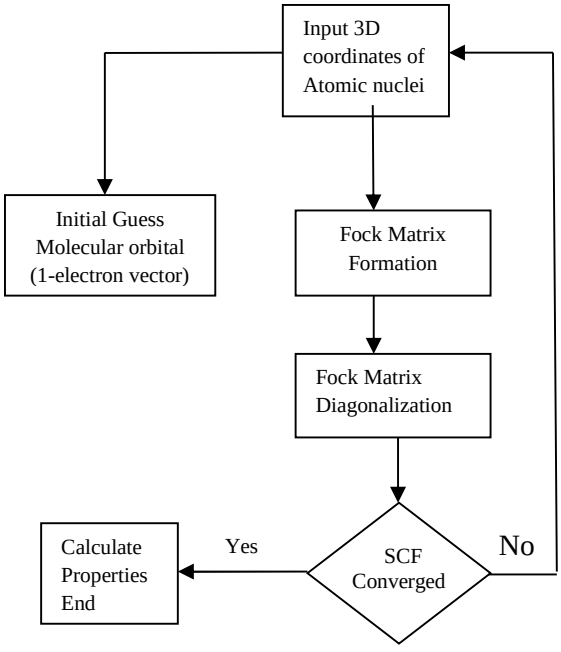

Figure 2.2: Flowchart of Hartree-Fock Method.

2.1.4 Determination of molecular conformations

Gaussian03 software (Frisch *et al*., 2003) is used for the present studies and the operating mode is shown in fig 2.4. Gaussian03 software is a computational program where the conformation is run using Hartree-Fock Self Consistent Field (HF-SCF) method. In this studies optimization of the molecules are based on the energy of interaction and dipole moment. The relation (H_A + H_B - H_{AB}) is used for calculating the hydrogen bond energy between 1:1 binary mixtures of the liquids, where H_A the energy of one single molecules and H_B is is the other molecules, for a binary mixture it is expressed in H_{AB}. In this computational program different basis sets are employed for the various conformer. A basis set is a set of functions or a series of number to describe where the electrons are in proximity to the nucleus and are used to create the molecular orbital, which are expanded as a linear combination of each coefficient of wave functions. But these basis functions are usually not actually the exact atomic orbital, even for the corresponding hydrogen-like atoms, due to approximations and simplifications of their analytic formulas. When a calculation is performed, the commonly used a basis has finite number of atomic orbitals, which is centered at the nucleus. Otherwise, the functions are centered on lone pair or on bond. Slater type orbital (STO) were initially used for calculation. They decay exponentially with the distance increase from the nucleus and can be expressed mathematically as $STO = \left(\, \right)^{0.5} e^{(-, r)}$. Later Gaussian type orbital were used as it is easier to calculate overlap and other such integrals with Gaussian basis functions, which led to huge computational savings and can be expressed as $GTO = \left(\right)^{0.75} e^{\left(-\sim r^2\right)}$. The basis sets normally employed are minimal basis set (as the name minimal, they are use to obtain

first look at one or more molecular properties giving quantitative result. Examples of minimal basis set are STO-3G and STO-6G), split-valence basis set (it takes responsibility for the electron that involved in bonding and chemical reaction, perform a thorough and careful calculation for the valence electron but not for the core electron. Example of split-valence basis set are 3-21G and 6-31G), polarized basis set (some of the electron might stray to other orbital and polarization must take in to account, a polarized basis set give the exact location of the electron. They are indicated by a '*', example of polarized basis set are 3-21G* or 3-21(d) and 6-31G(d)) and diffuse basis set (it extend the distance away from the nucleus to locate the random position of the electron. They are indicated by '+' example of diffuse basis set are 3-21+G and 6-31+G). The basis set selected is namely STO-3G, 6-31G, 6-31G (d) and 6-31G (d, p). STO-3G is the minimal basis set, represent electron density well in valence region and beyond but it cannot represent electron density well near the nucleus. It is a linear combination of 3 Gaussian type orbital fitted to one Slater type orbital. 6-31G is a split valence basis set where the core orbital is described by 6 Gaussian function and the valence is described by two Gaussian type orbital, first one having 3GTO and second having 1 GTO. 6-31G (d) and 6-31G (d, p) are polarised basis set where d functions to heavy atom other than hydrogen atom and P function to hydrogen atom.

2.1.5 Hydrogen bond energies calculation

The hydrogen bond energy at the site of molecular interaction is calculated by the general relation

$$H=H_A+H_B-H_{AB}$$

The energy of one liquid is assigned as H_A and the other as H_B in the binary system. Each liquid system is optimized in the Gaussian 03 software independently. The energy of the binary liquid in the 1:1concentration ratio is assigned as H_{AB}. The difference between the sum of the two pure liquids energy and the binary of the two liquid gives the total hydrogen bond energy exist between the two moieties. The hydrogen bond energy is expressed as kcal/mol. where the hydrogen bond distance is measured using Gausview 3.09 software tools as shown in fig 2.3, and is expressed in Å

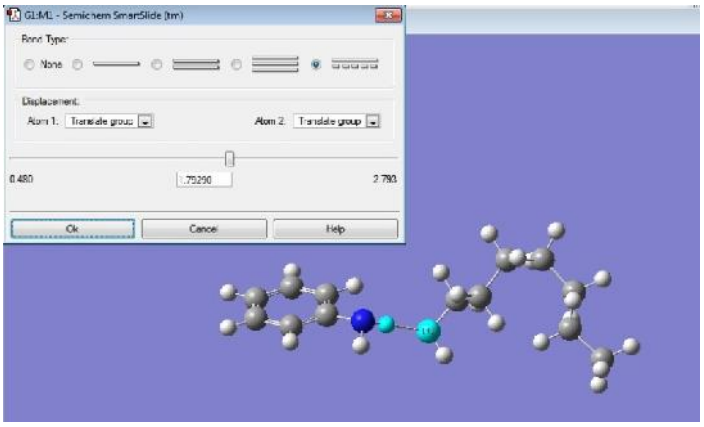

Figure 2.3: Technique for identifying the hydrogen bond distance.

2.1.6 Onsager Solvation Model

For the calculation of solvation effect, Onsager's solvation model is employed for the present study. In this method it is assumed that on solvation the solvent molecules surround the solute molecules. This model considers a polarisable dipole with polarizability ~ at the centre of a sphere, the sphere represents the solvent which is treated as a continuous medium of dielectric permittivity£ . The solute dipole induces a reaction field in the surrounding medium which inturn induces as electric field in the cavity (reaction field) which interact with the dipole. In Gaussian 03 software Onsager model is obtain by using the keyword SCRF=DIPOLE (dipole induced dipole model).

The radius of the cavity and the dielectric constant of the solvent is supplied as input and run for different particular basis set. Onsager's solvation model uses a spherical cavity for the solvent and approximates the solute to be a dipole. The reaction field as calculated in Gaussian 03 is given by the equation

$$R = \left[2\ll(£-1)/V(£+2)\right]$$

where V is the volume of the solvent molecule, « the dipole moment of the solute and £ the permittivity of the solvent. The cavity size V strongly effects the calculation (Onsager, 1936). In the present study V was determined using an in-built calculation in Gaussian 03, where V is defined as the volume inside a contour of 0.001 electron/bohr3 density. The molecular volume thus determined is accurate to two significant figures.

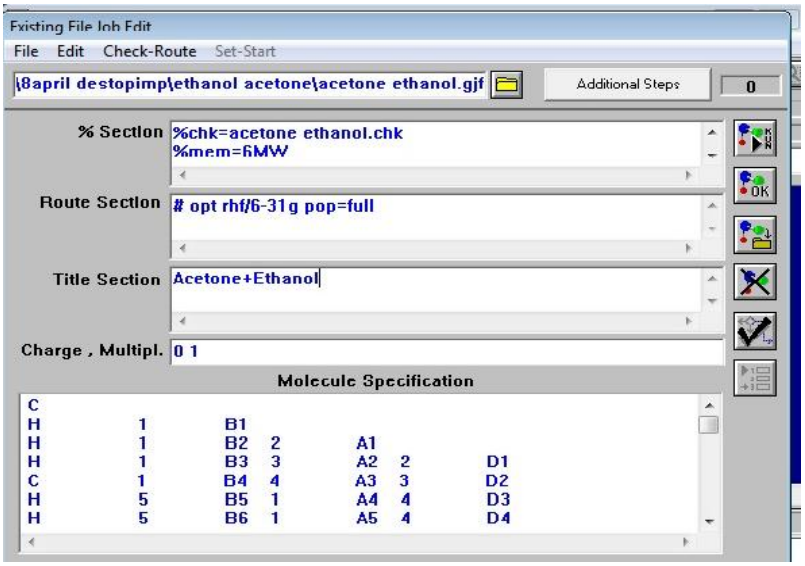

Figure 2.4: Operating mode of Gaussiam03.

2.2 Dielectric Studies

2.2.1 RCL meter for determination of static permittivity (£₀).

The PM 6303A Automatic LCR meter from M/S Fluke operating at a frequency of 1 khz as shown in fig. 2.5 was used for precise measurements of capacitance from which the static dielectric constant (ε_0) of liquids was determined. The measurement result, the numerical value, dimensions, and the equivalent electrical symbol, is displayed on the four digit liquid crystal display, which is updated at a rate of two measurements per second. A microprocessor controls the measurement process, computes the measurement value, and transfers the result to the display (RCL manual, 1995).

This instrument can measure, in addition to the basic *R, L, C* values, the Quality factor (*Q*), dissipation factor (*D*), parallel resistance ($R_{p)}$, series resistance (R_s), Impedance (*Z*), parallel capacitance (C_p) or parallel inductance (L_p), series capacitance (C_p) or series inductance (L_s) and the phase angle (¤).

The component measurement is based on the current and voltage technique.The component voltage and the component current are measured and converted into binary values. The CPU calculates the electrical parameters that are selected.

Each measurement cycle lasts approximately 0.5 seconds and consists of five single measurements, the result of which are stored and arithmetically evaluated. Finally the result is transferred to the display. The five single measurements are as follows:

1. Reference measurement: At the beginning of each measurement cycle, a reference measurement is performed. The measured value serves as reference for the subsequent four measurements.
2. Voltage measurement: 0^o
3. Voltage measurement: 90^o
4. Current measurement: 0^o
5. Current measurement: 90^o

At the end of the single measurements, the five values are stored. Using the measurement values, the microprocessor calculates the equivalent series resistance R_s, the equivalent series reactance X_s, and the quality factor $Q=X_s/R_s$ of the component. The auto mode decisions are based on the values of Q and D determined as shown in the fig 2.5.

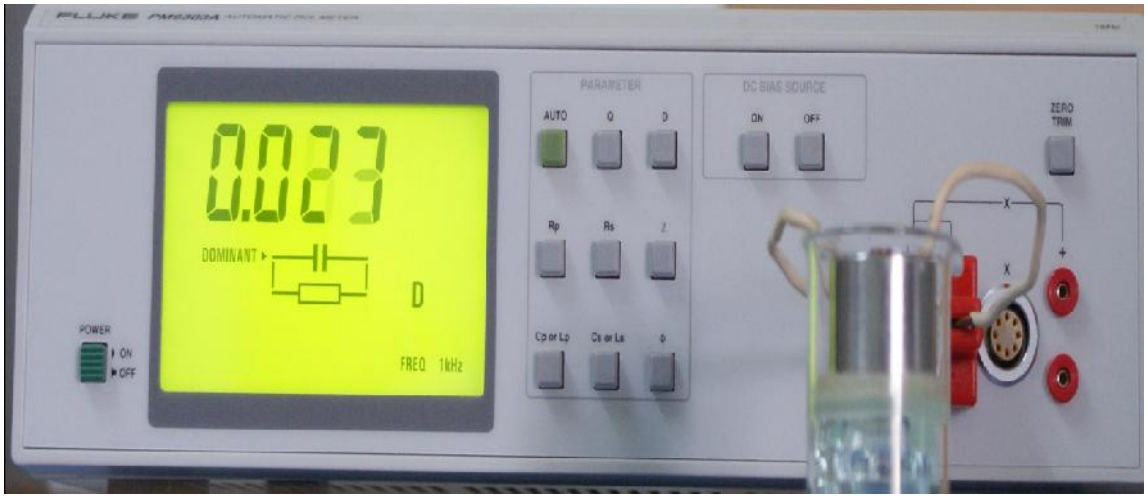

Figure 2.5: Experimental setup of RCL meter.

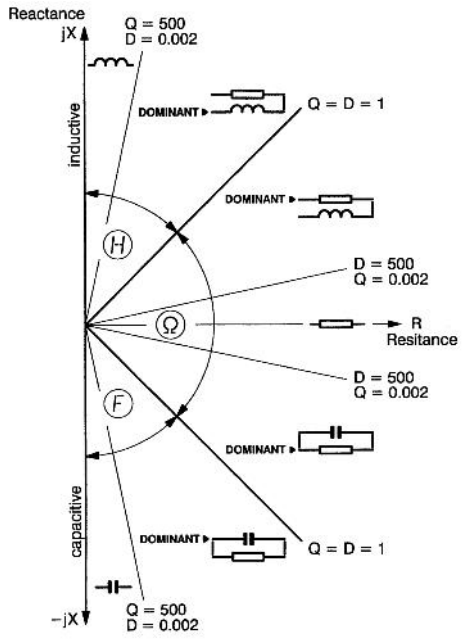

Figure 2.6: Operating mode of RLC meter.

A coaxial cylindrical capacitor cell was used for measurements. The two cylindrical shells have a very small spacing between them, which is filled with some dielectric medium.

The capacitance of the cylindrical capacitor is given by:

$$C = \frac{2\pi\varepsilon_o l}{log_e \frac{b}{a}} \quad \ldots (22)$$

Where l = length of cylindrical shells

b = radius of outer shell

a = radius of inner shell

ε_o = relative permittivity of free space

The photograph of the coaxial cell is shown in fig 2.7

Figure 2.7: Cylindrical capacitor Figure 2.8: Capacitor cell.

The capacitor was placed in a cell made of a 25 ml borosil beaker shown in fig. 2.8. Since the bottom of the beaker was not flat, it was cut circular glass and sealed with araldite. The sealing is required to ensure that there is no leakage since if there is any leakage; it would affect the volume of the liquid in the capacitor.

2.2.3 Abbe refractometer for determination of refractive index (*n*)

Refractive index (*n*) is measured to determine the high frequency dielectric permittivity (ε_{inf}) since $\varepsilon_{inf} = n^2$. Although ideally this measurement has to be done at UV frequencies, it is known that for most organic liquids measurements made using sodium vapor source are > 99.9% of the expected value and are hence routinely used in literature. Refractive indices have been measured using an Abbe refractometer shown in fig.2.9.

The basic principle of the refractometer is the application of the Snell's law. When the refractive phenomenon of the light occurs at the interface of two different media, it abides by Snell's law.

$$n_1 \sin\alpha_1 = n_2 \sin\alpha_2$$

In fig. 2.9, n_1 and n_2 represent the refractive indices of two media on both sides of the interface.

α_1 = Angle of incidence

α_2 = Angle of refraction

If the light enters from an optically denser medium to an optically rarer medium, the angle of incidence should be smaller than the angle of refraction. By changing the angle of incidence, the angle of refraction should be up to 90°, the angle of incidence at this moment should be called the critical angle. Abbe Refractometer for the determination of refractive index is just based on the principle to measure the critical angle.

Figure 2.9: Abbe refractometer.

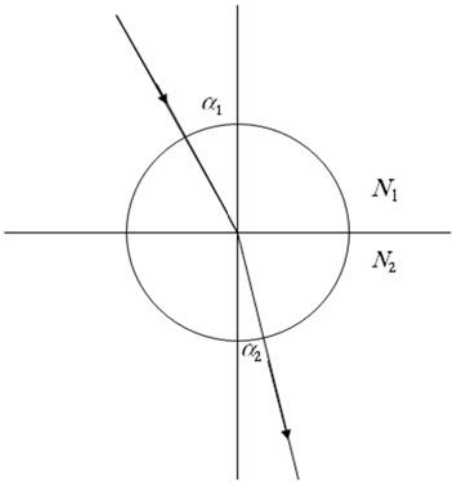

Figure. 2.10: Ray diagram of two media

In fig 2.11, when light rays of different angles project to the *AB* surface, if they are observed in the vertical direction on the *BC* surface with a telescope, a half dark and a half bright view field can be seen fig 2.12 the interface between the bright and the dark is the position of the critical angle.

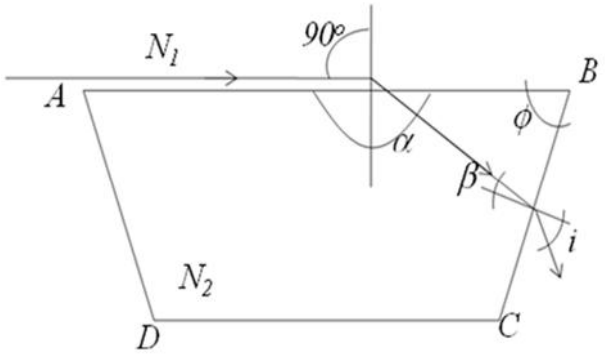

Figure 2.11: Refractive prism of refractive index N_2

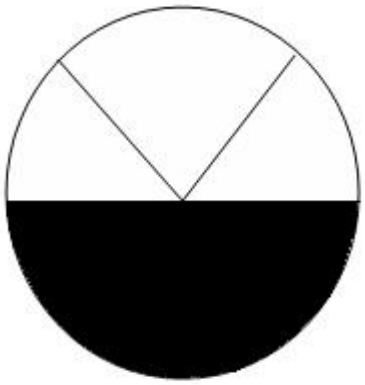

Figure 2.12: Interface between bright and dark

Fig 2.11 is a refractive prism, with its refractive index of N_2. Above the AB surface is the test piece (transparent solid or liquid), with its refractive index of N_1.

From Snell's law, we can obtain the equation:

$$n_1 = sin\varphi\sqrt{n_2^2 - sin^2 i} - cos\varphi sini \quad \ldots(23)$$

The refraction angle φ and the refractive index n_2 are known, when the critical angle i is measured. The refractive index n_1 of the test piece can be calculated by using eqn.23.

2.2.4 Dipole moment determination from Guggenheim's method

Dipole moment of the 1:1 binary system was determined from Guggenheim's method (Rojo *et al.*, 1999) as given by eqn. 24.

$$\mu^2 = \left[\frac{27KT}{4\pi N(\varepsilon_1+2)(n_1^2+2)}\right]\left[\frac{\Delta}{C}\right] \quad \ldots (24)$$

where, $\Delta = \left(\varepsilon_{12} - n_{12}^2\right) - \left(\varepsilon_1 - n_1^2\right)$

subscript 12 indicates solution and subscript 1 indicates solvent. K is the Boltzmann constant, N is the Avogadro number and T the absolutes temperature at which the experiment is conducted, the mean value of δ/c is calculated from the graph as shown in fig 2.13.

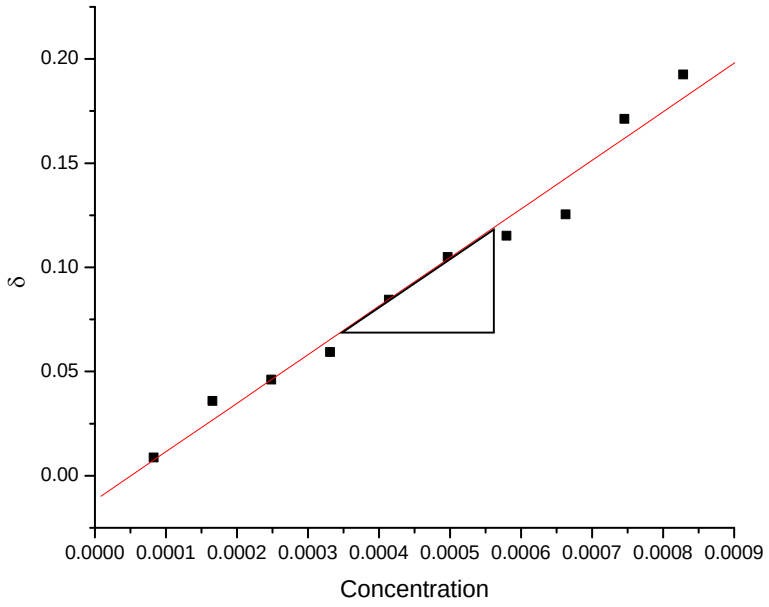

Figure 2.13: Typical graph for δ vrs concentration

The basis of the above equation is that for a molecular liquid the static permittivity (ε_0) has contributions from electronic and dipolar polarizations (neglecting atomic

polarization), where as the square of refractive index, which is the high frequency permittivity, has contributions only from electronic polarization. The difference between ε_0 and n^2 is thus an indicator of the dipolar polarization in the molecule. When a polar molecule is diluted in a non-polar solvent, the effect of the solvent is subtracted from the net polarization by defining

Eqn. 24 is an empirical relation and is valid strictly in the infinite dilution regime where there are no dipole-dipole interactions between the solute molecules.

2.3 Fourier Transform Infrared Spectroscopy

2.3.1 Introduction

Infrared is a part of electromagnetic spectrum that lies between the visible and the microwave region, in the frequency range between 3×10^{11} - 3.9×10^{14} Hz. In this frequency region atomic/molecular vibrational transitions are induced. There are three distinct region in infrared namely near-infrared (lies in the region between 4000-12800 cm^{-1}), mid-infrared (lies in the region between 400-4000 cm^{-1}) and far-infrared (lies in the region between 10-400 cm^{-1}). Each of these regions provides with distinct information. The present studies are done in the mid-infrared frequency region. For the sake of convenience, usually the wave number is used in place of frequency. The relation between the wave number and wavelength is given by $\bar{\nu} = \frac{1}{\lambda}$ and its unit is cm^{-1}.

When infrared radiation is passed through the sample, depending on the molecular vibration of the sample, some radiation is absorbed and some is transmitted creating a molecular finger print of the sample. This fingerprint is useful for the analysis of molecular structure of solid, liquid and gases.

2.3.3 IR theory

IR radiation emitted from black body source does not have sufficient energy to induce electronic transitions and the absorption is restricted to a certain vibrational states causing a net change in the dipole moment of the molecules. The IR beam is absorbed by the molecular vibrations of the sample only if the frequency of the radiation is in resonance with the molecular vibration, causing a change in the amplitude of the molecular vibration.

Since the position of atoms in molecules is random, there are various degrees of freedom for the atoms and hence there is a possibility of a number of different vibrational modes. If N be the number of atoms present in the molecules then the fundamental modes of vibration for the non-linear molecules is given by $3N$-6 degrees of freedom and for linear molecules $3N$-5 degrees of freedom.

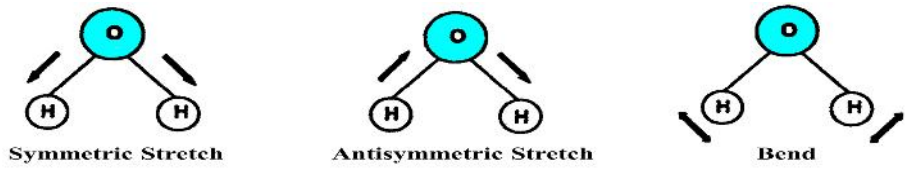

Figure 2.14: Modes of vibrations in molecules.

Vibrational modes belong mainly to two types (a) those in which there is a change in inter-atomic distance such as stretching (asymmetric and symmetric) and (b) those with a change in bond angle including modes such as bending (rocking, scissoring, wagging and twisting).

For the simplest of analysis, the atoms are treated according to Hooke's law as masses (of mass m) and the inter-atomic bonding is treated as a spring of spring constant (k). The strength of k determines the strength of the bond. The interatomic vibrations are

hence treated as simple harmonic motions about the mean atomic positions. According to Hooke's law the vibrational frequency of the spring can be written in terms of wave number as

$$\neg^{\rightarrow} = \frac{1}{2®c}\sqrt{\frac{k}{«}}\ cm^{-1}$$

Where k=force constant

« =reduced mass of the system

Thus, it is seen that increasing the mass of the atoms will reduce the frequency, and increasing the strength of the bond or the force constant will result in the increase in vibrational frequency. Hence if bond is more polar the infrared spectra arising from the bond is more intense.

However, the vibrational motion in a molecule is quantized. Only those transitions that follow the selection rule $\Delta J = \pm 1$ are allowed. Where J is the total quantum number.

As the force constant increases, the vibrational frequency (wave number) also increases. The force constants for bonds are: Single bond = 5 x 10^5 dyne/cm, Double bond = 10 x 10^5 dyne/cm, Triple bond = 15 x 10^5 dyne/cm. As the mass of the atoms increases, the vibration frequency decreases.

Using the following mass value:

C (carbon) = $\frac{12}{6.02\times10^{23}}$ a.u; H (hydrogen) = $\frac{1}{6.02\times10^{23}}$ a.u

Frequency of C–H stretching is calculated to be 3032 cm^{-1}. The actual range for C–H absorptions is 2850–3000 cm^{-1}. Now it can be seen that the calculated value is greater

than the range of the C-H stretch given. The range depends on the types of molecules to which C-H stretch is attached. It can vary depending on the mass of the atoms attached to it and also on the nature of the molecules. So there is no exact value for a particular bond, but the range can be expected from the IR spectra taken for the molecule required. The region of an IR spectrum where bond stretching vibrations are seen depends primarily on whether the bonds are single, double, or triple or if they are hydrogen bonds. The following table shows where absorption by single, double, and triple bonds are observed in an IR spectrum.

Table 2.1: Absorption region of various bonds.

BOND	ABSORPTION REGION (cm^{-1})
C–C, C–O, C–N	800–1300
C=C, C=O, C=N, N=O	1500–1900
C≡C, C≡N	2000–2300
C–H, N–H, O–H	2700–3800

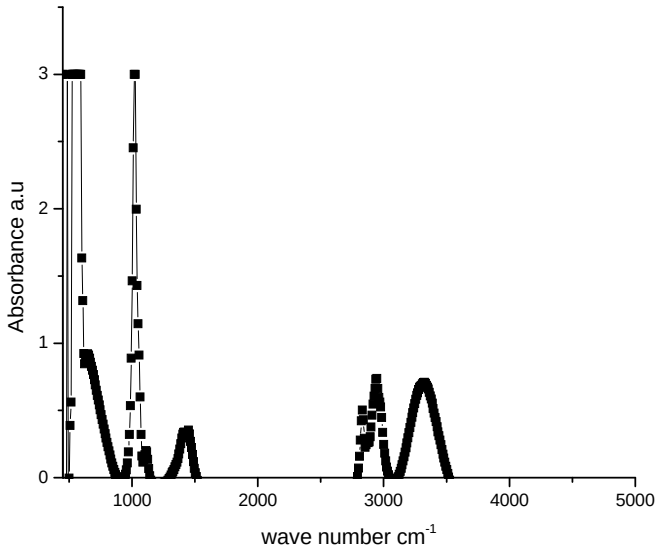

Figure 2.15: Typical IR absorption spectra.

2.3.2 Instrument and Software

The FTIR instrument from M/S ABB BOMEM, shown in fig 2.16 consists of a spectrometer and a computer with proprietary software. The spectrometer generates an interferogram using a Michelson interferometer arrangement. The proprietary software installed for data acquisition and fitting is called "*Horizon*".

Figure 2.16: FTIR spectrometer setup.

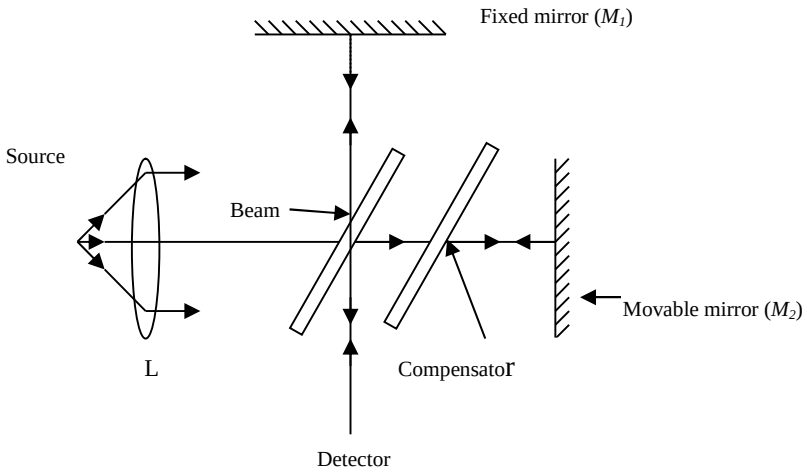

Figure 2.17: Block diagram of Michelson interferometer

The interferometer consists of a beam-splitter that splits the incoming infrared beam (containing infra red radiation of many frequencies) into two. One beam is reflected off a mirror fixed in space. The other beam is reflected off a movable mirror. The two reflected beams combine again causing an interference beam. The resulting beam is called an interferogram and it has the unique property that every data point (a function of the moving mirror position) has information about every infrared frequency that comes from the source. By measuring the interferogram, all frequencies are measured simultaneously.Thus a Michelson interferometer acts as a fourier transform spectrometer and the speed of measurement of all components is its advantage. Since most analysis requires spectra in the frequency domain, a fast fourier transform (FFT) is performed by the computer software.

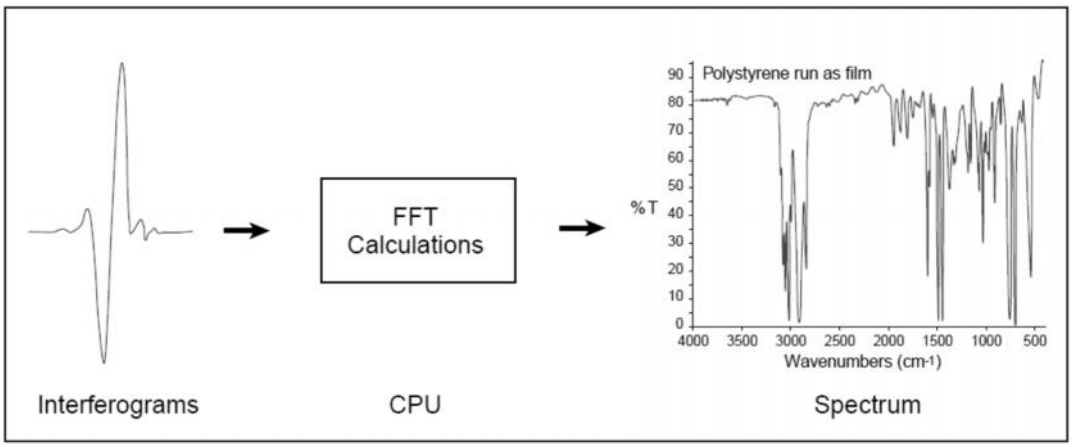

Figure 2.18: Working of FTIR.

FTIR spectra can be recorded either in the absorption mode or in the transmission mode. In fact, the two are inter-convertible even after the spectrum is recorded. All spectra of the present studies were recorded in the absorption mode.

The ABB-BOMEM MB-3000 FTIR spectrometer that was used comes with ZnSe windows that are useful under high-humidity conditions. Since the samples are all liquids, the ATR (attenuated total reflection) technique, shown in fig 2.19, was used for all the studies. In this method, by the principle of total internal reflection, the IR beam passes through IR transparent (zinc selenide) crystal and passes multiple times through the sample placed flush with the ZnSe crystal, as shown in fig 2.19. The IR beam penetrates the sample to a few microns in depth and absorbed at the characteristic absorption frequency giving the absorption spectra at the final output stage (Schmitz, 1972). The main advantage of this technique is that since the signal passes multiple times through the sample, the absorption spectral sensitivity increases.

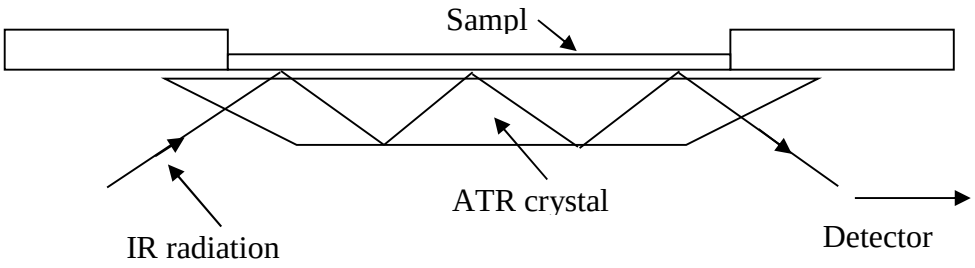

Figure 2.19: ATR technique

2.4 Contact angle measurement studies.

2.4.1 Introduction

The nature of wetting of surface by liquids is a function of cohesive and adhesive force. The molecular interaction among the liquids is a cohesive force and the interaction with the substrates is an adhesive force. They are the consequence parameter for the existence of the wetting. Complete wetting occur when the adhesive force dominate the cohesive force. On controlling the surface energy of the substrates by

coating, exposed to some particular frequency of light source or by changing the concentration of the liquids the wetting behaviour can be altered. Contact angle measurement is an important tool for the characterization of the wetting system and interfacial phenomenon. When water is made to contact with substrates, depending on the angle (¯) the substrates is designated as hydrophilic (which is less than 90^o), hydrophobic (if it is more than 90^o), superhydrophilic (if it is less than 30^o)and superhydrophobic (if it is more than 150^o) surface. Superhydrophobic are of two type; sticky surface and slippy surface which have a different wetting characteristic.

Depending on the surface morphology (roughness, smoothness, thickness and adhesive energy) of the substrate and surface tension of the liquids (cohesive force), the interaction of the liquid with the substrates can be determined and analyzed through contact angle studies. Contact angle (¯) is the angle between the surface of the solid and the outline tangent of a drop deposited on a solid surface. The angle between these two lines is called contact angle as shown in the fig 2.20.

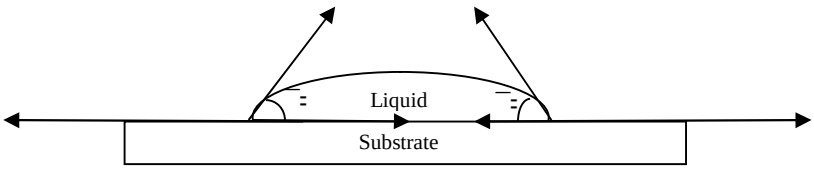

Figure 2.20: Typical figure of contact angle made by liquid on the substrate

The contact angle between substrates and liquids are related by the young equation (Young, 1805).

$$\cos\bar{} = \frac{Y_{SV} - Y_{SL}}{Y_{LV}}$$

Where, Y_{SV}=solid-vapor interfacial tension, Y_{SL}=solid-liquid interfacial tension and Y_{LV}=liquid-vapor interfacial tension.

2.4.2 Detail of instrument and technique

2.4.2.1 Goniometer instrument

Rame Hart contact angle goniometer consists of camera and software to capture the drop image and to analyze the drop profile. The modern day's goniometer consists of charge coupled device (CCD) camera, holder for goniometer micro syringe, a flat stage table to place the solid substrate which is to be examined. The CCD camera is a device which is specially designed to convert optical brightness into electrical amplitude signal using a many CCDs, and then reproduce the image of a subject using the electric signals without time delay. This instrument is used to measure the contact angle of sessile drop on a solid substrate. The instrument is useful for measuring advancing and receding contact angles, static and dynamic contact angle and surface tension and also for the surface energy of the solid substrate. They are also very good for dynamic and advancing contact angle measurement. Rame-Hart model 250 standard goniometer was used for the present studies. A photograph of the instrument is shown in fig 2.21.

Figure 2.21: The Rame-Hart Contact Angle Goniometer

It also has automated software controlled dispensing system with a nozzle and a piping system fitted to it to increase the accuracy and the speed of dispensing drops to produce sessile and pendant drops. A straight needle is used normally for manual dispensing of test liquid. The schematic representation of automated dispensing system is shown in fig 2.22.

Figure 2.22: Automated dispensing system

2.4.3 Technique

When a drop of the experimental liquid is carefully placed on the substrate on the flat stage table of the Goniometer, the CCD camera captures the profile of the liquid drop over the substrate and the picture is presented on the screen, the fiber optical lamp being illuminated from the background. The fixing of the crosshair cursor is very important in the measurement of contact angle. The horizontal solid-liquid interface must be aligned with the horizontal cursor line or the base line, as this determines the mathematical surface where the contact angle is to be measured.

2.4.3.1 Measurement of surface energy and surface tension

Contact angle goniometer can calculate the surface energy of the substrate (Carre, 2007; Hansen, 2004), surface tension (Roe *et al.,* 1967) and dynamic of the liquid on the substrates (Young, 1805). From Young's equation we can measure the contact angle and liquid-vapor interfacial tension directly but other quantity like solid-liquid and solid-vapor interfacial tension cannot be measured directly from the experiment. Dupree modified the Young's equation by introducing the concept of adhesion and it is the work done to separate the two phases given as $W=Y_{SV}+Y_{LV}-Y_{SL}$ Comparing the above equation with Young's equation, the adhesive energy is given as

$$W=Y_{LV}\,(1+\cos\theta) \qquad \text{...(25)}$$

This equation is known as Young-Dupree equation. To measure the solid vapor interfacial tension Fowke first split the total surface tension as the sum of the dispersive and polar component of surface energy. Later Owens-Wendt (Owens and Wendt, 1969) apply the geometric mean method and finally showed that adhesive energy can be expressed as the geometric mean of dispersive and polar component of surface free energy of solid and liquid phases as

$$Y_{LV}(1+\cos^{-}) = 2(\sqrt{Y_S^D}\sqrt{Y_L^D} + \sqrt{Y_S^P}\sqrt{Y_L^P}) \qquad \text{…(26)}$$

This equation can be solved by introducing a pair of polar and non-polar liquid. The standard polar liquid used was water and non-polar liquid as Diiodomethane. Owens-Wendt geometric mean method cannot be applicable for all samples so later on Wu (Wu, 1971) measured the adhesive energy of low energy surfaces and came to a conclusion that adhesive energy can be expressed as the harmonic mean instead

geometric mean of dispersive and polar component of surface free energy of two phases as.

$$Y_{LV}(1+\cos^{-})=4\left\{\frac{Y_S^D Y_L^D}{Y_S^D+Y_L^D}+\frac{Y_S^P Y_L^P}{Y_S^P+Y_L^P}\right\} \quad \ldots(27)$$

The choice of liquids used for Wu method is also same as Owens-Wendts method.

From the value of contact angle of sessile drop of a liquid over the solid substrate, one can measured the strength of interaction forces between the molecules of the solid substrate and the molecules of the liquid used.

Among many other techniques for the calculation of surface energy, multiliquid tool is taken up for the present studies. Multiliquid tool is an extension of Owens-Wendt geometric mean method where we use

$$Y_{LV}(1+\cos^{-})=2\sqrt{Y_S^d Y_L^d}+2\sqrt{Y_S^P Y_L^P} \quad \ldots(28)$$

The above equation can be simplified as

$$\frac{(1+\cos^{-})}{2}\frac{Y_{LV}}{\sqrt{Y_L^d}}=\sqrt{Y_S^d}+\sqrt{Y_S^P}\frac{\sqrt{Y_L^P}}{\sqrt{Y_L^d}} \quad \ldots(29)$$

This equation is of the form $Y=mx+c$, Where

$$Y=\frac{(1+\cos^{-})Y_L}{2\sqrt{Y_L^d}},\quad X=\frac{\sqrt{Y_L^P}}{\sqrt{Y_L^d}},\quad m=\sqrt{Y_S^P},\quad C=\sqrt{Y_S^d} \quad \ldots(30)$$

Using series of liquids with different polarity four different straight lines is obtained. From the best fit line polar and dispersive component of surface free energy of solid can be calculated. The probes liquids used were water, glycerol, and diiodomethane.

For the calculation of surface tension pendant drop method is employed as shown in fig 2.23. Pendant drop method is calculated from Young-Laplace equation as shown in eqn.31.

$$Y = \frac{\Delta^{\circ} g R_o^2}{} \qquad \ldots(31)$$

Where, Y is the surface tension liquid, Δ° is the density different between the drop and air, g is the acceleration due to gravity, R_o is the radius of curvature of the liquid drop and is the shape factor.

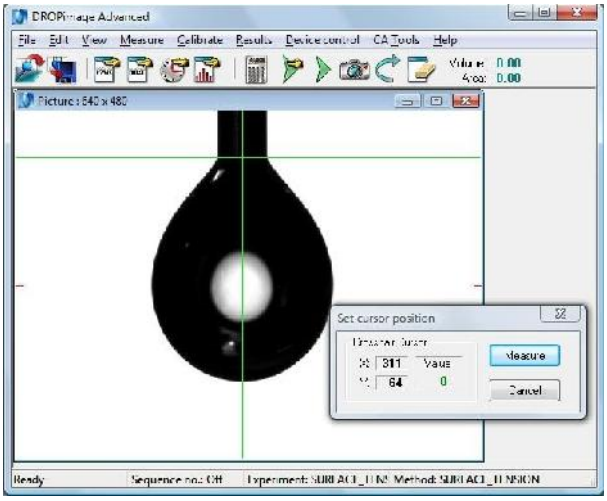

Figure 2.23: Pendant drop method for the calculation of surface tension

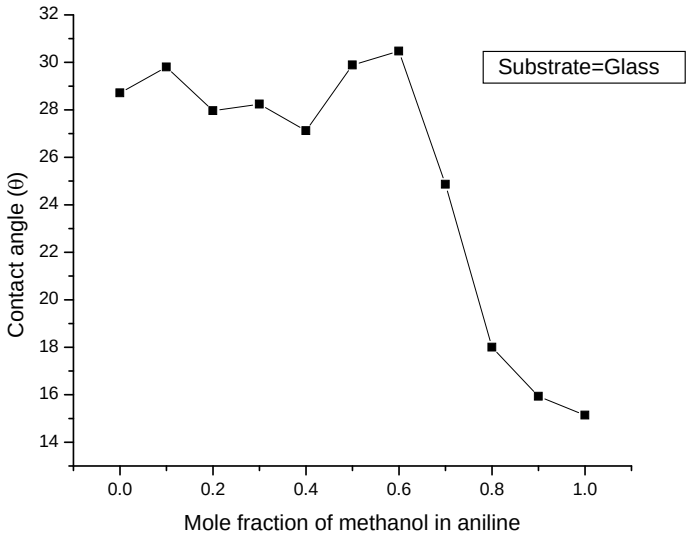

Figure2.24: Typical graph for contact angle of mole fraction of methanol in acetone.

2.4.3.2 Spin coater

Spin coater is an instrument which is used for coating liquids sample like amino acids, proteins etc over the substrates. The coating of sample film using spin coater is uniform as compare to drop and dry method. Spin coating technique has been applied for the coating of thin film over different substrates. The procedure involves dispensing a small volume of liquid sample on to the centre of the substrate and then spinning the substrate at a high speed, the centripetal acceleration will cause the sample liquid to coat over the substrate. Thin film accumulation on the substrate depend on the surface properties of substrate and liquid like surface energy, roughness, viscosity, surface tension and drying rate of sample liquid. One of the most important factors for uniform coating is speed of the spin coater. The speed of the substrate affects the centrifugal force applied to the liquid, there by effect the thickness of the film. The final film will be inversely proportional to the spin speed and spin time. Since there are several factors

affecting the coating process like spin speed, spin time and nature of liquid and substrate that effect the coating process.

Figure 2.25: Experimental setup of spin coater.

Amino acids and proteins were coated using the spin-coating technique. A commercial spin coater and a lab-made spin coater, shown in fig. 2.25 were used for this coating and the results were seen to be identical. Since the access to the commercial spin coater was limited and the lab-model worked well for this work, all studies reported in this thesis were performed using the lab-made model.

CHAPTER- 3

Studies of binary liquids and their interactions with solid substrates

Chapter - 3

Studies of binary liquids and their interactions with solid substrates

3.1 Introduction

This chapter contains the finding on two classes of binary liquids namely alcohol-aniline and alcohol-acetone. The alcohols studied are methanol, ethanol, isopropanol, butanol, hexanol and octanol. The studies performed are computational conformational analysis using Self Consistent Field – Hartree Fock technique (SCF-HF), dielectric studies for determination of dipole moment and refractive index (*n*), Fourier Transform Infrared (FTIR) and the study of wetting characteristics through the study of contact angle, surface energy and surface tension. Interaction between aniline and alcohol is characterized by theO-H--N bond while the interactions in the acetone-alcohol systems are characterizedby the C=O--H hydrogen bond. These two kinds of hydrogen bonds play an important role in biological systems and form the prototype for the hydrogen bonds seen in amino acids, which in turn determine the interactions in proteinsas discussedin chapter1 and seen in chapter 4. The choice of the six alcohols is based on the fact that they form a homologous series. By studying the interactions of aniline/acetone with these members of homologous series, it is expected that the influence of steric hindrance and hence the change in charge density at the hydrogen bonding site can be studied. Pentanol and heptanol could not be studied for logistic reasons.

Wetting of various substrates by binary liquids over the entire concentration range is studied since such an interactions play an important role in performance of many devices

(Xia *et al.,* 2001), concentration dependent wetting transitions are expected in case of wetting of substrates by binary liquid (Madhurima *et al.,* 2011)

3.2 Surface characterization

The substrates chosen for the present studies are borosilicate glass, silicon, aluminum oxide(Al_2O_3), indium tin oxide (ITO) and polymers namely; nylocast, epoxy FR4, fiber reinforce plastic (FRP), polypropylene, polyurethane, hylam and Teflon. The polymers are obtained commercially and are used as obtained after cleaning. These substrates have a wide application in the manufacturing of a variety of devices. Depending on the surface morphology and material property, the substrates have distinct surface energies which are calculated using the multiliquid tool discussed in chapter 2. Test liquids used for the characterization of the substrates are water, glycerol and diiodomethane. The results are arranged in order of decreasing surface energy and are shown in table 3.1.

Table3.1: Surface energy of different substrates.

Substrates	Surface energy (mj/m^2)			Substrates	Surface energy (mj/m^2)		
	Polar	Dispersive	Total		Polar	Dispersive	Total
Glass	28.70	26.98	55.6	Polypropylene	11.33	24.77	36.10
Nylocast	20.30	26.52	46.82	Al_2O_3	5.07	30.39	35.46
Silicon	5.10	36.36	41.46	Polyurethane	20.36	14.63	34.99
Epoxy FR4	8.44	31.05	39.49	ITO	0.46	30.60	31.06
Glass Epoxy	11.85	27.23	39.08	Hylam	5.32	20.57	25.89
FRP	31.40	35.49	38.63	Teflon	1.31	21.93	23.24

The surface energy of any material constitutes of two components - polar (short range interaction) and dispersive (long range interaction). Substrates chosen for the present studies have a wide range of polar and dispersive energy as seen from table 3.1, substrates ranging from high polar energy namely glass (29.22mj/m^2) to low polar energy namely ITO(0.46mj/m^2) and high dispersive energy namely silicon (36.36mj/m^2) to low dispersive energy polyurethane(14.63mj/m^2) are taken up for the present studies. The influence of polar and dispersive components of the total energy on wetting is studied.

3.3 Binary mixture of Aniline - Alcohols

The structure of aniline and the non-planarity of amino group in aniline has been reported (Ellena *et al.,* 1999). The structure is taken as the starting point for the present computations.Interactions between aniline and alcohols are due to the formation of hydrogen bonds of the kind N-H--O (Forlani, 2007). A few studies on aniline-alcohols binary liquids have been reported previously (Chaudhari and Mehrota, 2002). The decrease in the value of dielectric permittivity $\varepsilon_o$with an increase in the concentration of aniline in various alcohols is reported by Patil et al. (Patil *et al.,* 1999). Sigmoidal curves of permittivity with concentration variation in the alcohol rich region of the binary is attributed to volume reduction (Tsierkezos *et al.,* 2000). Alcohols are hydrogen bonded as a result exhibit extended network, aniline on the other hand does not show dipole-dipole interaction (Forlani, 2007).

From the present studies, it is observed that aniline and alcohol together exhibit hydrogen bond of the kind N-H--O, which breaks the extensive hydrogen bond network of alcohols, causing a blue shift in the IR OH peak. Further, the formation of smaller cluster is

seen from the red shift of NH_2 Scissoring. The wetting of various substrates by the binary liquids is seemingly concentration dependent. These are the general features observed for the six aniline-alcohol systems that are taken up in the present study and the results of each of the six system are discussed below.

3.3.1 Binary mixture of Aniline - Methanol

Aniline-methanol binary system has been studied previously by various researchers (Despande *et al.*,1971). From dielectric studies the Kirkwood *g* factor is determined and the two moieties showed a maximum interaction at 20% methanol concentration (Fattepur *et al.*, 1994). *In situ* magic angle spinning nuclear magnetic resonance spectroscopy showed the adsorption of aniline and methanol on zeolite (Ivanova *et al.*,2001);the adsorbed methanol are attached to the bridging hydroxyl group and aniline is bound to the zeolite.From the dielectric relaxation studies using Pico second time domain reflectometer measurements it is observed that the aniline rich region exhibits of hydrogen bonding between aniline and methanol while in the methanol-rich region, clusters of methanol similar to those in pure methanol are observed (Mandado *et al*., 2003).

3.3.1.1 Computational Analysis of aniline-methanol system

The interaction site between the aniline and methanol molecules is determined from computational studies. The details of the computational methods are discussed in chapter 2. A large number of initial conformations are chosen for both molecules of aniline and methanol and also for the binary system. The structure of methanol (Yamaguchi *et al.,* 1999; Adya *et al.,* 2000; Jorgensen, 1986) and aniline (Ellena *et al*., 1999) are well documented. Of the various conformations, the most stable conformer (with least energy) of aniline and

methanol are chosen to form the binary and the three lowest energy conformers of the binary system are reported here in fig.3.1.

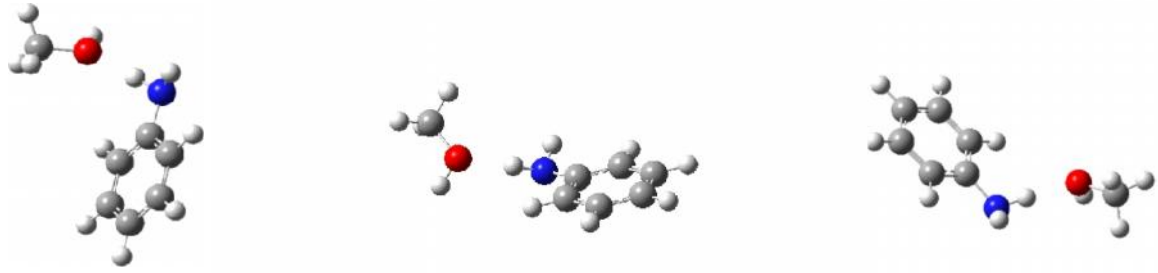

Structure (1). Structure (2). Structure(3).

Figure 3.1: Three conformations of the aniline-methanol 1:1 binary.

The most probable mode of interaction between aniline and methanol is taken from the minimum energy conformationas shown in fig. 3.1. The details of computational study are given in table 3.2. The conformer shown in fig. 3.1(1) is that with lowest energy at STO-3G. For higher basis sets structure 3 shown in fig. 3.1(3) possesses the lowest energy. Since, the hydrogen bonding is best represented by lower basis sets because of their directionality, the structure in fig. 3.1(1) is taken as the most probable conformation.

The 1:1 molecular conformations represent the middle region of concentration where the probability of formation of 1:1 complexes is larger. In order to understand the interaction in the aniline rich region (aniline as solvent; alcohol as the solute) and the alcohol rich (alcohol as solvent and aniline as solute), Onsager's solvation model is used. The details of this computational model have been discussed in chapter 2 and the results are given in table

3.3. On solvation by aniline, the dipole moment ($\vec{\mu}$) of methanol is more or less constant while there is an increase in the $\vec{\mu}$ of aniline due to the solvation by methanol. This is corroborated with IR and contact angle studies discussed below.

Table 3.2:Computational modeling data of the aniline-methanol 1:1 binary structure shown in fig.3.1.HF energy (hartree) and dipole moment (debye).

Basis	Parameter	Aniline	Methanol	Structure 1	Structure 2	Structure 3
STO-3G	HF Energy	-282.206100704	-113.549193204	-395.768990954	-395.768618282	-395.767582707
	Dipole Moment	1.3267	1.5094	3.1958	3.3431	3.6310
6-31G	HF Energy	-285.633042967	-114.988165278	-400.630823535	-400.630823536	-400.630823537
	Dipole Moment	1.456	2.2875	4.1539	4.8001	4.1527
6-31G(d)	HF Energy	-285.728226746	-115.035418040	-400.772841972	-400.772841908	-400.773012233
	Dipole Moment	1.6087	1.8656	3.3547	3.4274	3.1823
6-31G(d,p)	HF Energy	-285.745539086	-115.046709859	-400.800935132	-400.800936558	-400.801119791
	Dipole Moment	1.6037	1.8405	3.3414	3.4245	3.1554

Table 3.3:Solvation modeling dataof the three aniline-methanol 1:1 binary structure shown in fig.3.1.HF energy (hartree) and dipole moment (debye).

Basis	Parameter	Aniline rich region	Methanol rich region
STO-3G	HF Energy	-282.198621251	-113.549738472
	Dipole Moment	1.4652	1.5439
6-31G	HF Energy	-285.620191636	-114.985889555
	Dipole Moment	1.6065	2.5613
6-31G(d)	HF Energy	-285.716061909	-115.033385747
	Dipole Moment	1.7377	2.1397
6-31G(d,p)	HF Energy	-285.733090795	-115.044212334
	Dipole Moment	1.7336	2.1139

Hydrogen bond energies are calculated for the 1:1 binary system at various basis levels using the equation $ab_{e\_} = (E_A+E_B - E_{AB})$, where E_A and E_B are the energy of the individual component and E_{AB} is the energy of the binary system. The results are given in table 3.4. It is seen from HB energy that the bond is of intermediate strength (~ -6kcal/mol).

Table 3.4: Hydrogen bond energies of the three aniline-methanol 1:1 binary.

Basis set	Structure1 (kcal/mol)	Structure2 (kcal/mol)	Structure3 (kcal/mol)
STO-3G	-8.595033	-8.361177	-7.711344
6-31G	-6.033687	-6.033691	-6.033691
6-31G(d)	-5.771326	-5.771286	-5.878166
6-31G(d,p)	-5.464774	-5.465669	-5.580649

Hydrogen bond distance between oxygen of methanol and hydrogen of aniline are 1.80509 $\overset{o}{A}$ for structure (1), 1.82321 $\overset{o}{A}$ for structure (2) and 1.82023 $\overset{o}{A}$ for structure (3). Computational studies are performed to obtain a structure for the interacting moieties that can be used as a framework to interpret the experimental result.

3.3.1.2 Dielectric studies

The dipole moment ($\vec{\mu}$) of the binary system is determined experimentally from dielectric studies as discussed in chapter 2, using the Guggenheim's method. Benzene is used as the non-polar solvent and the 1:1 mixture of aniline - methanol as the solute. The plot of $\phi = \left(\varepsilon_{12} - n_{12}^2\right) - \left(\varepsilon_1 - n_1^2\right)$ versus concentration is shown in fig.3.2where subscript 12 indicates solution and subscript 1 indicates solvent. The experimentally determined value of $\vec{\mu}$ = 2.04Dwhile the corresponding value from the computation is about 3D, and are in

good agreement. A difference of 1D is within the experimental and computational error range (Sathyan *et al.*, 1995). The experimental data is shown in table 3.5.

Table 3.5: Dielectric data of aniline-methanol 1:1 mixture in benzene solution

Concentration (mol/cc)	£$_{12}$	n_{12}^2	¢
0.000145	2.28	2.26	0.001344
0.000289	2.36	2.25	0.088303
0.000434	2.40	2.26	0.116815
0.000579	2.42	2.27	0.129766
0.000724	2.51	2.27	0.211650
0.000868	2.52	2.26	0.240991
0.001013	2.54	2.29	0.229073
0.001158	2.65	2.27	0.357522
0.001303	2.61	2.28	0.306997
0.001447	3.13	2.24	0.872096

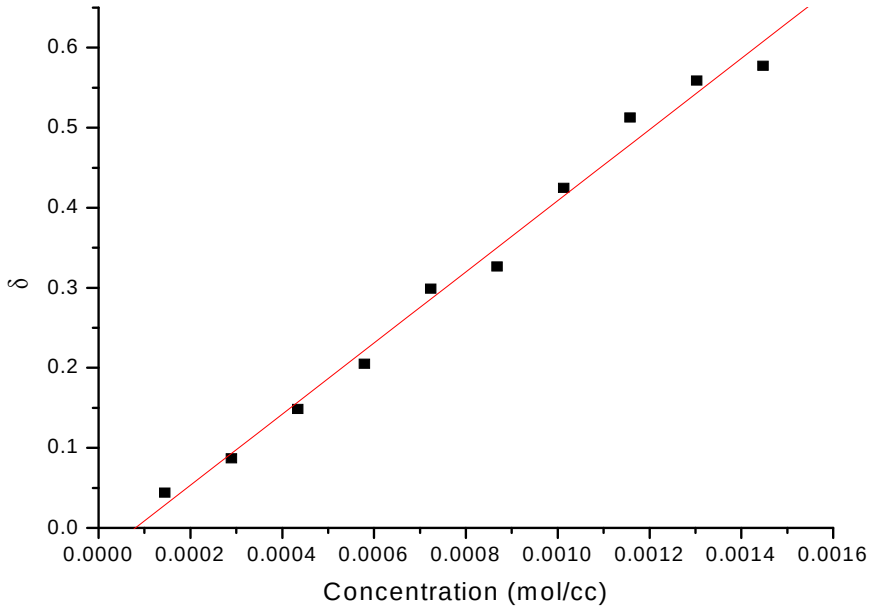

Figure 3.2: δ vs. concentration of the binary system used to determine the experimental dipole moment.

3.3.1.3 FTIR Studies

The FTIR spectra of aniline-methanol over the entire concentration range is reported. The O-H stretch region is magnified in fig.3.3 and NH_2scissoring in fig.3.4. Blue shift in the O-H peak is observed in methanol rich region and red shift in aniline rich region. A dramatic change in the OH peak position is seen on the introduction of about 20% aniline shown in fig.3.3, which indicates the breaking of methanol cluster by aniline.The N-Hstretch has the same frequency range of O-H and thus there is an overlap with the O-H peak. The smaller clusters of methanol formed at lower concentrations of anilineare seemingly unaffected with the introduction of aniline.

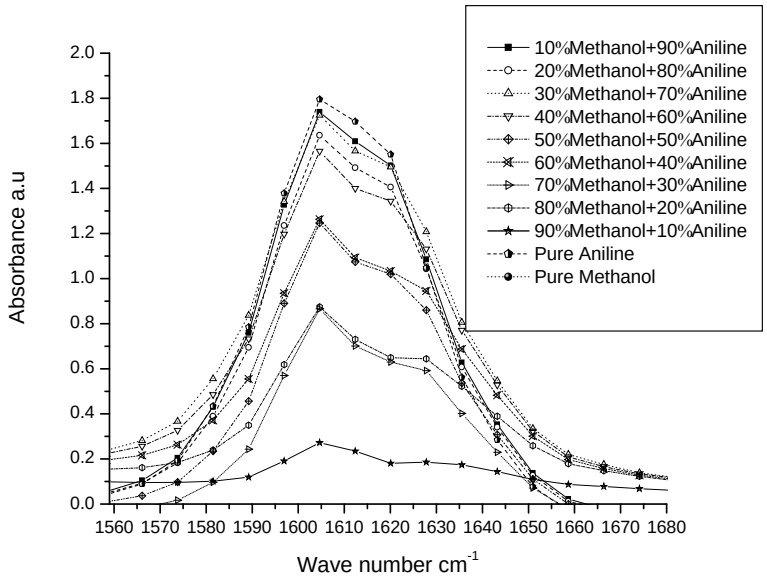

Figure 3.3: O-H stretching frequency of aniline-methanol mixture.

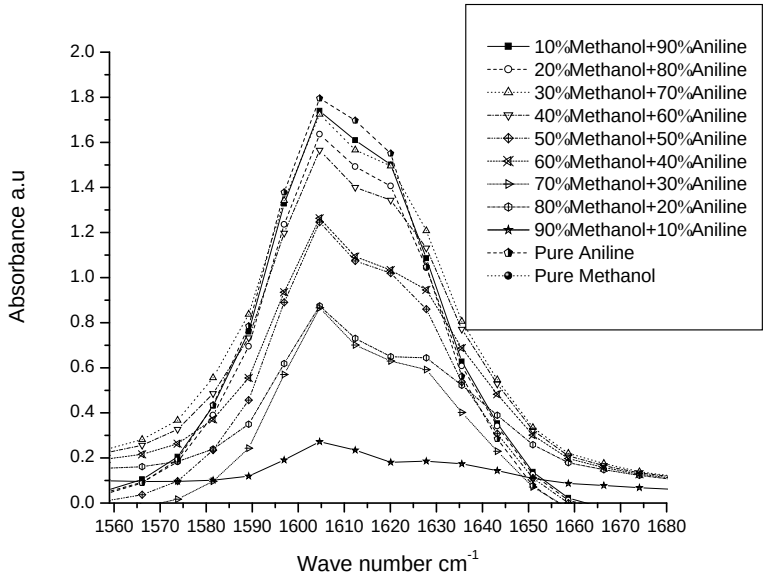

Figure 3.4: NH_2 Scissoring frequency of aniline-methanol mixture.

3.3.1.4 Wetting studies

Wetting of aniline-methanol over the entire concentration range on six substrates is measured through the contact angle made by the test liquids over the substrates, which is shown in fig.3.5. On most surfaces, a greater wetting is observed at higher concentration of methanol. At 10%-30% aniline a change in contact angle is observed. When the surface energy of the substrate matches with the surface tension of the liquid,rapid wetting is observed as seen in the case of Al_2O_3at ~70% concentration of methanol, as seen from table 3.1 and fig. 3.6,

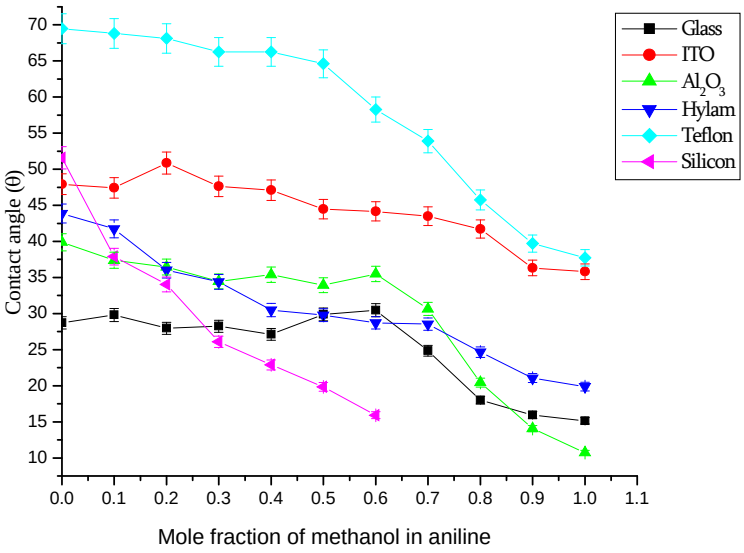

Figure 3.5: Variation of contact angle with mole fraction of methanol in aniline over different substrates.

Surface tension of pure liquids as obtained from literature (table 3.1) and surface tension of pure liquid calculated from the present studies are commensurate.

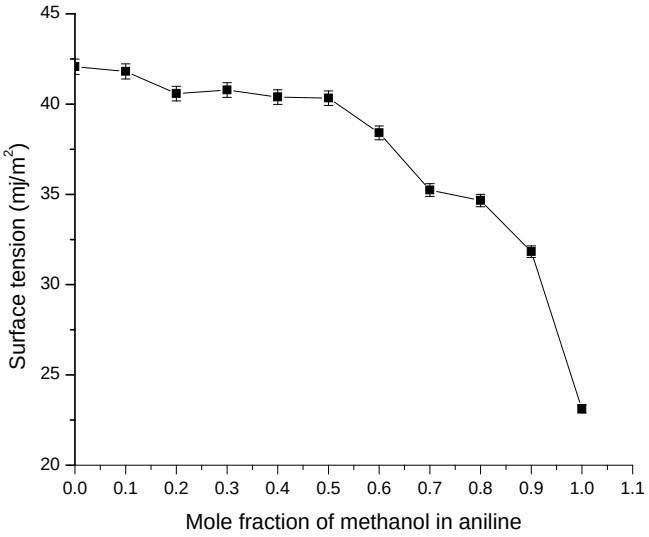

Figure 3.6: Variation of surface tension with mole fraction of methanol in aniline.

Summary

It is seen from the literature (Patil *et al.,* 1999) that, the Interaction between the two moieties namely aniline and methanol is maximum at 20% aniline concentration (methanol rich region) with a possibility of a secondary weak interaction between the phenyl group of aniline and the methyl group of methanol. The data of FTIR, contact angle, dielectric and computational analysis agree with the former observation but are in contradiction with the later. Maximum interaction between the moieties is seen between10%-30% aniline concentration and is attributed to the destruction of methanol clusters by aniline. Although the possibility of a second weak hydrogen bond between the phenyl ring and the methyl group cannot be fully discarded, we see no major evidence for the existence of the same. Almost all of the present studies over different substrates indicate that the 10%-30% aniline concentration region shows maximum interaction between the moieties. Rapid wetting is seen when the surface tension of the binary liquid is of the same magnitude as the surface energy of the substrates.

3.3.2 Binary mixture of Aniline-Ethanol

Liquid ethanol structure has been reported using neutron diffraction and molecular dynamics studies (Benmore *et al.,* 2000; Siaz *et al.,* 1997). The structure of liquid ethanol is seen to be dominated by hydrogen bond at room temperature. Aniline and ethanol form an associated liquid and the thermodynamics of this binary liquid are analyzed using the UNIQUAC model(Nagata and Sano, 1992) and found the equilibrium of the liquid-liquid interaction. Inhomogeneous distribution of aniline in the aniline-ethanol binary liquid is previously seen using laser photonionization studies by Mafune et al (Mafune *et al.,* 1994).The results of the present studies on this binary system are discussed below.

3.3.2.1 Computational Analysis

The three conformers shown in fig.3.7 are the most stable ones out of many initial comformers. The conformer shown in fig. 3.7(3) is that with lowest energy at STO-3G and also at higher basis set. This conformer is taken to be the most stable conformation and used for determination of interaction site between aniline and ethanol. Computational analysis are performed to determined the molecular interaction between aniline- ethanol binary system at different basis set, which are presented in table 3.6. On solvation by aniline, the dipole moment ($\vec{\mu}$) of ethanol is more or less constant where as there is an increase in the $\vec{\mu}$ of aniline on solvation by methanol as shown in table 3.7. This is consistent with the results of IR and contact angle studies discussed below. The calculated hydrogen bond energy is shown in table 3.8.

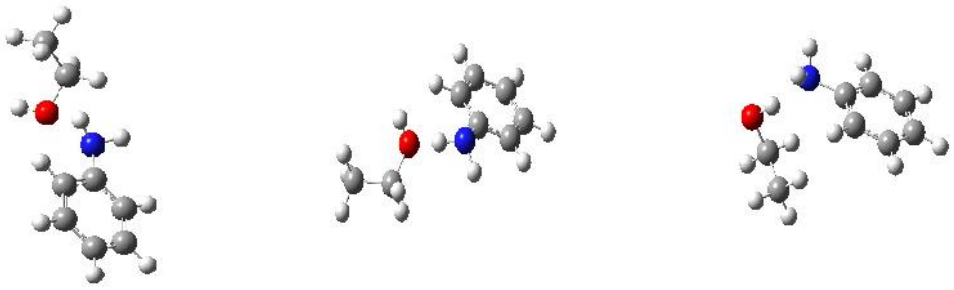

Structure (1). Structure (2). Structure (3).

Figure 3.7: Three conformations of the aniline-ethanol 1:1 binary.

Table 3.6: Computational modeling data of the aniline-ethanol 1:1 binary structure shown in fig 3.7.HF energy (hartree) and dipole moment (debye).

Basis	Parameter	Aniline	Ethanol	Structure 1	Structure 2	Structure 3
	HF Energy	-282.206100704	-152.032674708	-434.353122003	-434.353142317	-434.353542285
STO-3G	Dipole Moment	1.3267	1.4364	3.4779	3.3711	3.0316
	HF Energy	-285.633042967	-154.013229094	-439.655520179	-439.655520166	-439.653146044
6-31G	Dipole Moment	1.456	2.1048	4.1503	4.1519	2.5209
	HF Energy	-285.728226746	-154.075744647	-439.813111028	-439.814045772	-439.814696840
6-31G(d)	Dipole Moment	1.6087	1.7376	3.3514	1.6635	2.8082
	HF Energy	-285.745539086	-154.090161446	-439.844336054	-439.844336551	-439.845556635
6-31G(d,p)	Dipole Moment	1.6037	1.7030	3.3878	3.4548	2.7168

The hydrogen bond distance between oxygen of methanol and hydrogen attached to nitrogen site of aniline are 1.79614 $\overset{o}{A}$ for structure1, 1.79501 $\overset{o}{A}$ for structure 2 and 1.93558 $\overset{o}{A}$ for structure 3.

Table 3.7: Solvation modeling data of the three aniline-ethanol 1:1 binary structure shown in fig 3.7.HF energy (hartree) and dipole moment (debye).

Basis	Parameter	Aniline rich region	Ethanol rich region
STO-3G	HF Energy	-282.206506083	-152.133126111
	Dipole Moment	1.5584	1.4869
6-31G	HF Energy	-285.631669179	-154.009355460
	Dipole Moment	1.6443	2.4135
6-31G(d)	HF Energy	-285.726944066	-154.072616060
	Dipole Moment	1.8246	2.0196
6-31G(d,p)	HF Energy	-285.744068735	-154.086547127
	Dipole Moment	1.7923	1.9930

Hydrogen bond energies are calculated for the 1:1 binary system at various basis levels using the same equation used in aniline-methanol system. The results are given in table 3.8. It is seen from HB energy that the bond is of intermediate strength (~ -5kcal/mol).

Table 3.8: Hydrogen bond energies of the three aniline-ethanol 1:1 binary.

Basis set	Structure1 (kcal/mol)	Structure2 (kcal/mol)	Structure3 (kcal/mol)
STO-3G	-9.002637	-9.015384	-9.266479
6-31G	-5.803262	-5.803253	-4.313468
6-31G(d)	-5.735271	-6.321877	-6.730383
6-31G(d,p)	-5.418896	-5.419208	-6.184823

3.3.2.2 Dielectric studies

The experimental dipole moment of the 1:1 binary system of aniline-ethanol is determined from fig. 3.8 and table 3.9. The experimental results shown in fig.3.8 yield an experimental dipole moment of « = 1.75D. While the corresponding value from the computation is about 3D.

Table 3.9: Dielectric data of aniline-ethanol 1:1 mixture in benzene solution

Concentration (mol/cc)	£$_{12}$	n_{12}^2	¢
0.000130	2.28	2.26	0.005837
0.000260	2.32	2.26	0.042737
0.000390	2.35	2.26	0.070312
0.000520	2.35	2.26	0.075302
0.000650	2.48	2.26	0.199092
0.000780	2.54	2.26	0.265832
0.000910	2.55	2.26	0.267305
0.001040	2.63	2.26	0.350242
0.001170	2.73	2.27	0.442926
0.001300	2.75	2.26	0.475635

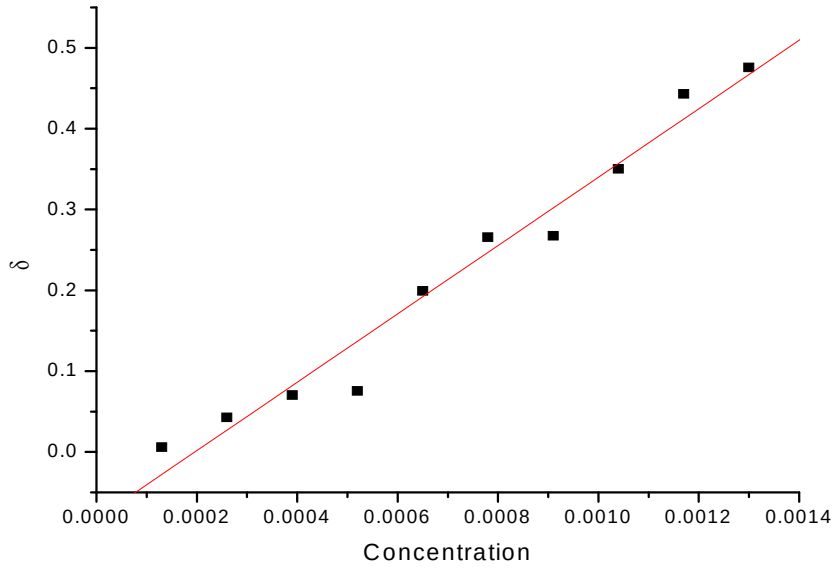

Figure 3.8: δ vs. concentration of the binary system used to determine the experimental dipole moment.

3.3.2.3 FTIR studies

The FTIR spectrum of aniline-ethanol over the entire concentration range is report. At lower concentration of aniline (approximately at 20%) there is a significant change in the OH peak, which indicates the breaking of the hydrogen bond cluster of alcohols by aniline, similar to that in aniline-methanol. On increasing aniline concentration, the OH peak position does not show significant shift as seen from fig.3.9. From fig.3.10 it is observed that NH_2 scissoring frequency also does not shift with addition of ethanol. A change in the OH peak is observed at lower concentration of aniline approximately from 20% as shown in fig.3.9. The introduction of aniline at lower concentration of ethanol does not have adverse effect on smaller cluster of ethanol where as the larger clusters are broken by aniline leading to a significant blueshift in the IR peak position in fig.3.9.

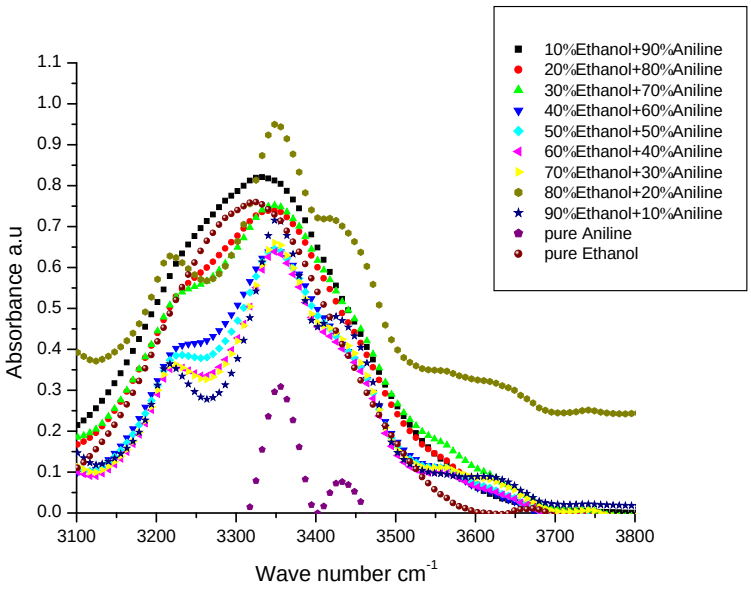

Figure 3.9: O-H stretching frequency of aniline-ethanol mixture.

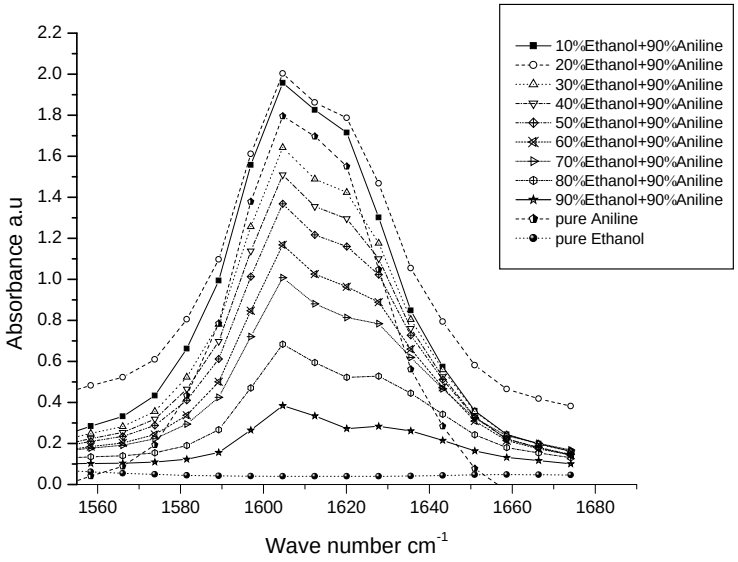

Figure 3.10: NH_2 Scissoring frequency of aniline-ethanol mixture.

3.3.2.4 Wetting studies

The contact angle made by aniline-ethanol binary system over the entire concentration region over the previously discussed substrates is measured and is reported in fig.3.11 along with surface tension in fig.3.12. Ethanol region show a better wetting than aniline region and this is due to same magnitude of surface tension of liquids and surface energy of the substrates data. A dramatic wetting is observed at about 10%-30% aniline for this system. This result follows the same trend as that of aniline - methanol system.

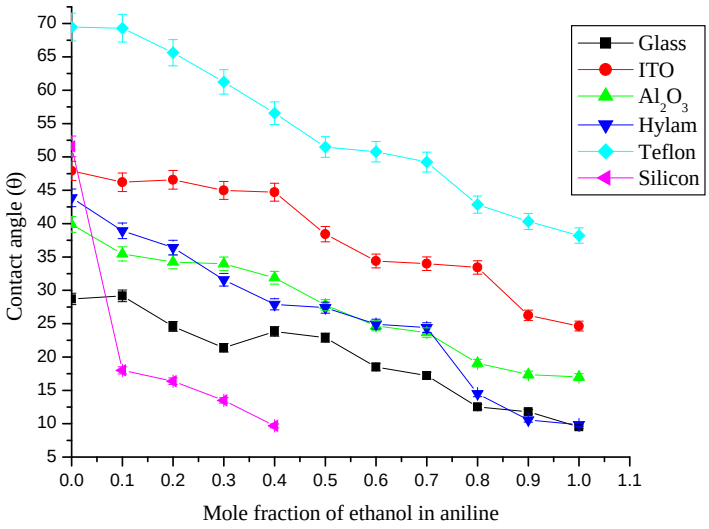

Figure 3.11: Variation of contact angle with mole fraction of ethanol in aniline over different substrates.

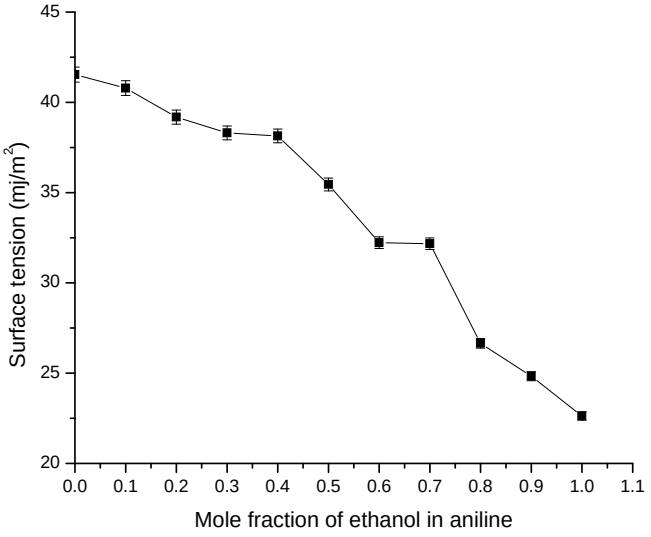

Figure 3.12: Variation of surface tension with mole fraction of ethanol in aniline.

Summary

Aniline and ethanol interact by means of hydrogen bonds of the kind N-H--O. The interaction between the two moieties over the entire concentration region of the binary liquid shows regions of distinct behavior. Ethanol forms a hydrogen-bonded network and the network is broken by the addition of polar aniline as observed from the dipole moment and FTIR data. On further addition of aniline to the ethanol solution, there is no further significant change. Aniline rich region of the binary liquid is characterized by the presence of non-hydrogen bonded associations between the moieties.

When such a binary liquid is taken as a sessile drop and its wetting characteristics observed over substrates of different surface characteristics, it is seen that the 10%-30% aniline concentration region shows maximum interaction between the moieties. Rapid

wetting is seen when the surface tension of the binary liquid is of the same magnitude as the surface energy of the substrates.

3.3.3 Binary mixture of Aniline - Isopropanol

Molecular interactions in the aniline-isopropanol binary system discussed previously are expected to be the same as seen in the previous systems discussed previously. Neutron diffraction of deuteriated-1-propanol is used to study the molecular conformation as well as intermolecular structural correlation (Sahoo *et al.,* 2008) where the nature of hydrogen bond and molecular association is suggested. Hydrogen bonded binary mixture of isopropanol and aniline for various mole fraction are analyzed previously at different temperature by dielectric permittivity studies at radio frequencies. The formation of hydrogen bond isverifiedthrough computational and supported by parallel studies of FTIR (Krishna *et al.,* 2010).In the binary mixture of propan-1-ol with alkyl benzoates studied using low frequency impedance analyser, the formation of hydrogen bond has been reported (Mohan *et al.,* 2011).

3.3.3.1 Computational Analysis

As with the previous cases, the three most stable conformers of aniline-isopropanol system taken up for further study are shown in fig.3.13. The structure shown in fig.3.13 (3) possesses the lowest energy both at lower and higher basis sets, which is taken as the most stable conformer.

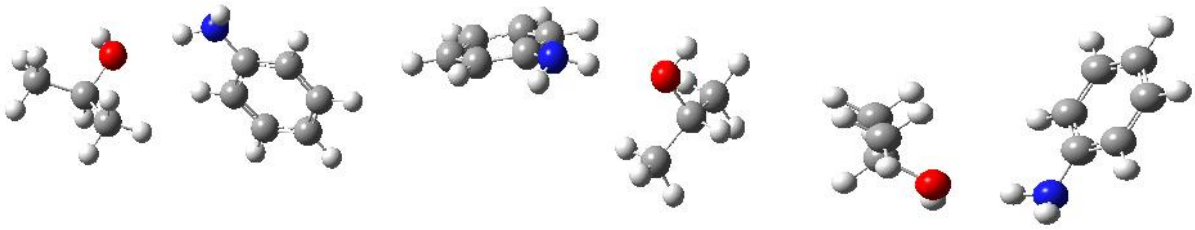

Structure (1) Structure (2) Structure (3)

Figure 3.13: Three conformations of the aniline-isopropanol 1:1 binary system.

The result of computational conformal analysis at different basis sets used to determined aniline-isopropanol interactions are presented in table 3.10.

Table 3.10:Computational modeling data of aniline-isopropanol 1:1 binary structure shown in fig. 3.13.HF energy (hartree) and dipole moment (debye).

Basis	Parameter	Aniline	Isopropanol	Structure 1	Structure 2	Structure 3
STO-3G	HF Energy	-282.206100704	-190.716353715	-472.936321060	-472.936382774	-472.936868744
	Dipole Moment	1.3267	1.4481	3.3552	3.2375	2.7424
6-31G	HF Energy	-285.633042967	-193.037562840	-478.680174673	-478.680198694	-478.680174707
	Dipole Moment	1.456	2.0902	4.1093	4.1147	4.1040
6-31G(d)	HF Energy	-285.728226746	-193.115416025	-478.853131053	-478.853139675	-478.853144184
	Dipole Moment	1.6087	1.8521	3.3618	3.4731	3.2740
6-31G(d,p)	HF Energy	-285.745539086	-193.128929944	-478.887520081	-478.887523061	-478.888523610
	Dipole Moment	1.6037	1.8326	3.3399	3.4595	3.3265

The hydrogen bond distance between oxygen of isopropanol and hydrogen attached to nitrogen of aniline are 1.80435 $\overset{o}{A}$ for structure 1, 1.80495 $\overset{o}{A}$ for structure 2 and 1.80495 $\overset{o}{A}$ for structure 3.

Solvation modeling data are presented in table 3.11. On solvation by aniline, the dipole moment ($\vec{\mu}$) of alcohols is more or less constant where as there is an increase in the $\vec{\mu}$ of aniline on solvation by alcohols as shown in table3.11.

Table 3.11: Solvation modeling data of aniline-isopropanol 1:1 binary structure shown in fig.3.13.HF energy (hartree) and dipole moment (debye).

Basis set	Parameter	Aniline rich region	Isopropanol rich region
STO-3G	HF Energy Dipole moment	-282.206438093 1.5194	-190.716499868 1.4885
6-31G	HF Energy Dipole moment	-285.631663645 1.6399	-193.032866015 2.5600
6-31G(d)	HF Energy Dipole moment	-285.726890392 1.7838	-193.1109444118 2.0823
6-31G(d,p)	HF Energy Dipole moment	-285.744070398 1.7936	-193.124277022 2.0757

The hydrogen bond energy of the binary 1:1 conformation for the three structures of the systems are given in table 3.12. It is seen from HB energy that the bond is of intermediate strength (~-6kcal/mol).

Table 3.12: Hydrogen bond energy of the three aniline-isopropanol 1:1 binary.

Basis set	Structure 1 (kcal/mol)	Structure 2 (kcal/mol)	Structure 3 (kcal/mol)
STO-3G	-8.7401820	-8.7401820	-9.0451330
6-31G	-6.0196325	-6.0196325	-6.0045804
6-31G(d)	-5.9594022	-5.9594022	-5.9622316
6-31G(d,p)	-8.1915349	-8.1915349	-8.8193894

3.3.3.2 Dielectric studies

Dipole moment of the 1:1 binary system is determined from fig.3.14.The experimental results shown in table 3.13 and fig.3.14 yield an experimental dipole moments of « =2.12D, while the corresponding value from the computation is about 3D

Table 3.13: Dielectric data of aniline-isopropanol 1:1 mixture in benzene solution

Concentration (mol/cc)	£$_{12}$	n_{12}^2	¢
0.000118	2.30	2.25	0.022268
0.000236	2.33	2.26	0.051523
0.000354	2.34	2.26	0.059271
0.000471	2.34	2.26	0.067707
0.000589	2.40	2.26	0.113242
0.000707	2.43	2.27	0.143237
0.000825	2.48	2.27	0.183668
0.000943	2.53	2.28	0.235419
0.001061	2.55	2.27	0.261861
0.001179	2.57	2.28	0.273434

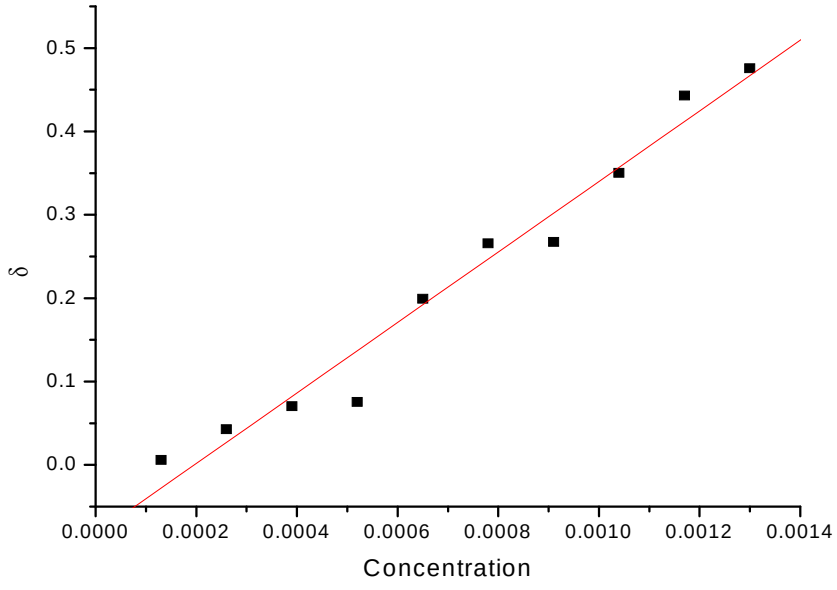

Figure 3.14: δ vs. concentration of the binary system used to determine the experimental dipole moment.

3.3.3.3 FTIR Studies

The IR spectrum of aniline-isopropanol over the entire concentration range is reported. A change on the O-H peak is observed at lower concentration of aniline approximately from 20% as shown in fig.3.15, which is also indicate by complete wetting in contact angle studies. The introduction of aniline inisopropanolrich region is seen to break the clusters of alcohol, leading to a red shift in the IR peak as seen from fig. 3.16.

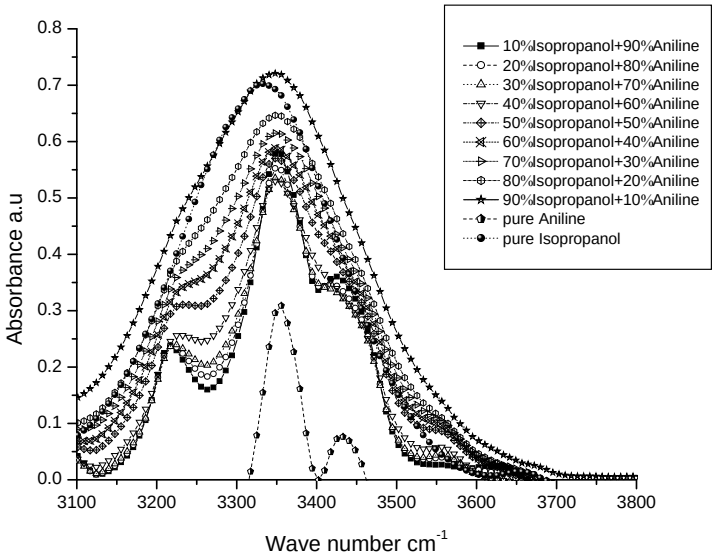

Figure 3.15: O-H stretching frequency of aniline-isopropanol mixture.

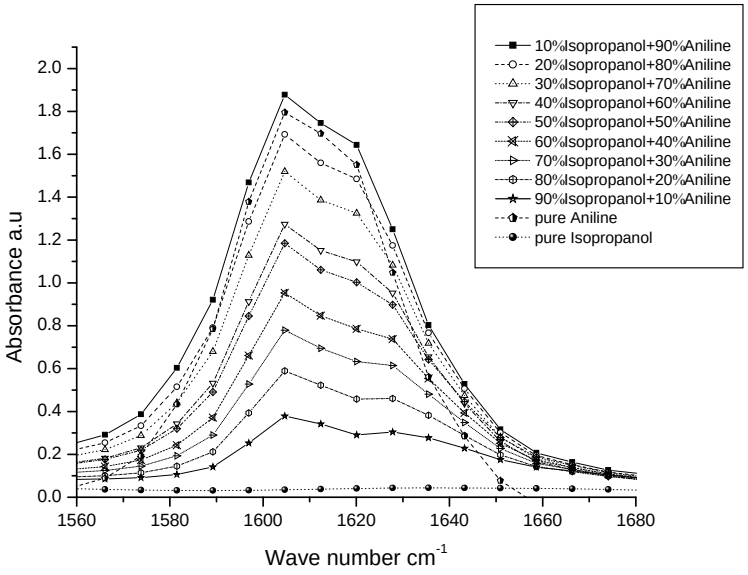

Figure 3.16: NH_2 Scissoring frequency of aniline-isopropanol mixture.

3.3.3.4 Wetting studies

The contact angle made by aniline-isopropanol binary system over the entire concentration region on the same substrates as before is measured and is reported in fig.3.17 along with surface tension in fig.3.18. As with the previous case a dramatic wetting is observed at about 20% aniline for these systems. Wetting of Al_2O_3 is similar to that in aniline-methanol. At higher concentrations of isopropanol complete wetting is observed.

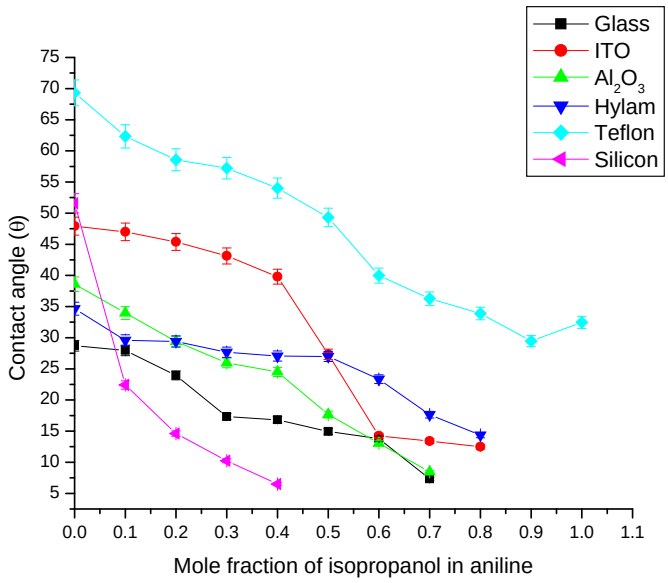

Figure 3.17: Variation of contact angle with mole fraction of isopropanol in aniline over different substrates.

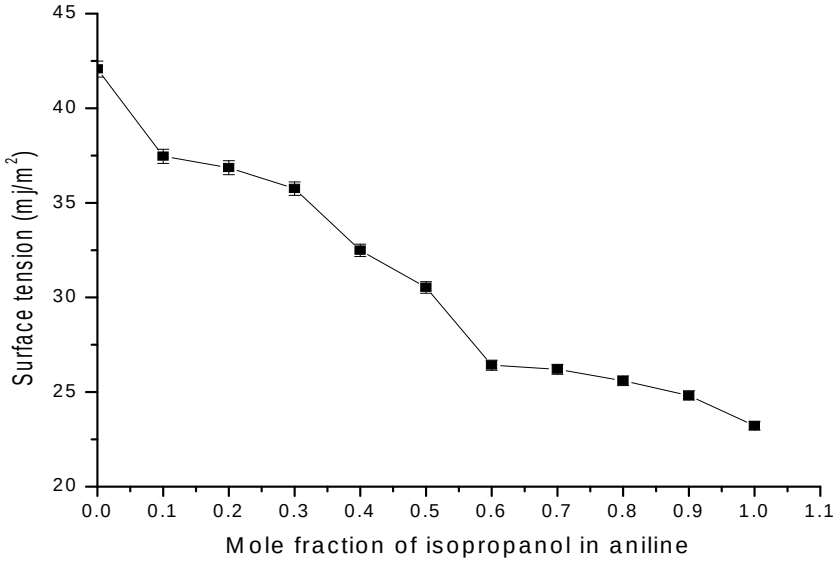

Figure 3.18: Variation of surface tension with mole fraction of isopropanol in aniline.

Summary

When the surface energy of the substrates has the same magnitudeas the surface tension of the test liquid, rapid wetting is observed. This is also seen in the case of wetting by aniline-isopropanol binary liquid at the 0.8 mole fraction of isopropanol in aniline. The wetting trend of this system follows the same trend of the previous systems discussed. Except for Teflon, which is hydrophobic, other substrates show complete wetting at higher concentration of alcohol. From our observation it appears that there is a destruction of alcohols cluster by aniline ~ 20%-50% aniline concentration. Rapid wetting is observed in our studies mainly for Al_2O_3 and ITO substrates.

3.3.4 Binary mixture of Aniline - Butanol

From the previous studied it is expected that aniline-butanol system will show molecular interaction of the kind N-H--O hydrogen bonding. The structure of tert-butanol alcohol has been reported previously (Kusalik *et al.*, 2000). Monte Carlo simulation studied of adsorption and ordering at the vapor-liquid interface of water/1-butanol solution at 298.15k shows the formation of hydrogen bond between water and 1-butanol (Chen *et al.*, 2002).From the ultrasonic velocity studies of binary mixture of aniline and butanol at 303k, the molar volume show a continuous increase in molecular interaction in toluene+n-butanol, reaching a maximum at 0.2 mole fraction and aniline + n-butanol system shows decreasing(Lakshmanan and Govindasamy, 2011).

3.3.4.1 Computational Analysis

The three most stable conformers of aniline-butanol systems are show in fig.3.19. Among the three conformers the structure 3 show in fig.3.19 (3) possesses the lowest energy for lower basis set and structure 2 show in fig.3.19 (2) possesses the lowest energy for higher basis set i.e. 6-31G(d,p).

Computational conformational analysis at different basis sets are used to determined aniline-butanol interactions. The results are presented in table 3.14.

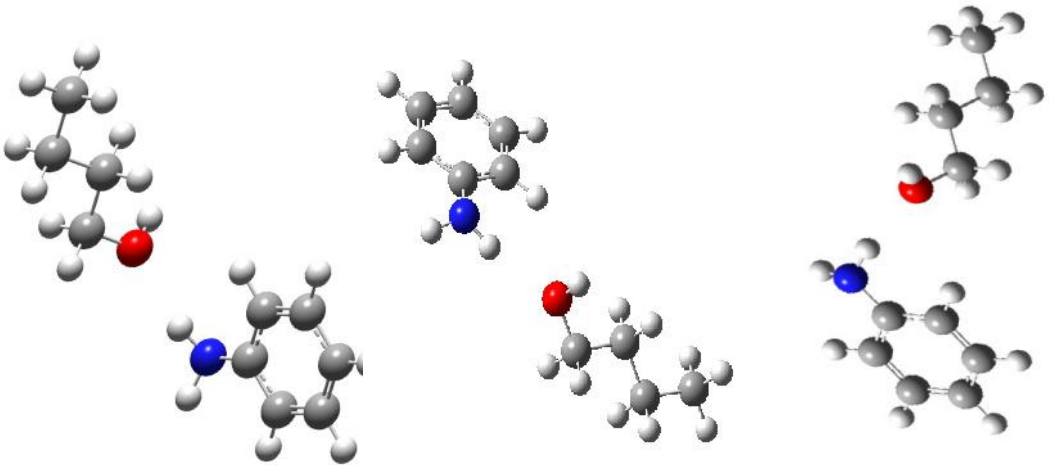

Structure (1). Structure (2). Structure (3).

Figure 3.19: Three conformations of the aniline-butanol1:1 binary.

Table 3.14: Computational modeling data of aniline-butanol 1:1 binary structure shown in fig. 3.19.HF energy (hartree) and dipole moment (debye).

Basis	Parameter	Aniline	Butanol	Structure 1	Structure 2	Structure 3
	HF Energy	-282.206100704	-229.293544703	-511.513429532	-511.513334843	-511.513827732
STO-3G	Dipole Moment	1.3267	1.5104	2.9575	2.7268	2.7751
	HF Energy	-285.633042967	-232.049943700	-517.692737193	-517.692737188	-517.692652292
6-31G	Dipole Moment	1.456	2.2904	4.1855	4.1749	4.3821
	HF Energy	-285.728226746	-232.145061178	-517.882661986	-517.882661987	-517.882661986
6-31G(d)	Dipole Moment	1.6087	1.6896	3.6036	3.6062	3.6036
	HF Energy	-285.745539086	-232.165547347	-517.919940633	-517.919940642	-517.919864694
6-31G(d,p)	Dipole Moment	1.6037	1.8260	3.5983	3.5995	4.1814

The hydrogen bond energy of the binary 1:1 conformation for the three structures of the system is given in table 3.16. It is seen from HB energy that the bond is of intermediate strength (~ -6kcal/mol).

Solvation modeling data are presented in table 3.22.

Table 3.15: Solvation modeling data of aniline-butanol1:1 binary structure shown in fig. 3.19.HF energy (hartree) and dipole moment (debye).

Basis	Parameter	Aniline rich region	Butanol rich region
STO-3G	HF Energy	-282.213157257	-229.293906593
	Dipole Moment	1.5278	1.5735
6-31G	HF Energy	-285.633563222	-232.050674299
	Dipole Moment	1.9156	2.4806
6-31G(d)	HF Energy	-285.731303520	-232.145472418
	Dipole Moment	1.6912	2.0090
6-31G(d,p)	HF Energy	-285.748029737	-232.165936485
	Dipole Moment	1.6538	1.9853

Table 3.16: Hydrogen bond energy of the three aniline -butanol conformer.

Basis set	Structure 1 (kcal/mol)	Structure 2 (kcal/mol)	Structure 3 (kcal/mol)
STO-3G	-8.6496762	-8.5902479	-8.8995507
6-31G	-6.1185525	-6.1185494	-6.0652763
6-31G(d)	-5.8823176	-5.8823182	-5.8355819
6-31G(d,p)	-5.5549381	-5.5561040	-5.5090778

The hydrogen bond energy between oxygen of butanol and hydrogen attached to nitrogen of aniline are 1.81027 $\overset{o}{A}$ for structure 1, 1.80199 $\overset{o}{A}$ for structure 2 and 1.79047 $\overset{o}{A}$ for structure 3.

3.3.4.2 Dielectric studies

Dipole moment of the 1:1 binary system is determined using the same procedure as discussed before. The data is given in table 3.17, the experimental results shown in figures 3.20 yield an experimental dipole moment of $\vec{\mu}$ =1.81D, while the corresponding value from the computation is about 3D.

Table 3.17: Dielectric data of aniline-butanol 1:1 mixture in benzene solution

Concentration (mol/cc)	ε_{12}	n_{12}^2	α
0.000094	2.33	2.26	0.046680
0.000188	2.35	2.26	0.068419
0.000282	2.37	2.26	0.092506
0.000376	2.43	2.26	0.152329
0.000469	2.45	2.26	0.170800
0.000563	2.46	2.25	0.191680
0.000657	2.47	2.26	0.196628
0.000751	2.48	2.26	0.207154
0.000845	2.55	2.26	0.267307
0.000939	2.56	2.26	0.280838

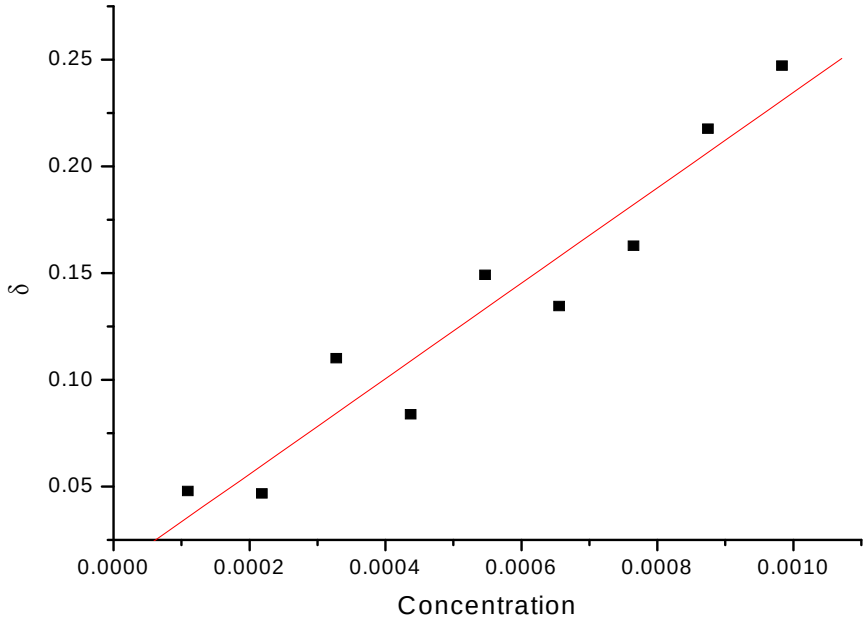

Figure 3.20: δ vs. concentration of the binary system used to determine the experimental dipole moment.

3.3.4.3 FTIR studies

The IR spectrum of aniline-butanol over the entire concentration range is reported. The O-H peak and NH_2scissoring frequency follow the same result of the previous system. The peak intensities have not been normalized since the shift in peak position is being observed. Shift in OH peak is observed at lower concentration of aniline approximately from 20% as shown in fig.3.21. The introduction of aniline in butanol rich region is seen to break the clusters of alcohol, leading to a red shift in the IR peak as seen from fig. 3.22.

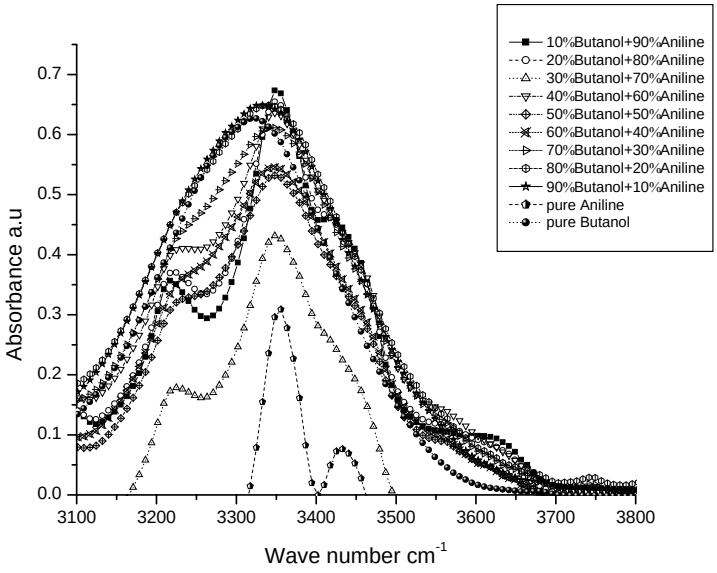

Figure 3.21: O-H stretching frequency of aniline-butanol mixture.

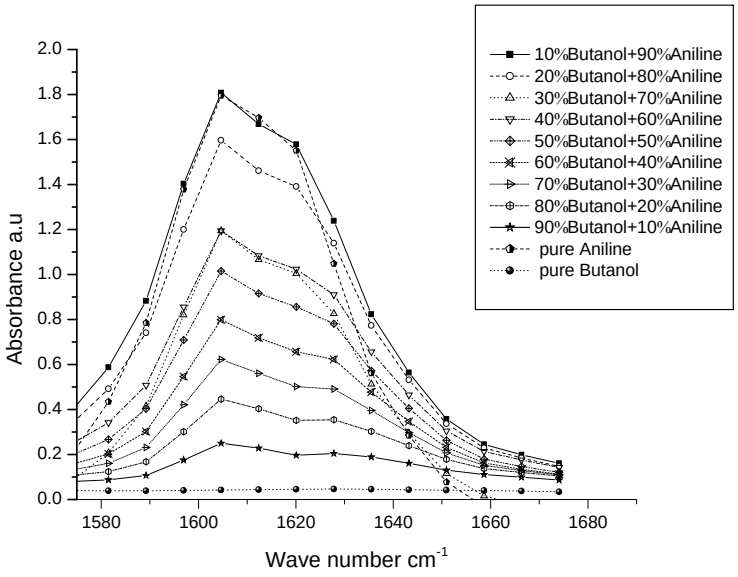

Figure 3.22: NH2 Scissoring frequency of aniline-butanol mixture.

3.3.4.4 Wetting studies

Wetting of substrates by aniline-butanol system is shown in fig.3.23 and surface tension in fig.3.24. The result follows the same trend of the previous studies.

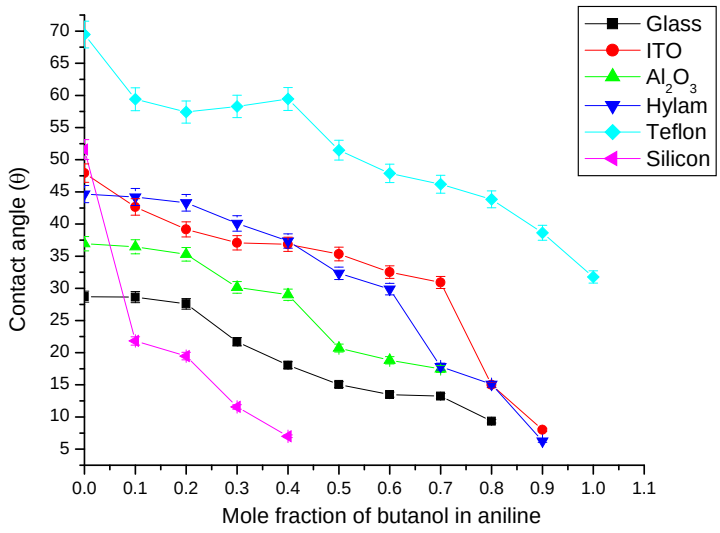

Figure 3.23: Variation of contact angle with mole fraction of butanol in aniline over different substrates.

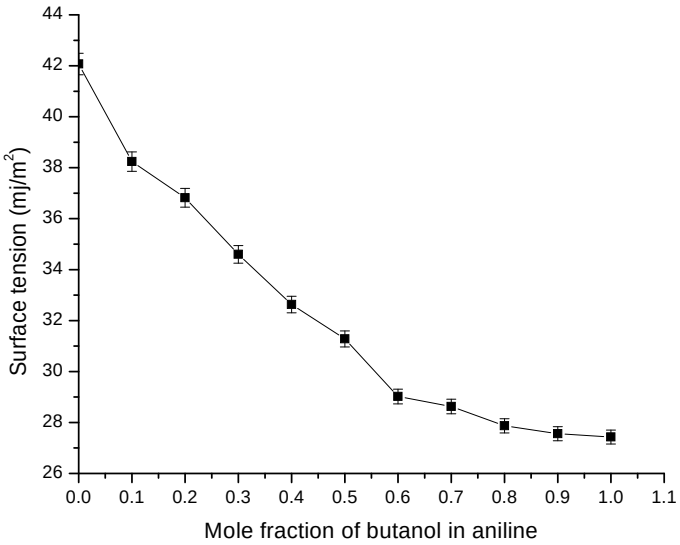

Figure 3.24: Variation of surface tension with mole fraction of butanol in aniline.

Summary

The studies on molecular interaction in aniline- butanol have been indicated. At around 10%-30% aniline concentrations (i.e alcohols rich region) the interaction between the binary liquid and substrates is maximum; the result so far has in well similarity with aniline-isopropanol system.

3.3.5 Binary mixture of Aniline - Hexanol

A few studied on aniline – hexanol binary mixture has been known so far, interaction of the type N-H--O hydrogen bond is expected as seen from the previous studies. The dielectric relaxation studies of N,Ndimethylformamide (DMF) and 1-heptanol binary mixture is reported by Ramachandran et al (Ramachandran *et al.*, 2007), the change in the relaxation is observed which indicate the existence of molecular interaction in this system.

3.3.5.1 Computational analysis

The three conformers of aniline-hexanol system are shown in fig. 3.25, among them structure 1 shown in fig.3.25(1) is taken as the most stable conformer.

Computation analysis of aniline-hexanol at different basis sets are presented in table 3.18.

The hydrogen bond energy of the binary 1:1 conformation for the three structures of the system are given in table 3.20. It is seen from HB energy that the bond is of intermediate strength (~-6kcal/mol).The hydrogen bond energy between oxygen of hexanol and hydrogen attached to nitrogen of aniline are 1.78891 $\overset{o}{A}$ for structure 1, 1.78886 $\overset{o}{A}$ for structure 2 and 1.79474 $\overset{o}{A}$ for structure 3.

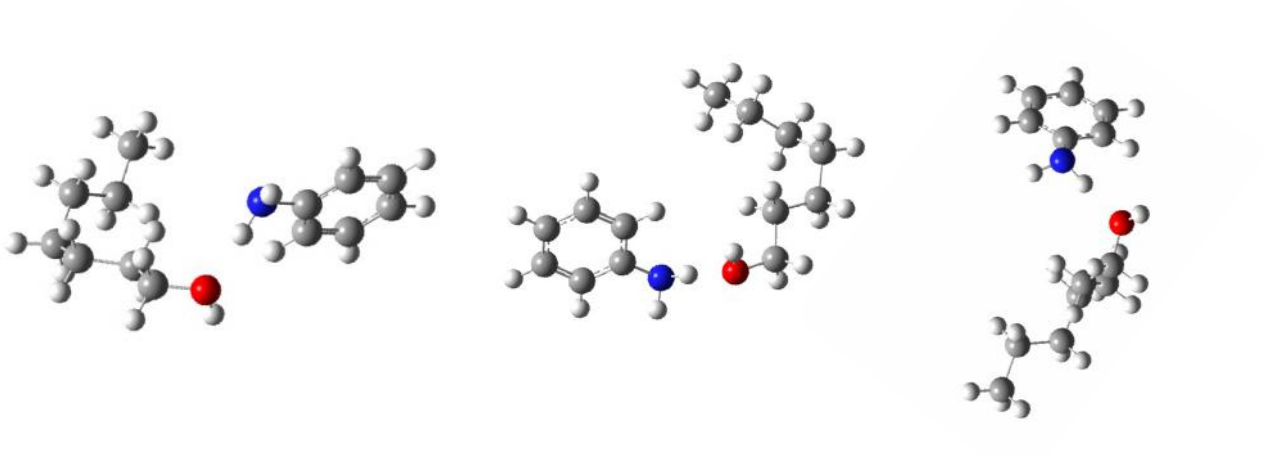

Structure (1) Structure (2) Structure (3)

Figure 3.25: Three conformations of the aniline-hexanol 1:1 binary.

Table 3.18:Computational modeling data of aniline-hexanol1:1 binary structure shown in fig. 3.25.HF energy (hartree) and dipole moment (debye).

Basis	Parameter	Aniline	Hexanol	Structure 1	Structure 2	Structure 3
	HF Energy	-282.206100704	-345.028454931	-627.248767513	-627.248767473	-627.248021911
STO-3G	Dipole Moment	1.3267	1.5178	2.7405	2.7412	6.4437
	HF Energy	-285.633042967	-349.099466546	634.742382956	-634.742181349	-634.740766218
6-31G	Dipole Moment	1.4560	2.2904	3.5593	4.4722	3.7562
	HF Energy	-285.728226746	-349.243153788	-634.980913520	-634.980711913	-634.982334074
6-31G(d)	Dipole Moment	1.6087	1.8703	3.2360	5.6580	3.0955
	HF Energy	-285.745539086	-349.272735062	-635.027353601	-635.027151994	-635.028220018
6-31G(d,p)	Dipole Moment	1.6037	1.8439	3.2376	5.4071	2.9670

Solvation modeling data are presented in table 3.19.

Table 3.19: Solvation modeling data of aniline-hexanol1:1 binary structure shown in fig. 3.25.HF energy (hartree) and dipole moment (debye).

Basis set	Parameter	Aniline rich region	Hexanolrich region
STO-3G	HF Energy Dipole moment	-282.213001238 1.5106	-345.028838569 1.7004
6-31G	HF Energy Dipole moment	-285.633381187 1.8778	-349.100257137 2.8740
6-31G(d)	HF Energy Dipole moment	-285.731160508 1.6534	-349.243604673 2.3482
6-31G(d,p)	HF Energy Dipole moment	-285.747904283 1.6191	-349.273158592 2.3182

Table 3.20: Hydrogen bond energy of the three aniline-hexanolconformer.

Basis set	Structure 1	Structure 2	Structure 3
STO-3G	8.918096	8.918070	8.450223
6-31G	6.195684	6.069174	5.181165
6-31G(d)	5.982044	5.855533	6.873456
6-31G(d,p)	5.697448	5.570937	6.241133

3.3.5.2 Dielectric studies

Dipole moment of the 1:1 binary system is determined from fig.3.26 and table 3.21.The experimental results shown in fig.3.26 yield an experimental dipole moments of « $\vec{}$ =1.58D, while the corresponding value from the computation is about 3D.

Table 3.21: Dielectric data of aniline-hexanol1:1 mixture in benzene solution

Concentration (mol/cc)	$£_{12}$	n_{12}^2	¢
0.000094	2.33	2.26	0.046680
0.000188	2.35	2.26	0.068419
0.000282	2.37	2.26	0.092506
0.000376	2.43	2.26	0.152329
0.000469	2.45	2.26	0.170800
0.000563	2.46	2.25	0.191680
0.000657	2.47	2.26	0.196628
0.000751	2.48	2.26	0.207154
0.000845	2.55	2.26	0.267307
0.000939	2.56	2.26	0.280838

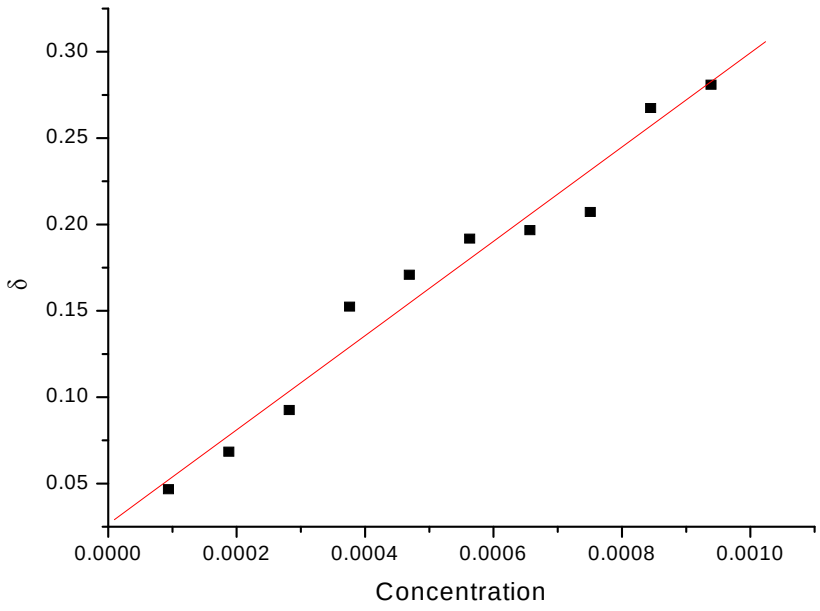

Figure 3.26: δ vs. concentration of the binary system used to determine the experimental dipole moment.

3.3.5.3 FTIR studies

The IR spectrum of aniline-hexanol over the entire concentration is reported. Blue shifting O-H peak is observed from ~ 20% aniline concentration as shown in fig. 3.27. Red shift in NH_2 scissoring is observed as indicated in fig.3.28.

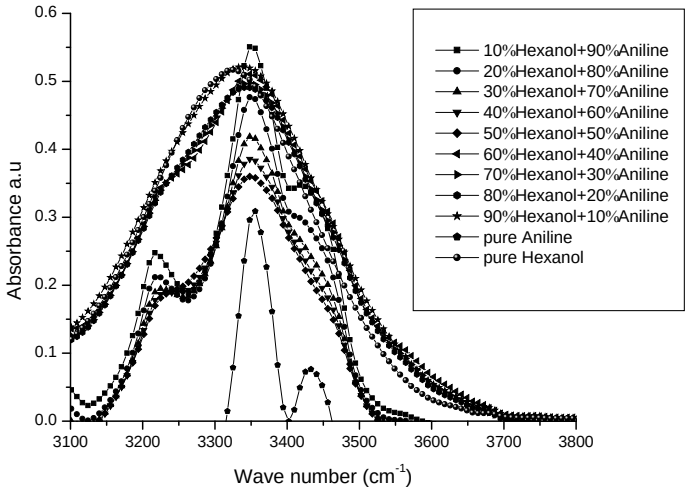

Figure 3.27: O-H stretching frequency of aniline-hexanol mixture.

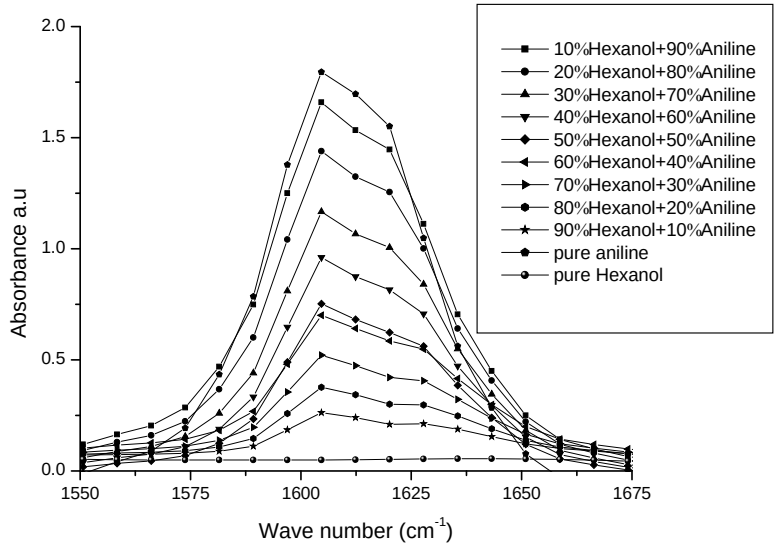

Figure 3.28: NH_2 Scissoring frequency of aniline-hexanol mixture.

3.3.5.4 Wetting studies

Wetting of substrates by aniline-hexanol system is shown in fig.3.29 and its surface tension in fig 3.30.

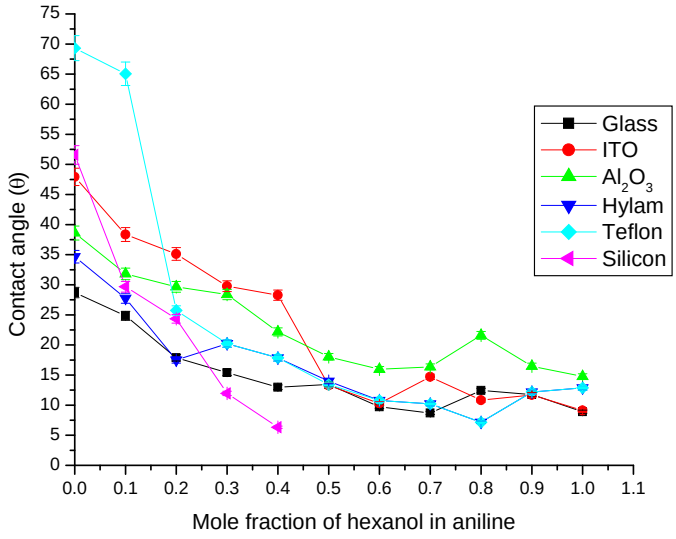

Figure 3.29: Variation of contact angle with mole fraction of hexanol in aniline over different substrates.

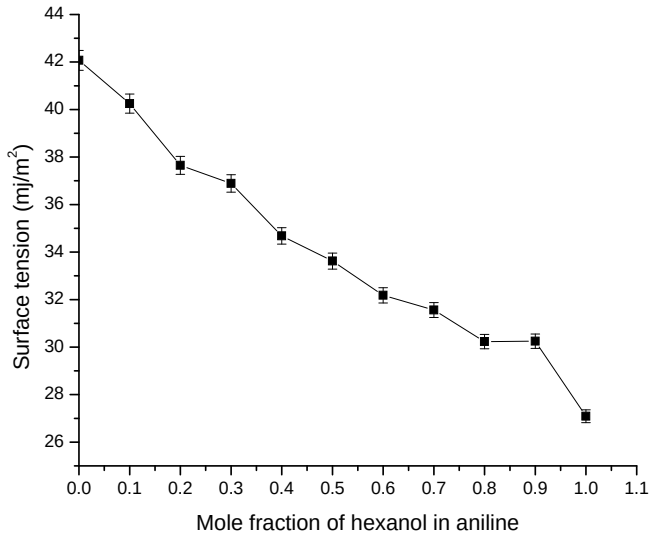

Figure 3.30: Variation of surface tension with mole fraction of hexanol in aniline

Summary

The studies of aniline-hexanol binary system is presented, where molecularinteraction between the two moieties appears at approximately 20% aniline concentration (hexanol rich region) which is indicated by rapid wetting in contact angle studied followed by FTIR spectroscopy analysis. Secondary weak interaction is expected by the IR spectra of this binary at different concentration does not show the effect of it (Patil *et al.,* 1999).

3.3.6 Binary mixture of Aniline - Octanol

From the studies of infrared spectroscopy, the structure of 1-octanol has been reported previously (Paolantoni *et al.,* 2005; Sassi *et al.,* 2002). Molecular dynamics and free-energy perturbation studies shows structure, dynamics, and solvation in 1-octanol and its water-saturated solution (De Bolt *et al.,* 1995).Interaction of N,Ndimethylformamide (DMF) and 1-Octanolbinary mixture is observed in the changing of dielectric relaxation using time domain reflectometry (Ramachandran *et al.,* 2007).

3.3.6.1 Computational Analysis

The three most stable conformers of aniline-octanol systems are shown in fig.3.31. Among the three conformers, structure 2shown in fig.3.31 (2) possesses the lowest energy for lower basis set and structure 2 shown in fig.3.31 (2) possesses the lowest energy for higher basis set.

Computational conformal analysis at different basis sets are used to determine aniline-octanol interactions. The results are presented in table 3.22.

The hydrogen bond energy of the binary 1:1 conformation for the three structures of the system are given in table 3.24. It is seen from HB energy that the bond is of intermediate strength (~ -6kcal/mol).

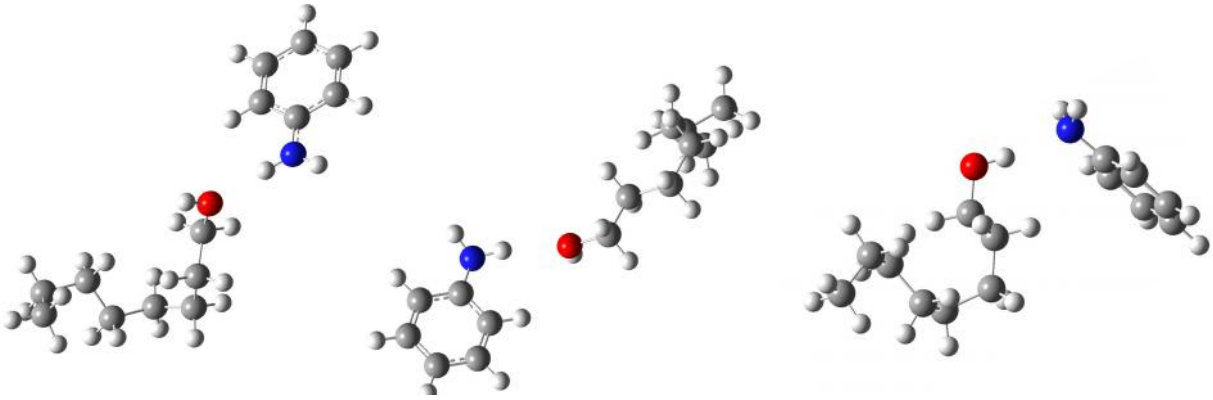

Structure (1). Structure (2). Structure (3).

Figure 3.31: Three conformations of the aniline-octanol1:1 binary.

Table 3.22: Computational modeling data of aniline-octanol1:1 binary structure shown in fig.3.31 HF energy (hartree) and dipole moment (debye).

Basis	Parameter	Aniline	Octanol	Structure 1	Structure 2	Structure 3
	HF Energy	-282.206100704	-383.605075453	-665.825412522	-665.827210698	-665.825747084
STO-3G	Dipole Moment	1.3267	1.4209	3.4255	3.2306	3.0567
	HF Energy	-285.633042967	-388.115036549	-673.757206404	-673.758905235	-673.754870038
6-31G	Dipole Moment	1.4560	2.0199	4.5888	4.5101	2.5333
	HF Energy	-285.728226746	-388.274454112	-673.753961534	-674.013606111	-674.013364499
6-31G(d)	Dipole Moment	1.6087	1.6896	4.5888	3.6432	2.8650
	HF Energy	-285.745539086	-388.307067725	-674.061310173	-674.063011627	-674.062413322
6-31G(d,p)	Dipole Moment	1.6037	1.6525	3.5012	3.7308	2.7647

Solvation modeling data are presented in table 3.23.

Table 3.23: Solvation modeling data of aniline-octanol1:1 binary binary structure shown in fig.3.31 HF energy (hartree) and dipole moment (debye).

Basis set	Parameter	Aniline rich region	Octanol rich region
STO-3G	HF Energy Dipole moment	-282.206438093 1.5194	-383.605231606 1.4813
6-31G	HF Energy Dipole moment	-285.631663645 1.6399	-388.110040174 2.3897
6-31G(d)	HF Energy Dipole moment	-285.726890392 1.7838	-388.270082496 2.0098
6-31G(d,p)	HF Energy Dipole moment	-285.744070398 1.7936	-388.302211803 1.9835

The hydrogen bond distance between oxygen of octanol and hydrogen attached to nitrogen of anilne are1.79314 $\overset{o}{A}$ for structure 1, 1.79866 $\overset{o}{A}$ for structure 2 and 1.93941 $\overset{o}{A}$ for structure 3.

Table 3.24: Hydrogen bond energy (kcal/mol)of the three aniline - Octanol conformer.

Basis set	Structure 1 (kcal/mol)	Structure 2 (kcal/mol)	Structure 3 (kcal/mol)
STO-3G	-10.061834	-9.143402	-9.143402
6-31G	-6.793246	-4.261120	-4.261120
6-31G(d)	-6.855705	-6.704091	-6.704091
6-31G(d,p)	-6.529126	-6.153683	-6.153683

3.3.6.2 Dielectric studies

Dipole moment of the 1:1 binary system is determined from fig. 3.32 and table 3.25.The experimental results shown in fig.3.32, yield an experimental dipole moment of « =1.27D, while the corresponding value from the computation is about 3D.

Table 3.25:Dielectric data of aniline-octanol 1:1 mixture in benzene solution

Concentration (mol/cc)	£$_{12}$	n_{12}^2	¢
0.000083	2.25	2.25	0.008716
0.000166	2.25	2.25	0.035919
0.000248	2.25	2.25	0.046123
0.000331	2.25	2.25	0.059328
0.000414	2.24	2.24	0.084507
0.000497	2.24	2.24	0.104915
0.000580	2.24	2.24	0.115120
0.000663	2.24	2.24	0.125324
0.000745	2.24	2.24	0.171189
0.000828	2.23	2.23	0.192524

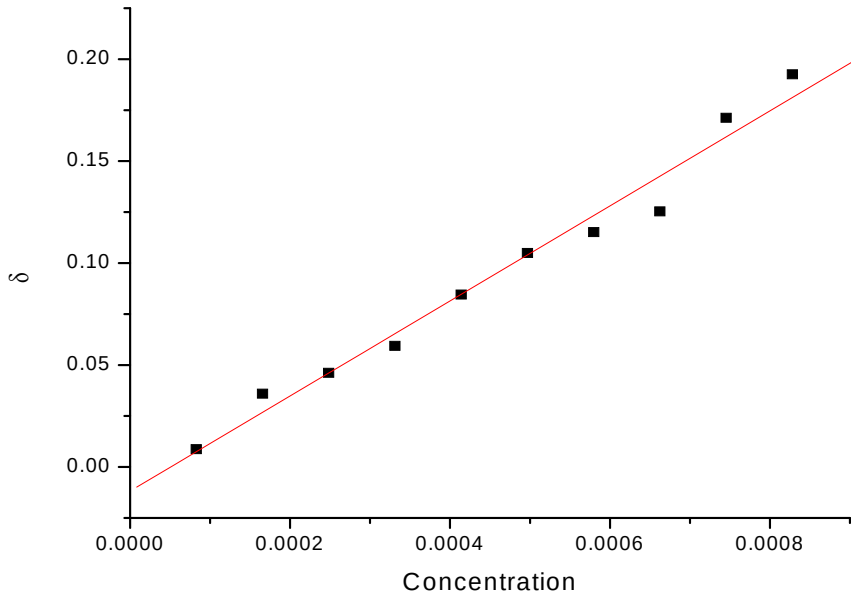

Figure 3.32: δ vs. concentration of the binary system used to determine the experimental dipole moment.

3.3.6.3 FTIR studies

The IR spectrum of aniline-octanol over the entire concentration is reported. The O-H and NH_2 scissoring frequency of aniline-hexanol binary system as shown in fig.3.33 and fig.3.34.

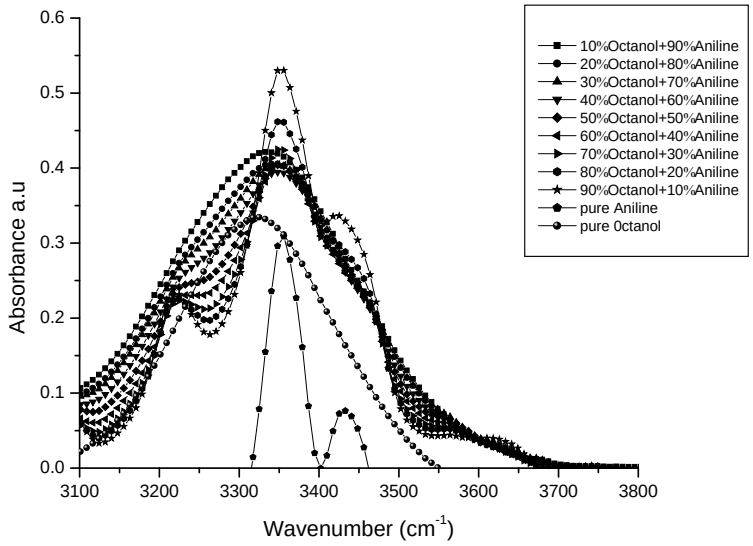

Figure3.33: O-H stretching frequency of aniline-octanol mixture

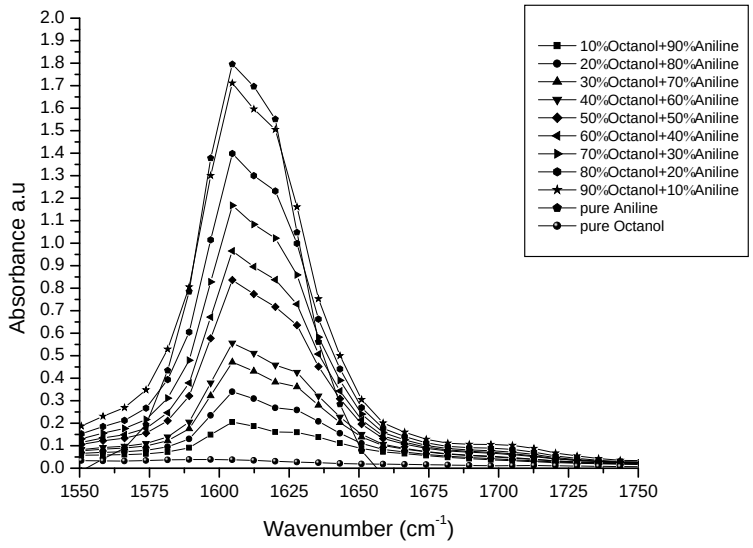

Figure 3.34: NH_2 Scissoring frequency of aniline-octanol mixture.

3.3.6.4 Wetting studies

Wetting of substrates by aniline-octanol system is shown in fig.3.35 and the corresponding surface tension in fig.3.36.

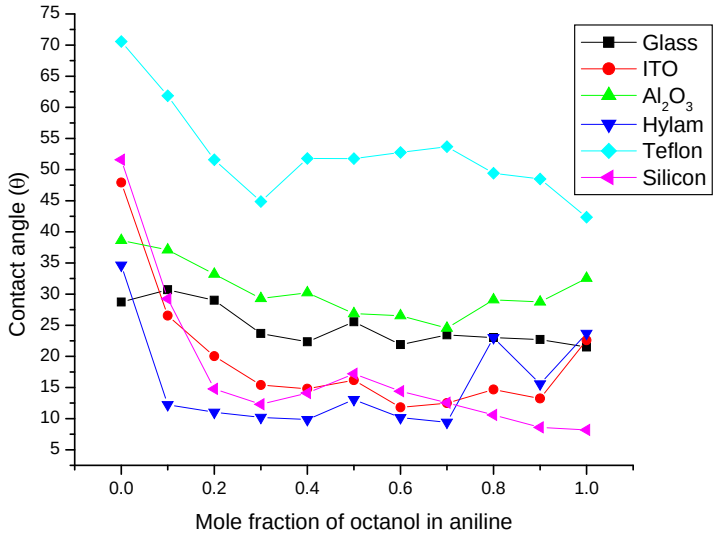

Figure 3.35: Variation of contact angle with mole fraction of octanol in aniline over different substrates

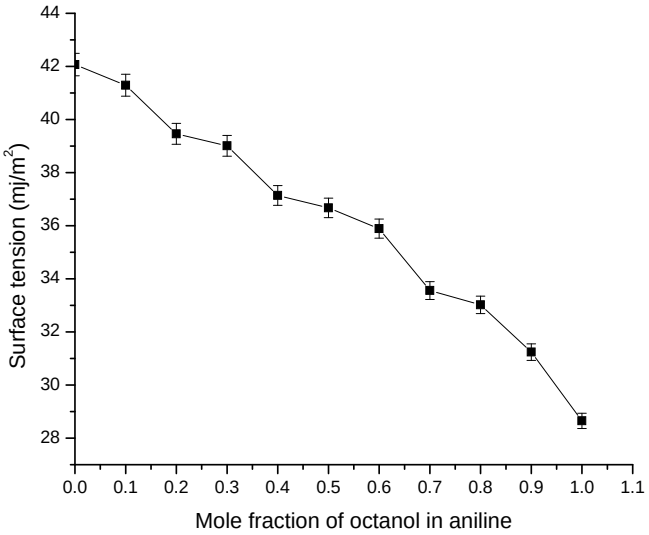

Figure 3.36: Variation of surface tension with mole fraction of octanol in aniline

Summary

Binary system of aniline-octanol studies is discussed. It is seen that the behaviour of the molecular interactions follows the same trend as that of the aniline-hexanol binary system.By comparing the contact angle of all alcohols used for the present studies i.e. from lower alcohol methanol to higher alcohol octanol, the homologous chain length effect is observed and discusses detail in chapter 5.

3.4 Binary mixture of Acetone-Alcohols

The interaction between acetone and alcohols is through the C=O--H hydrogen bonds, which is expected to be a linear bond however the presence of a second weak C-H--O hydrogen bond has also been reported. This bond is seen to cause the formation of a ring like conformation in acetone- methanol system (Sathyan *et al.,* 1995). Interaction between ketones and alcohols from photochemical studies has been reported previously (Weizmann *et al.,* 1938). The formation of C=O···H-O hydrogen bond in $H_2CO\cdots H_2O$ and $H_2CO\cdots 2H_2O$ was determined through Ab initio calculations (Morokuma *et al.,* 1971). The hydrogen bond interaction between acetone and water is investigated at the ab initio MBPT/CC level using different approximations and basis sets (Countinho *et al.,* 1999). The study of acetone – alcohol system is of interest for this reason. The C=O--H weak hydrogen bond is useful as a prototype for the C=O--H bond seen in many biological systems such as protein – protein interface (Jiang *et al.,* 2002), in amino acid residues (Scheiner *et al.,* 2001), engineered protein cavity (Musah and Goodin,1997). The existence of C-H--O bond in creatine has been reported by Popelier and Bader (Popelier and Bader, 1992). The aim for this part of the work is to understand the effect of increasing chain length of alcohol on the various properties, especially the wetting properties. The alcohols taken up for the study are the same as those in the aniline-alcohol systems discussed in previous pages. Certain physico-chemical properties of acetone-alcohol binary liquids have been reported in this study.

3.4.1 Binary mixture of Acetone-Methanol

Hydrogen bond formation in acetone-methanol binary mixtures has been investigated previously through infrared matrix isolation in solid argon, red shift in both C=O stretching mode of acetone as well as O-H stretching mode of methanol suggest that the two molecules are bound through the hydrogen bond between the carbonyl oxygen and the hydroxyl hydrogen atoms (Han and Kim, 1996). Blue shifting C-H--O hydrogen bond formation is observed through argon matrix-isolation infrared spectra of 1-methoxy-2-(dimethylamino) ethane (Matsuura *et al.,* 2003). The dielectric relaxation of methanol-ketone systems is seen to be influenced by the conformation of the molecules and steric hindrance, the number of carbon atom in the homologous series has no role on the dielectric relaxation time (Madhurima *et al.,* 2006).

3.4.1.1 Computational analysis

The salient feature of the conformation of acetone-methanol systems is the likelihood of formation of a ring-like structure due to the presence of a second weak hydrogen bond between methyl hydrogen and alcohol oxygen. Although detailed studies on the acetone-methanol conformation are available in literature, the system is studied again for two reasons. Firstly previous, studies were performed at STO-3G and 6-31G level and now 6-31G (d) and 6-31G (d,p) are included. Secondly the influence of homologous series of alcohols on the molecular interaction with acetone is being studied. Starting from the monomers described previously, many conformations of acetone-methanol binary system are studied. Three conformers with the lowest energies are taken for further analysis and are shown in fig. 3.37 (1), (2) and (3). The computational results are presented in table 3.26.

Data of the solvation model studies, as discussed in chapter 2, are presented in table 3.27 and the hydrogen bond energies for the three conformers are given in table 3.28.

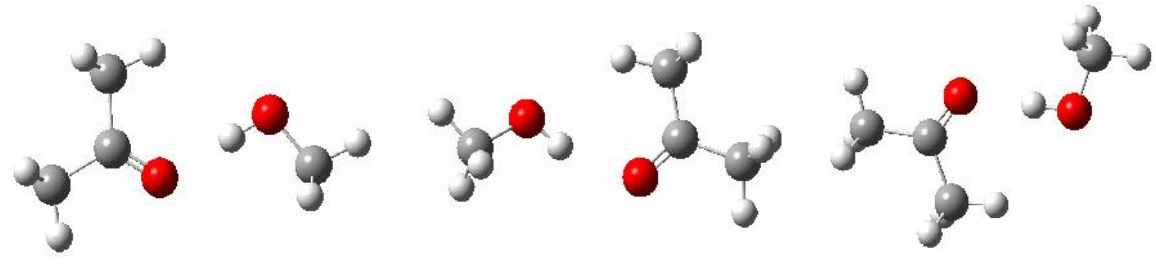

Structure (1). Structure (2). Structure (3).

Figure 3.37: Three conformations of the acetone-methanol 1:1 binary.

Table 3.26: Computational modeling data of acetone-methanol 1:1 binary structure shown in fig. 3.37.HF energy (hartree) and dipole moment (debye).

Basis	Parameter	Acetone	Methanol	Structure 1	Structure 2	Structure 3
STO-3G	HF Energy	-189.536032779	-113.549193204	-303.092430458	-303.092430490	-303.092430488
	Dipole Moment	1.9186	1.5094	3.0324	3.0280	3.0288
6-31G	HF Energy	-191.875161568	-114.988165278	-306.875492977	-306.875492954	-306.875511557
	Dipole Moment	3.6072	2.2875	2.989	2.9894	3.3626
6-31G(d)	HF Energy	-191.962236330	-115.035418040	-307.007599288	-307.007599275	-307.007599281
	Dipole Moment	3.1188	1.8656	3.6832	3.6828	3.6830
6-31G(d,p)	HF Energy	-191.972071644	-115.046709859	-307.028709769	-307.028366338	-307.028709772
	Dipole Moment	3.1406	1.8405	3.6444	3.0315	3.6449

The dipole moment in the acetone rich region is larger than that of pure acetone and in the methanol rich region the value is close to that of methanol. The dipole moment in the acetone rich region is close to the computational value for the conformer in fig.3.37 (c) and it corresponds to a structure where the oxygen of O-H group is available for interaction with

the surface. These observations are discussed below in comparison with IR and contact angle data.

Table 3.27: Solvation modeling data of the three acetone-methanol 1:1 binary structure shown in fig. 3.37.HF energy (hartree) and dipole moment (debye).

Basis	Parameter	Acetone rich region	Methanol rich region
	HF Energy	-189.525402000	-113.549794307
STO-3G	Dipole Moment	2.1370	1.5478
	HF Energy	-191.874118894	-114.989428342
6-31G	Dipole Moment	4.5990	2.3995
	HF Energy	-191.954720255	-115.036191631
6-31G(d)	Dipole Moment	3.7890	1.9519
	HF Energy	-191.964876785	-115.047402686
6-31G(d,p)	Dipole Moment	3.8566	1.9128

Table 3.28: Hydrogen bond energies of the three acetone-methanol 1:1 binary.

Basis set	Structure1 (kcal/mol)	Structure2 (kcal/mol)	Structure3 (kcal/mol)
STO-3G	-4.520869	-4.520890	-4.520888
6-31G	-7.634335	-7.634321	-7.645994
6-31G(d)	-6.240579	-6.240571	-6.240575
6-31G(d,p)	-6.244207	-6.028701	-6.244209

The hydrogen bond energies at various basis sets are shown in table 3.28. The hydrogen bond energy are approximately-5kcal/mol. Hydrogen bond distance between oxygen of C=O acetone and hydrogen of O-H of methanol are 1.80329 $\mathring{A}$ for structure 1, 1.80325 $\mathring{A}$ for structure 2 and 1.80327 $\mathring{A}$ for structure 3. Second weak hydrogen bond between oxygen of O-H and hydrogen attached to side chain of acetone are 2.92922 $\mathring{A}$, for structure 1, 2.92604 $\mathring{A}$ for structure 2 and 2.63238 $\mathring{A}$ for structure 3.

3.4.1.2 Dielectric studies

Dipole moment of the 1:1 binary liquid is determined using Guggenheim's method as discuss in chapter 2. The result is presented in table 3.29 and fig. 3.38.

Table 3.29: Dielectric data of acetone-methanol 1:1 mixture in benzene solution

Concentration (mol/cc)	£$_{12}$	n_{12}^2	¢
0.000176	2.23	2.24	-0.028008
0.000352	2.32	2.23	0.073952
0.000527	2.39	2.24	0.137976
0.000703	2.52	2.24	0.258997
0.000879	2.64	2.24	0.381992
0.001055	2.71	2.23	0.466937
0.001231	2.86	2.22	0.619920
0.001406	3.03	2.22	0.795880
0.001582	3.21	2.21	0.981832
0.001758	3.36	2.21	1.128857

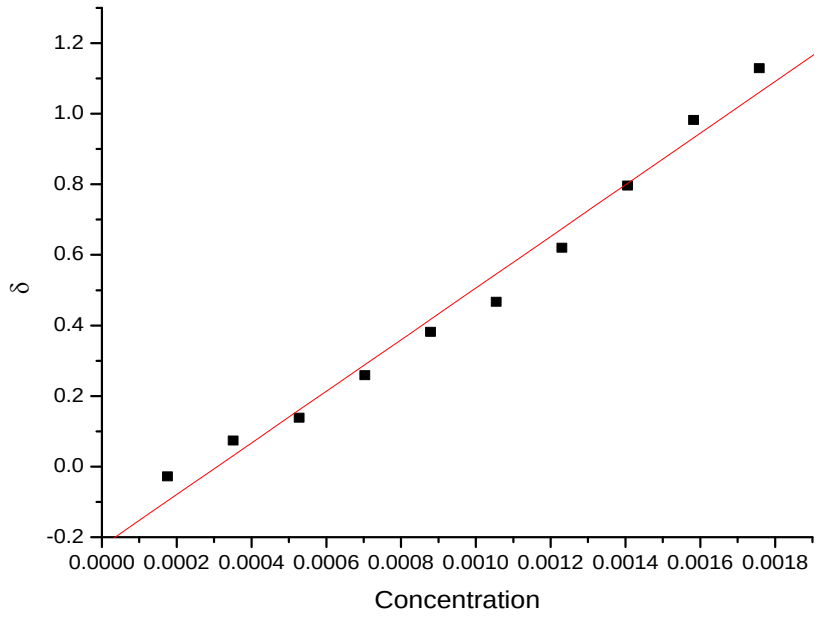

Figure 3.38: δ vs. concentration of the binary system used to determine the experimental dipole moment.

The experimentally determined dipole moment « = 2.83D compare well with the simulation result of 1:1 conformer in table 3.26.

3.4.1.3 FTIR studies

The FTIR spectra of acetone-methanol over the entire concentration range is reported. the O-H peak in figure 3.39 shows a red shift , C=O in figure 3.40 and C-H stretching in figure 3.41 shows a blue shifting hydrogen bond.

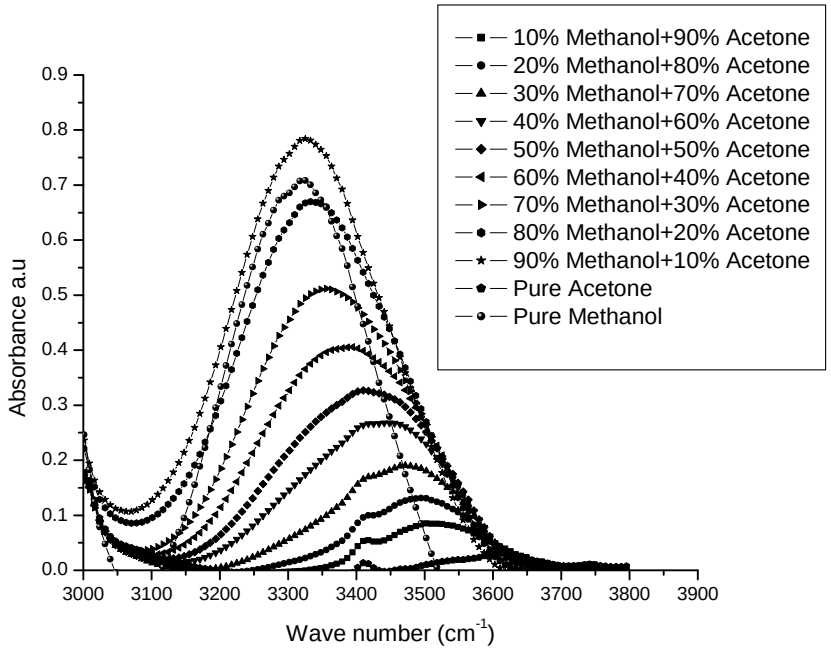

Figure 3.39: O-H stretching frequency of acetone-methanol mixture.

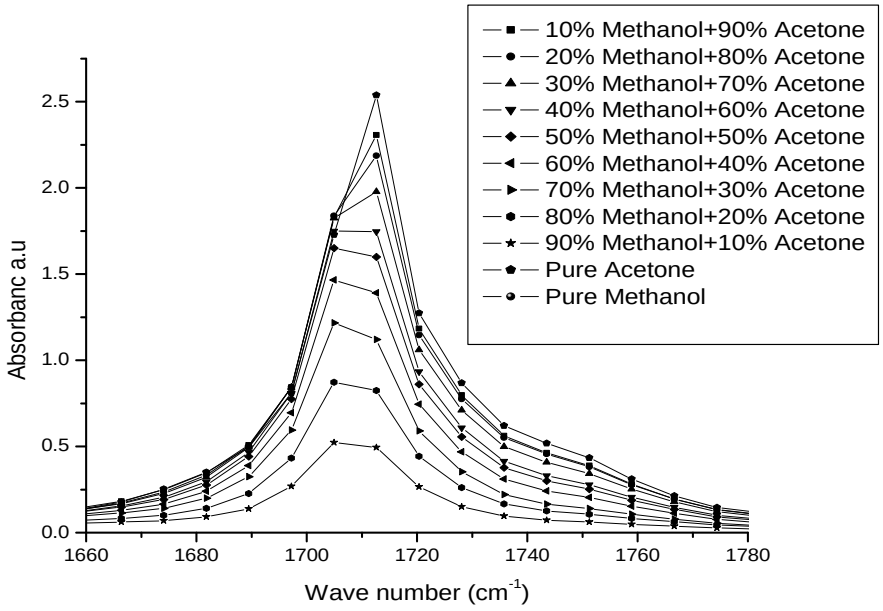

Figure 3.40: C=O stretching frequency of acetone-methanol mixture.

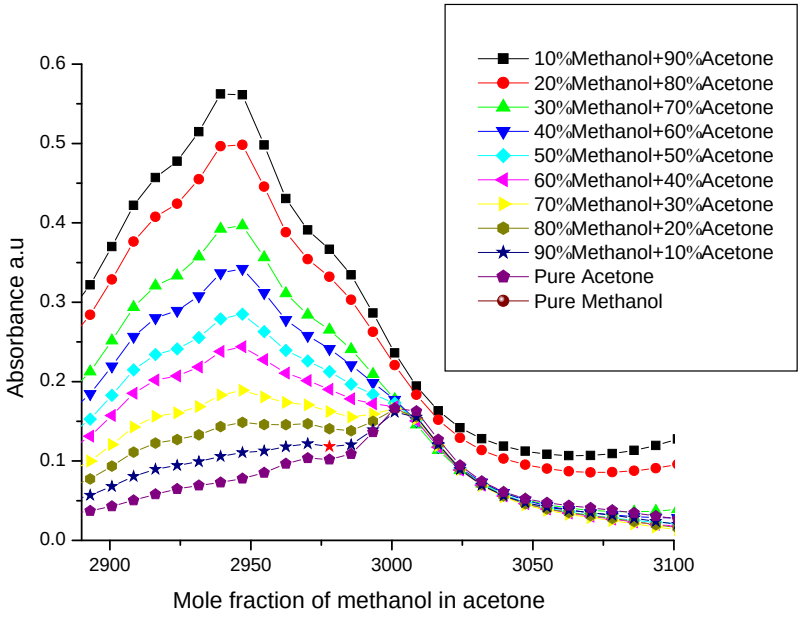

Figure 3.41: C-H stretching frequency of acetone-methanol binary mixture.

3.4.1.4 Wetting studies

As shown in fig. 3.42 the variation of contact angle of the binary at 0.2 mole fraction of methanol (acetone rich region) is less than that at 0.8 mole fraction of methanol, unlike the result of the solvation study. Clearly the over simplification of the solvation model of treating methanol as a continuous dielectric medium in which an acetone molecules is placed is inadequate to describe the specific molecular interactions between the two species, especially in the extensively hydrogen bonded methanol rich region. By comparing the results of surface tension from fig. 3.43 and contact angle measurement, it is clear that the two of the three regions of interaction between acetone-methanol binary liquid and the surfaces, namely at 0.2 and 0.8 mole fraction of methanol are due to conformal changes in the binary liquid. The change at 0.5 mole fraction of methanol is related directly to a change in surface tension of the liquid.

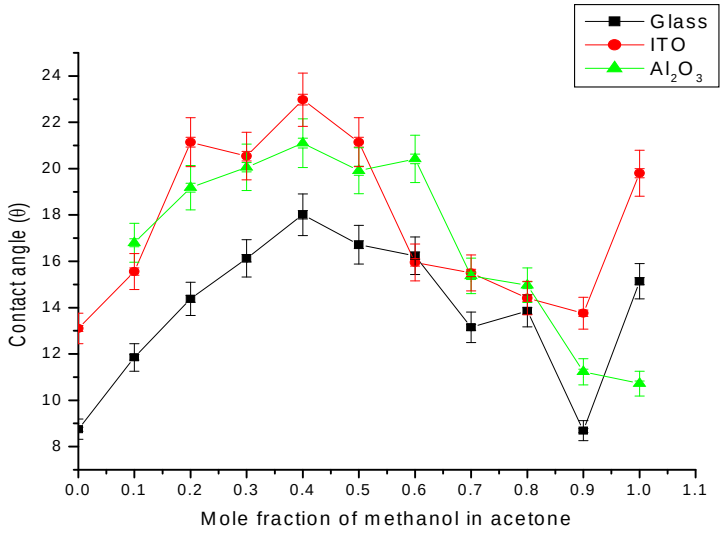

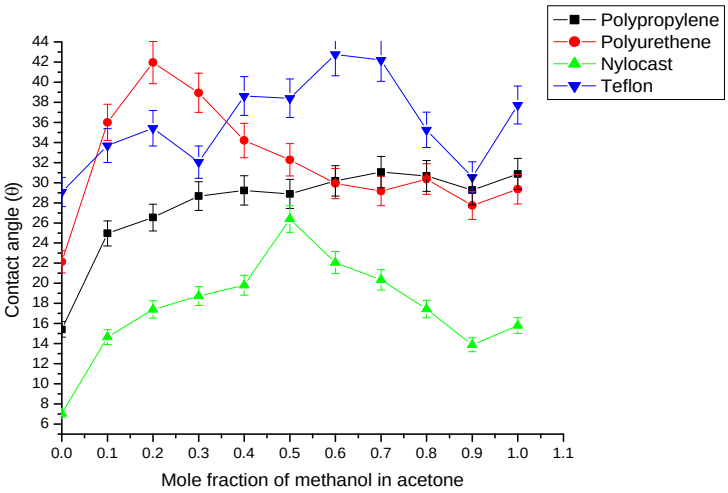

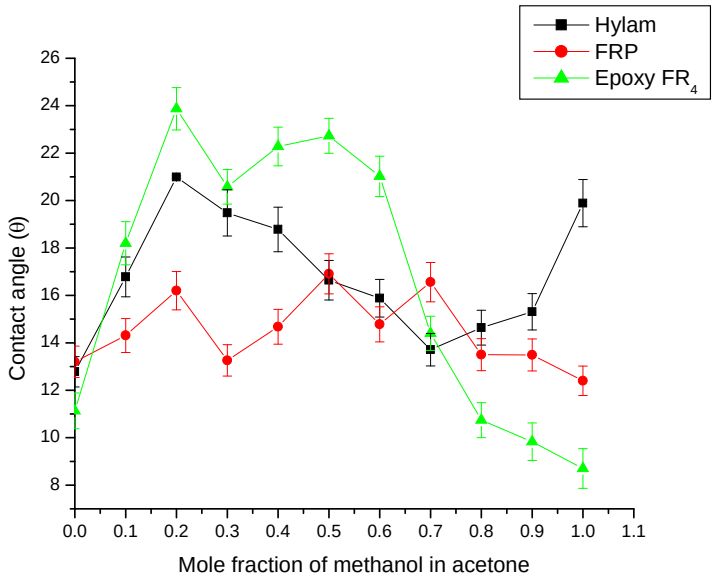

Figure 3.42: Variation of contact angle with mole fraction of methanol in acetone over different substrates

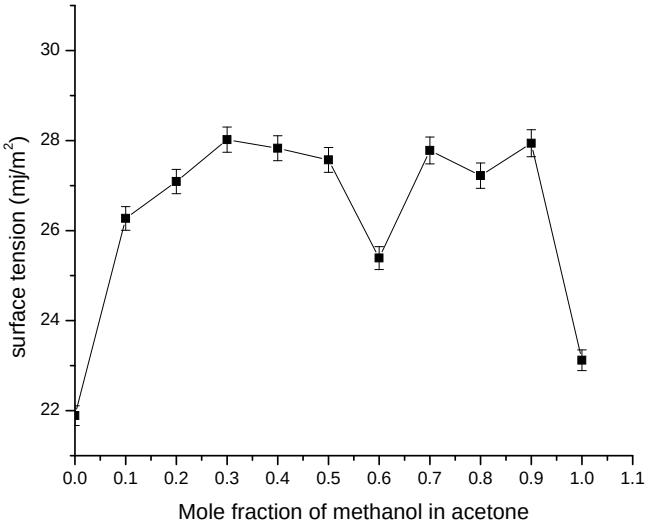

Figure 3.43: Surface tension of mole fraction of methanol in acetone.

Summary

Wetting studies of acetone-methanol system over different substrates are shown in figure 3.49. The binary liquids have a greater contact angle for the 0.5(1:1) concentration. Two other peaks in the contact angle data are seen. A contact angle maxima at 0.2 mole fraction of methanol and lower contact angle minima at 0.1 mole fraction of acetone are seen. Hence three distinct regions of interaction of the moieties are identified at 0.2, 0.5 and 0.9 mole fraction of methanol. Hydrogen bond formation is identified along with the confirmation of a secondary interaction through IR spectroscopy.

3.4.2 Binary mixture of Acetone-Ethanol

Interaction of the type C=O--H hydrogen bond is expected in this system. From the ultrasonic studies of binary mixture of acetone and water it is observed that on the addition of acetone in the solution, the intermolecular free length increase linearly, which is due to the formation of hydrogen bond between the solute and solvent (Sonar *et al.*,2011).

Intermolecular hydrogen bonding has been observed in the tertiary mixture of methanol+ethanol+acetone through UV-VIS spectroscopy study of solvation (Ray and Bagchi, 2002)

3.4.2.1 Computational analysis

Similar to that of acetone-methanol system, the most stable conformer shown in fig. 3.44(1) for acetone-ethanol binary is chosen for the present studies.

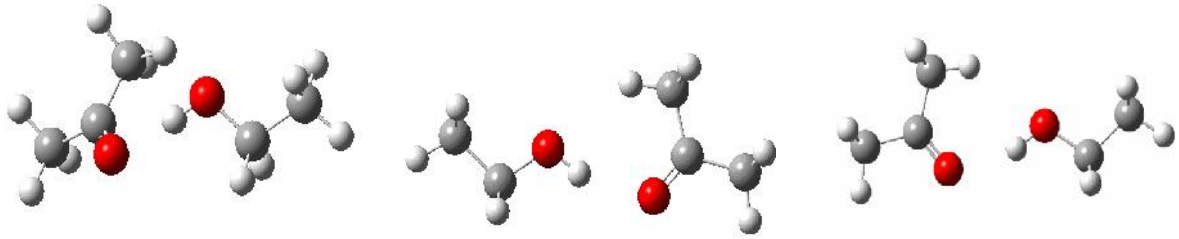

Structure (1) Structure (2) Structure (3)

Figure 3.44: Three conformations of the acetone-ethanol 1:1 binary.

Table 3.30: Computational modeling data of the acetone-ethanol 1:1 binary structure shown in figure 3.44.HF energy (hartree) and dipole moment (debye).

Basis	Parameter	Acetone	Ethanol	Structure 1	Structure 2	Structure 3
STO-3G	HF Energy	-189.536032779	-152.0326747	-341.575584035	-341.575584025	-341.575583991
	Dipole Moment	1.9186	1.4364	2.9454	2.9452	2.9477
6-31G	HF Energy	-191.875161568	-154.0132291	-345.900323787	-345.900323448	-345.900323468
	Dipole Moment	3.6072	2.1048	3.0811	3.0811	3.0824
6-31G(d)	HF Energy	-191.962236330	-154.0757446	-346.047792987	-346.047793054	-346.047793057
	Dipole Moment	3.1188	1.7376	3.6889	3.6870	3.6883
6-31G(d,p)	HF Energy	-191.972071644	-154.0901614	-346.072024728	-346.072024726	-346.072024728
	Dipole Moment	3.1406	1.7030	3.6509	3.6504	3.6499

On solvation there is a change in the energy and dipole moment both for the acetone rich region and acetone rich region shown in table 3.31.

Table3.31:Solvation modeling dataof the three acetone-ethanol 1:1 binary structure shown in fig.3.44.HF energy (hartree) and dipole moment (debye).

Basis	Parameter	Acetone rich region	Ethanol rich region
	HF Energy	-189.537342493	-152.133689577
STO-3G	Dipole Moment	2.1139	1.5954
	HF Energy	-191.880506133	-154.014047096
6-31G	Dipole Moment	4.3785	2.4477
	HF Energy	-191.965566720	-154.076335859
6-31G(d)	Dipole Moment	3.6577	1.9650
	HF Energy	-191.976608781	-154.090683106
6-31G(d,p)	Dipole Moment	3.8772	1.9258

The hydrogen bond energies of acetone-ethanol binary data is shown in table 3.32 and the average energy is approximated to be -5kcal/mol

Table: 3.32: Hydrogen bond energies of the three acetone-ethanol 1:1 binary.

Basis set	Structure1 (kcal/mol)	Structure2 (kcal/mol)	Structure3 (kcal/mol)
STO-3G	-4.314970	-4.314963	-4.314942
6-31G	-7.488131	-7.487918	-7.487931
6-31G(d)	-6.157182	-6.157224	-6.157226
6-31G(d,p)	-6.144407	-6.144405	-6.144407

Hydrogen bond distance between oxygen of C=O acetone and hydrogen of O-H of ethanol are 1.81269 $\overset{o}{A}$ for structure 1, 1.81275 $\overset{o}{A}$ for structure 2 and 1.81249 $\overset{o}{A}$ for structure 3. Second weak hydrogen bond between oxygen of O-H and hydrogen attached to side chain of

acetone are 2.92913 Å for structure 1, 2.92912 Å for structure 2 and 2.92993 Å for structure 3.

3.4.2.2 Dielectric studies

Dipole moment of the 1:1 binary liquid is determined and the result is presented in table 3.33 and fig. 3.45.

Table 3.33: Dielectric data of acetone-ethanol 1:1 mixture in benzene solution

Concentration (mol/cc)	£$_{12}$	n_{12}^2	¢
0.000152	2.25	2.24	-0.011003
0.000304	2.38	2.24	0.124985
0.000456	2.49	2.24	0.237976
0.000607	2.62	2.24	0.361992
0.000759	2.75	2.25	0.486000
0.000911	2.83	2.24	0.571992
0.001063	2.88	2.24	0.618997
0.001215	2.96	2.23	0.710965
0.001367	3.17	2.22	0.932901
0.001518	3.23	2.21	1.001832

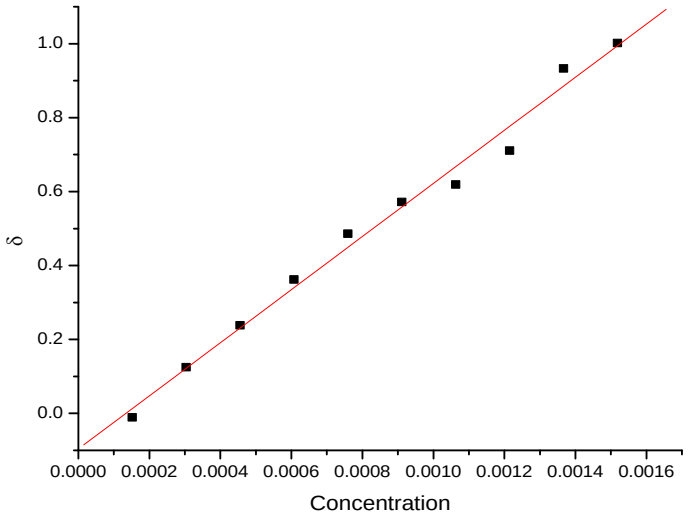

Figure 3.45: δ vs. concentration of the binary system used to determine the experimental dipole moment.

The experimentally determined dipole moment « = 2.34D compare well with the simulation result of 1:1 conformer in table 3.37.

3.4.2.3 FTIR studies

The FTIR spectrum of acetone-ethanol over the entire concentration range is report. The O-H peak in fig. 3.46 shows a red shift. The C=O peak in fig. 3.47 and C-H peak in fig 3.48 shows blue shifting hydrogen bond.

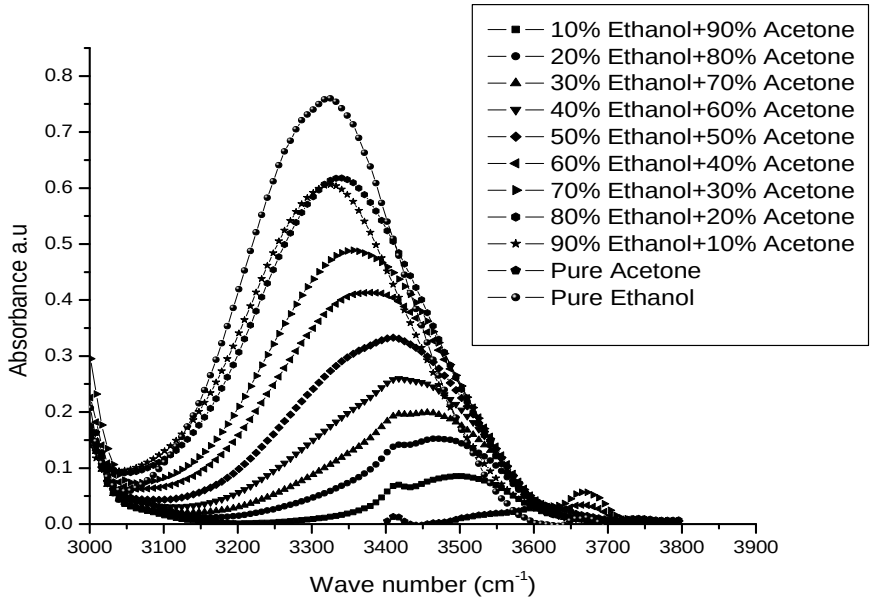

Figure 3.46: O-H stretching frequency of acetone-ethanol binary mixture.

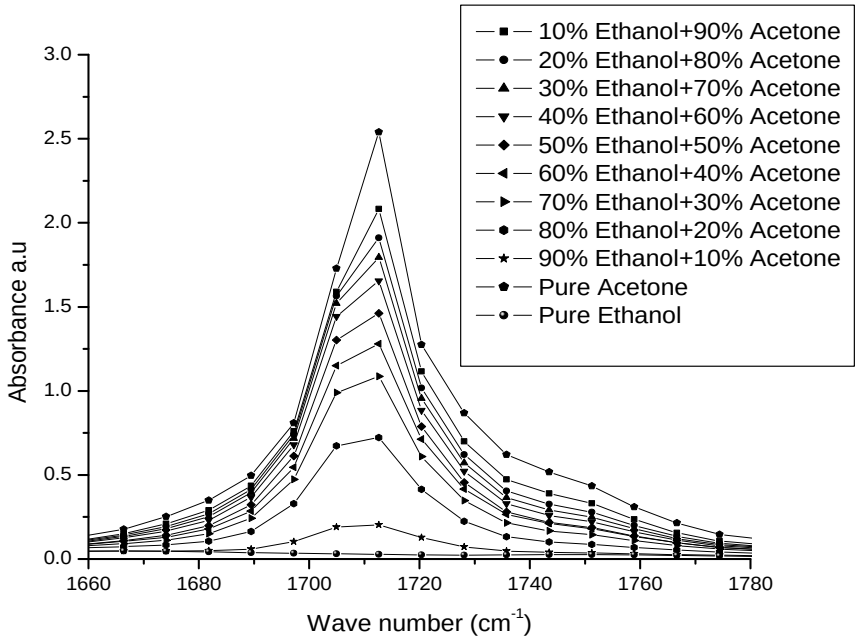

Figure 3.47: C=O frequency of acetone-ethanol binary mixture.

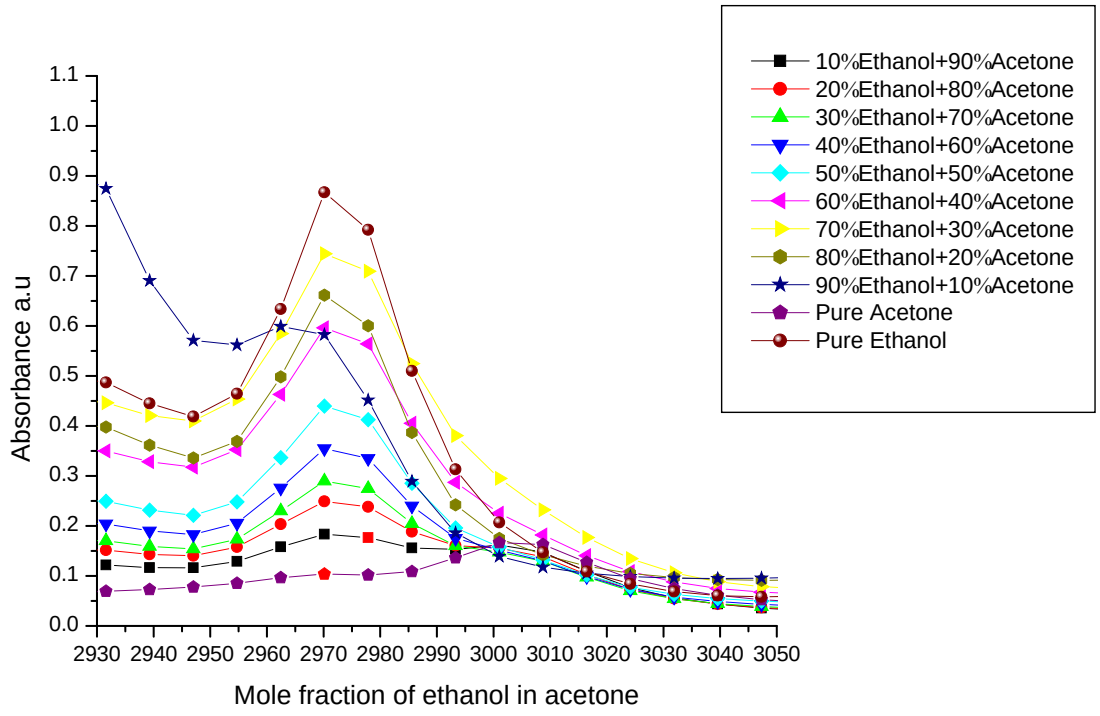

Figure 3.48: C-H stretching frequency of acetone-ethanol binary mixture.

3.4.2.4 Wetting studies

Following the same trend of acetone -methanol system, the contact angle made by acetone-ethanol binary liquid over different substrate is shown in fig.3.49 and the calculated surface tension is shown in fig.3.50.

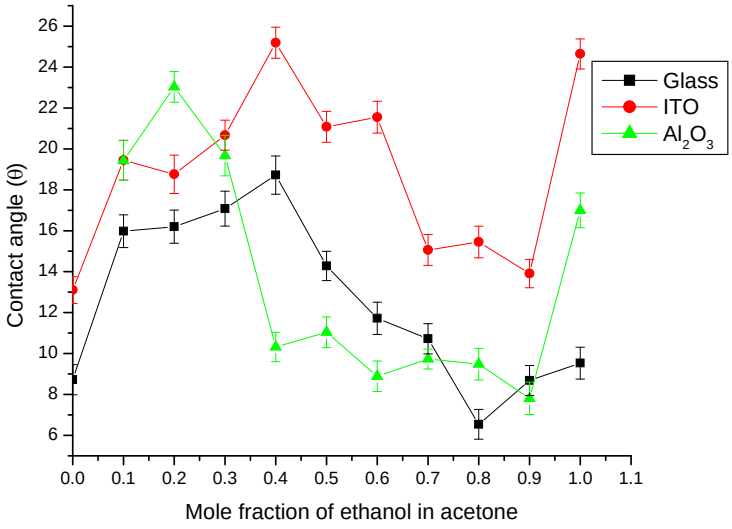

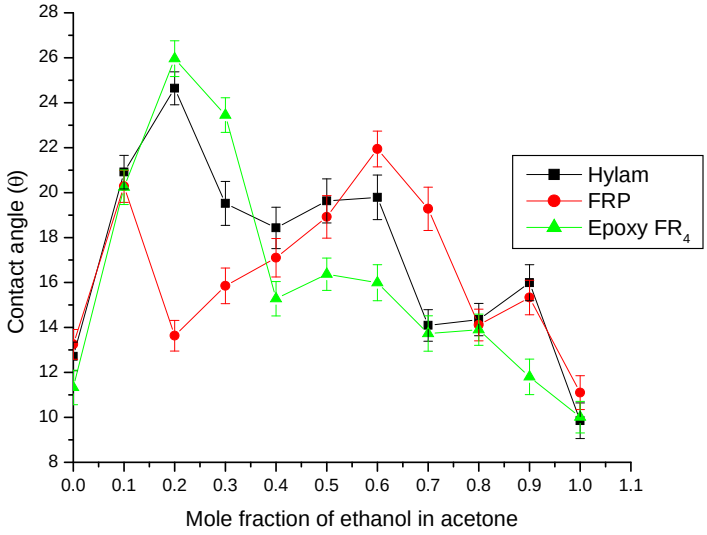

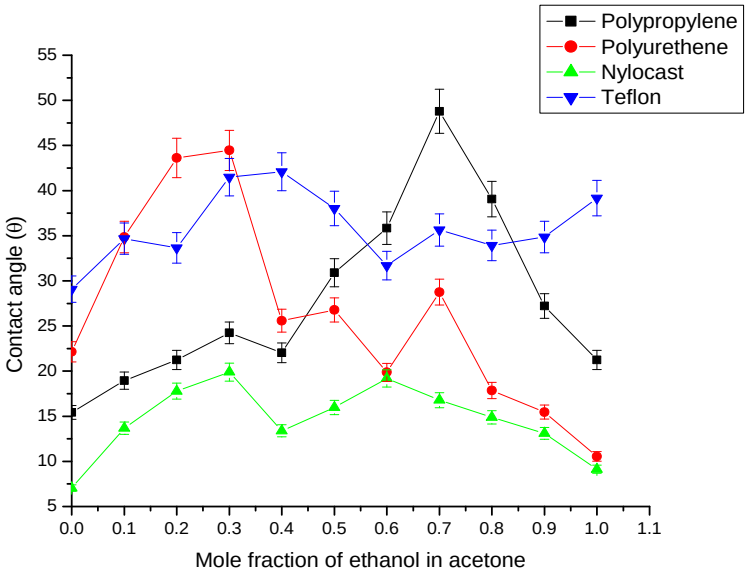

Figure 3.49: Variation of contact angle with mole fraction of ethanol in acetone over different substrates.

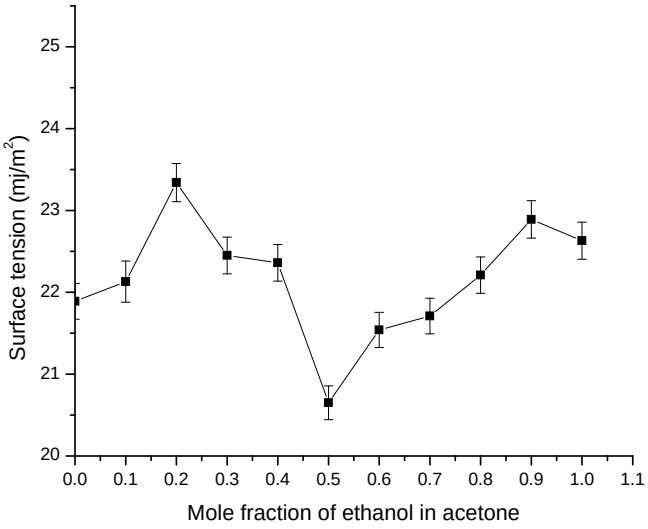

Figure 3.50: Variation of surface tension with mole fraction of ethanol in acetone

3.4.3 Binary mixture of Acetone-Isopropanol:

Acetone-isopropanol binary mixture is expected to show molecular interaction through the formation of hydrogen bonding of the type C=O—H, as observed in acetone-ethanol binary system discuss previously. From the study of density, ultrasonic speed and viscosity of the binary mixtures of 2-methyl-2propanol with ketones, weak and strong interaction for aliphatic and aromatic ketones are observed due to the change in excess intermolecular free length (Rajagopal and Chenthilnath, 2010).Ultrasonic velocity studies show an absorption peak of liquids mixture at the intermediate concentration of acetone-isopropanol mixture indicating that there exists molecular association between the two moieties at the intermediate concentrations (Burton, 1948).

3.4.3.1 Computational analysis

Three conformations of acetone-isopropanol are shown in the fig. 3.51, among which fig. 3.51(1) has the most stable conformer.Computational simulation data of acetone - isopropanol data is shown in table 3.34. Structure 1 possesses the most stable conformer.

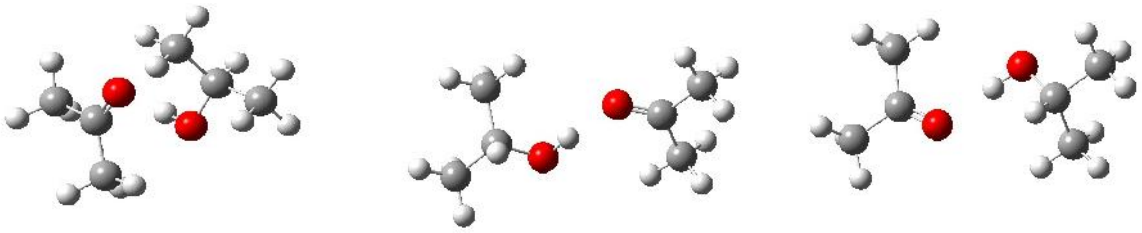

Structure (1) Structure (2) Structure (3)

Figure 3.51: Three conformations of the acetone-isopropanol 1:1 binary.

Table 3.34: Computational modeling data of the acetone-isopropanol 1:1 binary structure shown in fig. 3.51.HF energy (hartree) and dipole moment (debye).

Basis	Parameter	Acetone	Isopropanol	Structure 1	Structure 2	Structure 3
STO-3G	HF Energy	-189.536032779	-190.716353715	-380.259119309	-380.259118503	-380.259119306
	Dipole Moment	1.9186	1.4481	2.8872	2.9009	2.8869
6-31G	HF Energy	-191.875161568	-193.037562840	-384.924600093	-384.924600116	-384.924600111
	Dipole Moment	3.6072	2.0902	3.6652	3.6586	3.6605
6-31G(d)	HF Energy	-191.962236330	-193.115416025	-385.087478073	-385.087493208	-385.087493206
	Dipole Moment	3.1188	1.8521	3.5431	3.7703	3.7703
6-31G(d,p)	HF Energy	-191.972071644	-193.128929944	-385.111714911	-385.114848672	-385.114848664
	Dipole Moment	3.1406	1.8326	4.3489	3.7314	3.7319

On solvation, both the acetone rich region and the isopropanol rich region as shown in table 3.35 shows a change in their energy when compared to its pure form.

Table 3.35: Solvation modeling data of the three acetone-isopropanol 1:1 binary structure shown in fig. 3.51.HF energy (hartree) and dipole moment (debye).

Basis	Parameter	Acetone rich region	Isopropanol rich region
STO-3G	HF Energy(hartree)	-189.537032880	-190.717023203
	Dipole Moment(debye)	2.0676	1.5454
6-31G	HF Energy(hartree)	-191.878250891	-193.038693036
	Dipole Moment(debye)	4.0528	2.3465
6-31G(d)	HF Energy(hartree)	-191.965045662	-193.116105585
	Dipole Moment(debye)	3.5732	1.9009
6-31G(d,p)	HF Energy(hartree)	-191.974869043	-193.133603750
	Dipole Moment(debye)	3.5946	1.8572

The hydrogen bond energy at different basis set is calculated in acetone-isopropanol binary mixture and the energy is approximately-5kcal/mol.

Table 3.36:Hydrogen bond energies of the three acetone - isopropanol 1:1 binary.

Basis set	Structure1 (kcal/mol)	Structure2 (kcal/mol)	Structure3 (kcal/mol)
STO-3G	-4.224905	-4.224399	-4.224903
6-31G	-7.452116	-7.452131	-7.452127
6-31G(d)	-6.165771	-6.175268	-6.175267
6-31G(d,p)	-6.722773	-8.689239	-8.689234

Hydrogen bond distance between oxygen of C=O acetone and hydrogen of O-H of isopropanol are 1.82612 $\overset{o}{A}$ for structure 1, 1.82625 $\overset{o}{A}$ for structure 2 and 1.82616 $\overset{o}{A}$ for structure 3. Second weak hydrogen bond between oxygen of O-H and hydrogen attached to side chain of acetone are 2.91511 $\overset{o}{A}$, for structure 1, 2.92038 $\overset{o}{A}$ for structure 2 and 2.91559 $\overset{o}{A}$ for structure 3.

3.4.3.2 Dielectric studies

Dipole moment of the 1:1 binary liquid is determined and the result are presented in table 3.37 and fig. 3.52.

Table 3.37: Dielectric data of acetone-Isopropanol 1:1 mixture in benzene solution

Concentration (mol/cc)	£$_{12}$	n_{12}^2	¢
0.000134	2.26	2.23	0.013952
0.000267	2.33	2.23	0.083952
0.000401	2.39	2.23	0.146937
0.000534	2.48	2.23	0.233952
0.000668	2.54	2.23	0.290965
0.000801	2.6	2.22	0.359920
0.000935	2.68	2.23	0.430965
0.001069	2.76	2.23	0.516937
0.001202	2.84	2.22	0.602901
0.001336	2.92	2.22	0.682901

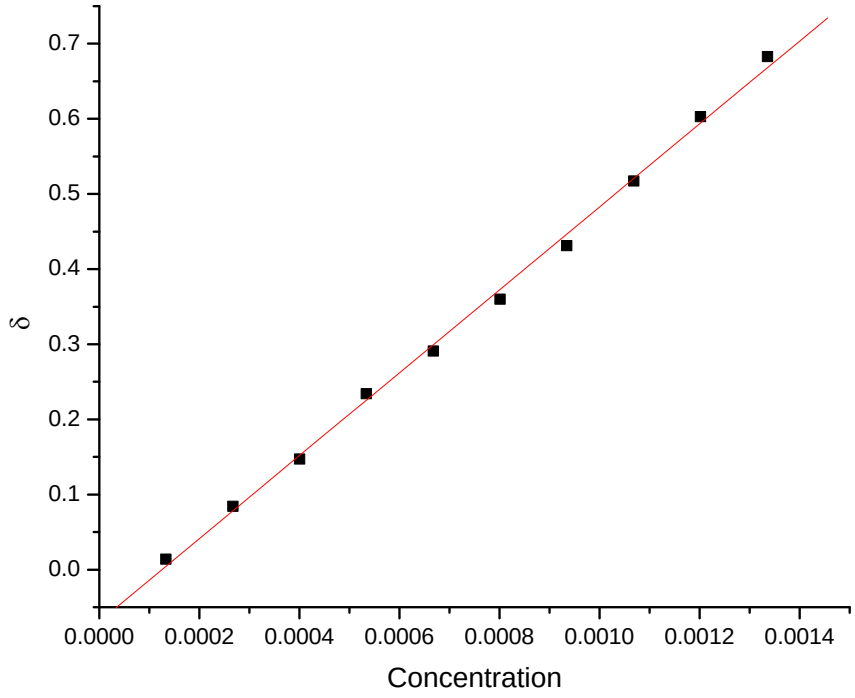

Figure 3.52: δ vs. concentration of the binary system used to determine the experimental dipole moment.

The experimentally determined dipole moment $\vec{\mu}$ = 2.15D, compares well with the simulation result of 1:1 conformer in table 3.34.

3.4.3.3 FTIR studies

The IR spectrum of acetone-isopropanol over the entire concentration range is reported. Fig. 3.53 show the red shifting of O-H peak, while the two corresponding peaks shown in fig.3.54(C=O) and fig.3.55 (C-H) shows blue shifting hydrogen bond. Figure 3.61: IR spectra of acetone–isopropanol binary mixture.

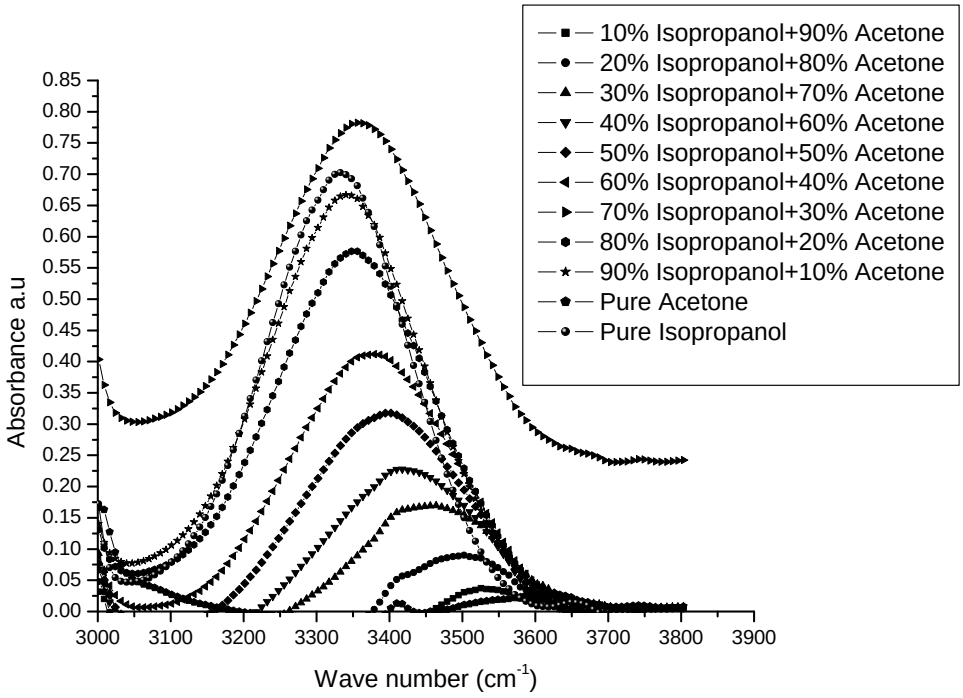

Figure 3.53: O-H stretching frequency of acetone- isopropanol binary mixture.

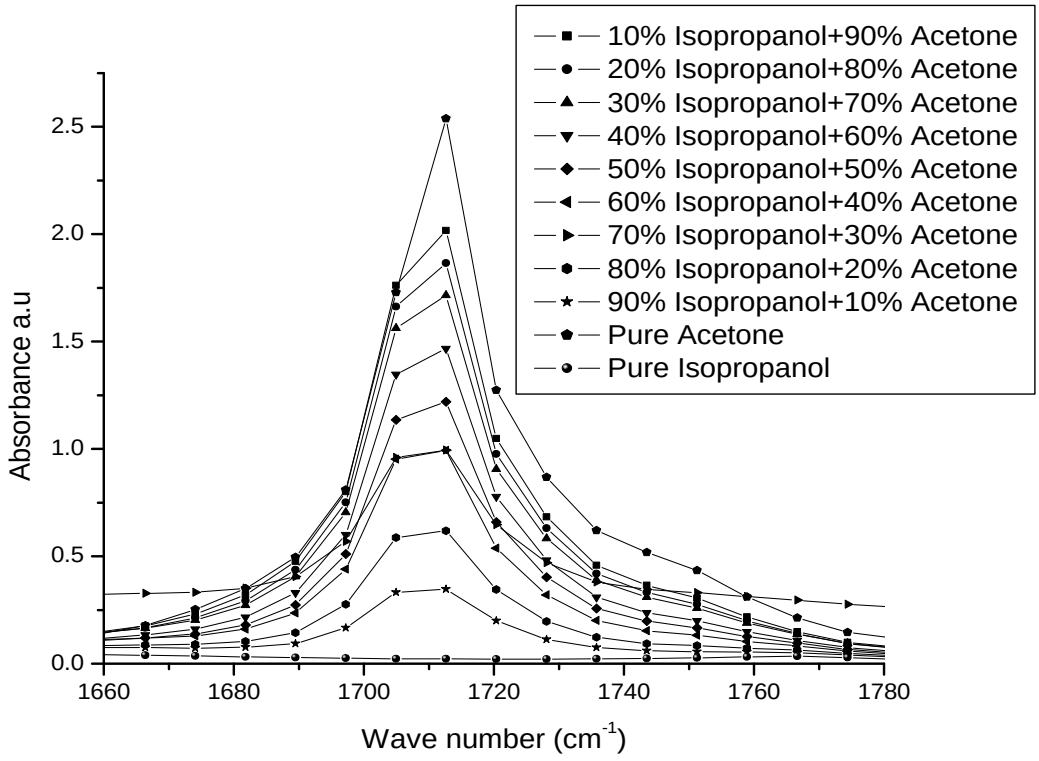

Figure 3.54: C=O frequency of acetone-isopropanol binary mixture.

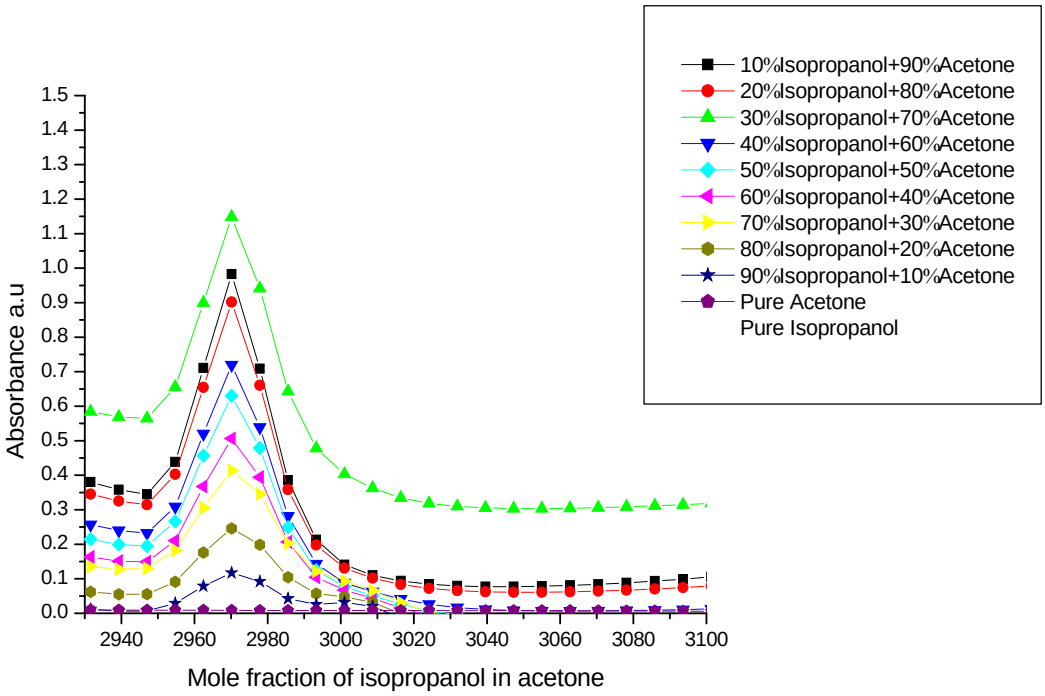

Figure 3.55: C-H stretching frequency of acetone -isopropanol binary mixture.

3.4.4.4 Wetting studies

Contact angle made by the acetone-isopropanol binary is shown in figure 3.56 and the corresponding surface tension is shown in figure 3.57. The wetting behavior of acetone-isopropanol show the similar trend as that of acetone-ethanol binary system.

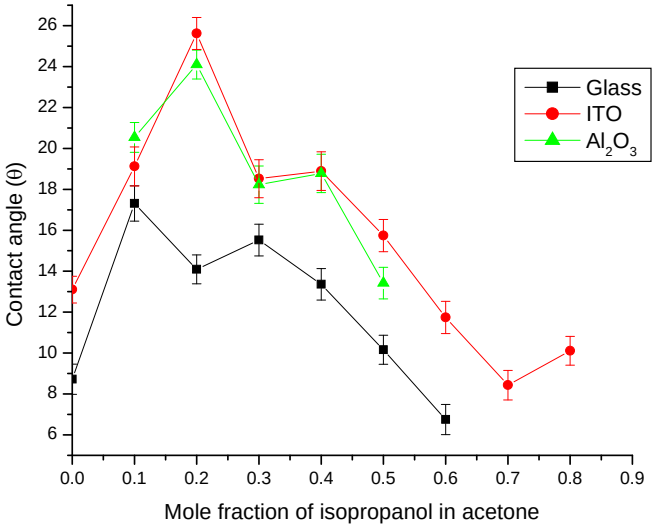
Contact angle (θ)
Mole fraction of isopropanol in acetone
Glass
ITO
Al2O3

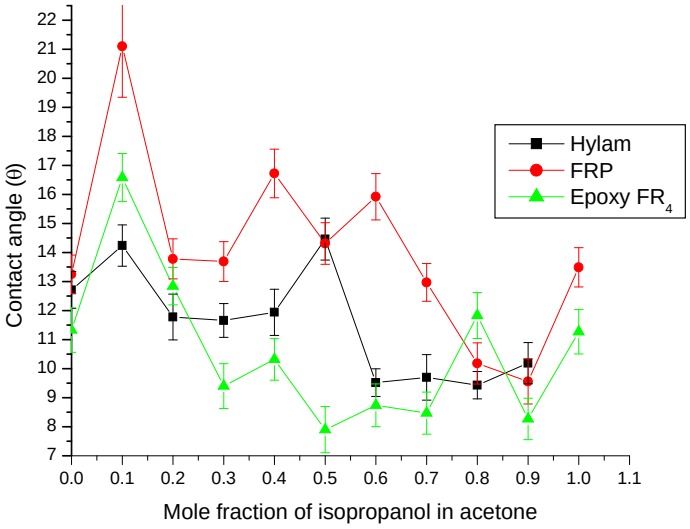
Contact angle (θ)
Mole fraction of isopropanol in acetone
Hylam
FRP
Epoxy FR4

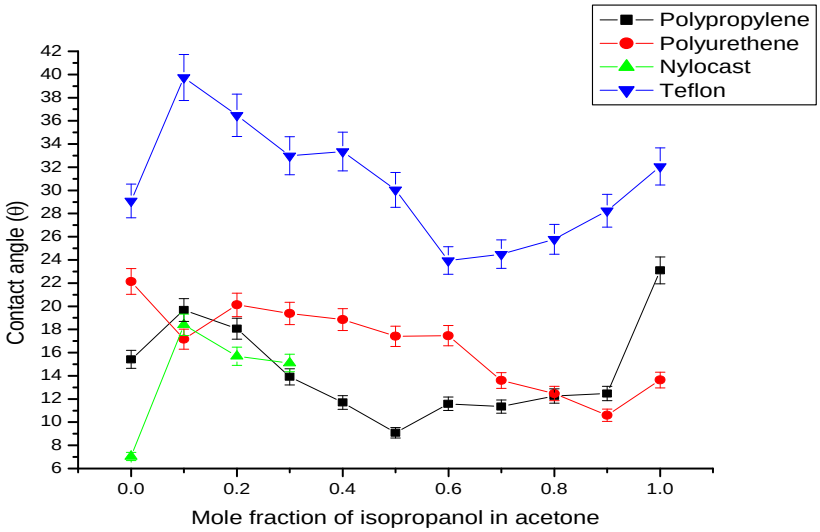

Figure 3.56: Variation of contact angle with mole fraction of isopropanol in acetone over different substrates

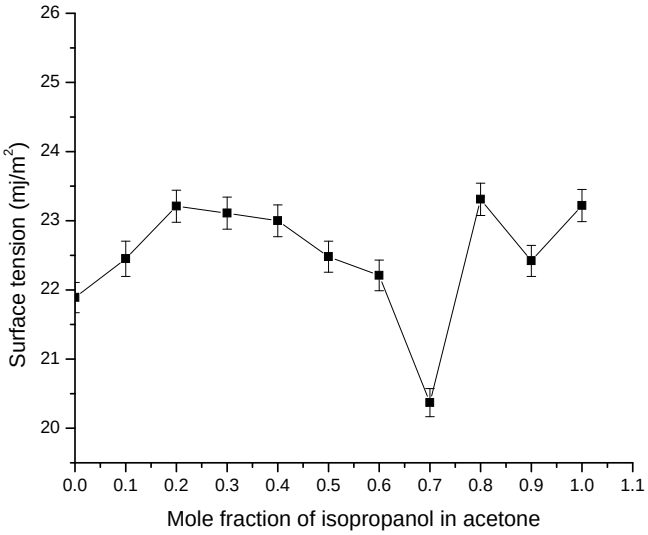

Figure 3.57: Variation of surface tension with mole fraction of isopropanol in acetone

Summary

The binary system of acetone-isopropanol follows the same trend as that of methanol-acetone and ethanol-acetone binary system.

3.4.4. Binary mixture of Acetone-Butanol

The type of interaction site in acetone-butanol system is similar to acetone-isopropanol binary system.The molecular interactions in acetone and tertiary butanol has been studied from ultrasonic studied, where the absorption peak exist at the intermediate concentration of this mixture (Burton, 1948).

3.4.4.1 Computational analysis

The three most stable conformer of acetone-butanol is shown in fig. 3.58, among them structure 1 shown in fig. 3.58 (1) possesses the most stable conformer.

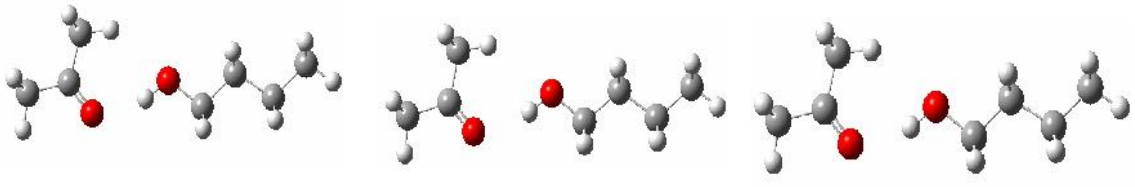

Structure (1). Structure (2).

Figure 3.58: Three conformations of the acetone-butanol 1:1 binary.

Computational simulation data of acetone-butanol binary system is shown in table 3.38.

Table 3.38: Computational modeling data of the acetone-butanol 1:1 binary structure shown in fig. 3.58.HF energy (hartree) and dipole moment (debye).

Basis	Parameter	Acetone	Butanol	Structure 1	Structure 2	Structure 3
STO-3G	HF Energy	-189.536032779	-229.2935447	-418.836405236	-418.835944272	-418.835944166
	Dipole Moment	1.9186	1.5104	2.9360	2.9436	2.9455
6-31G	HF Energy	-191.875161568	-232.0499437	-423.937380796	-423.937380797	-423.937380902
	Dipole Moment	3.6072	2.2904	3.1102	3.1091	3.1106
6-31G(d)	HF Energy	-191.962236330	-232.1450612	-424.117197647	-424.117101131	-424.117101130
	Dipole Moment	3.1188	1.6896	3.7083	3.6767	3.6774
6-31G(d,p)	HF Energy	-191.972071644	-232.1655473	-424.146863046	-424.147034951	-424.147393870
	Dipole Moment	3.1406	1.8260	4.7389	3.1106	3.6423

On solvation the acetone and isopropanol rich region shows a change in their energy when compare to their 1:1 binary as shown in table 3.38.

Table: 3.39:Solvation modeling data of the three acetone-butanol 1:1 binary structure shown in fig. 3.58.HF energy (hartree) and dipole moment (debye).

Basis	Parameter	Acetone rich region	Butanol rich region
	HF Energy	-189.536905549	-229.293654521
STO-3G	Dipole Moment	2.0486	1.5345
	HF Energy	-191.877772654	-232.051426787
6-31G	Dipole Moment	3.9836	2.3515
	HF Energy	-191.964623343	-232.145784940
6-31G(d)	Dipole Moment	3.5048	1.9288
	HF Energy	-191.974408104	-232.166177679
6-31G(d,p)	Dipole Moment	3.5198	1.8747

The calculated hydrogen bond energies is shown in table 3.40 and the average energy is approximated to be -5 kcal/mol.

Table 3.40: Hydrogen bond energies of the three acetone-butanol 1:1 binary.

Basis set	Structure1 (kcal/mol)	Structure2 (kcal/mol)	Structure3 (kcal/mol)
STO-3G	-4.284473	-3.995213	-3.995147
6-31G	-7.702996	-7.702997122	-7.703063
6-31G(d)	-6.212441	-6.151876489	-6.151876
6-31G(d,p)	-5.800794	-5.908666163	-6.133891

Hydrogen bond distance between oxygen of C=O acetone and hydrogen of O-H of butanol are 1.81883A for structure 1, 1.81345A for structure 2 and 1.81344A for structure 3. Second weak hydrogen bond between oxygen of O-H and hydrogen attached to side chain of acetone are 2.91002A, for structure 1, 2.92675A for structure 2 and 2.92795A for structure 3

3.4.4.2 Dielectric studies

Dipole moment of the 1:1 binary liquid is determined and the result is presented in table 3.41and figure 3.68.

Table 3.41: Dielectric data of acetone-butanol 1:1 mixture in benzene solution

Concentration (mol/cc)	£$_{12}$	n_{12}^2	¢
0.000121	2.28	2.24	0.018997
0.000242	2.36	2.24	0.101992
0.000364	2.41	2.24	0.148997
0.000485	2.46	2.24	0.204985
0.000606	2.51	2.24	0.257976
0.000727	2.59	2.24	0.334985
0.000848	2.68	2.23	0.430965
0.000970	2.74	2.23	0.496937
0.001091	2.82	2.21	0.588857
0.001212	2.88	2.21	0.654805

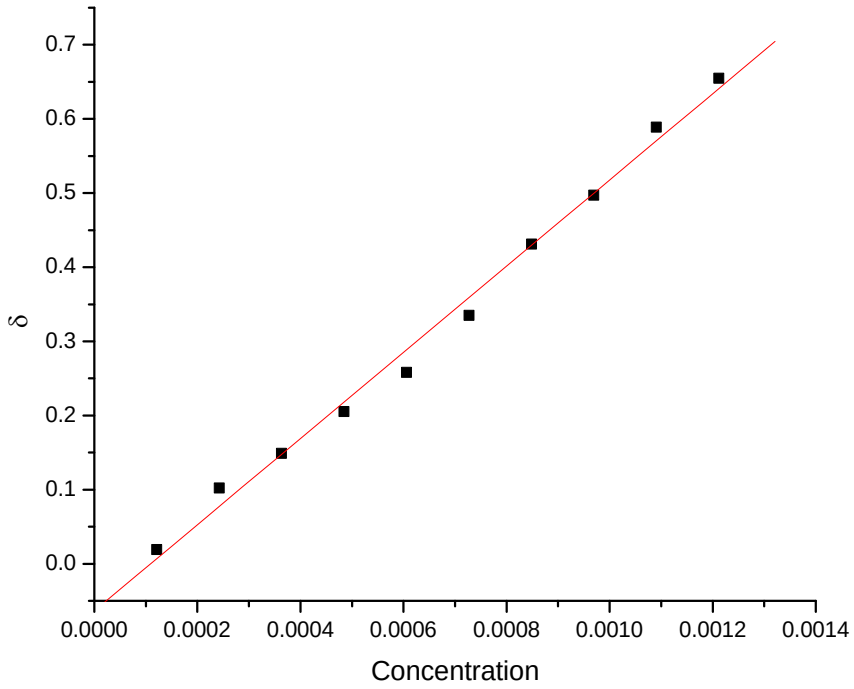

Figure 3.59: δ vs. concentration of the binary system used to determine the experimental dipole moment.

The experimentally determined dipole moment $\vec{\mu}$ =2.22D compare well with the simulation result of 1:1 conformer in table 3.48.

3.4.4.3 FTIR studies

The IR spectrum of aniline-butanol over the entire concentration range is reported. The OH peak showed in fig. 3.60 shows a red shifting hydrogen bond and C=O and C-H show a blue shifting hydrogen bond as seen in fig. 3.61 and fig.3.62.

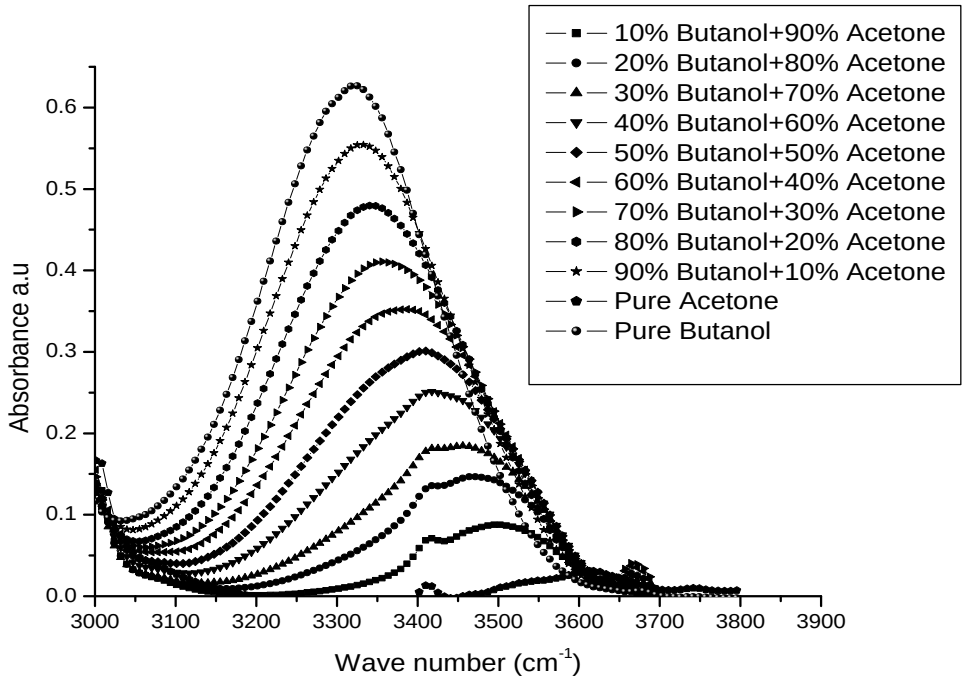

Figure 3.60: O-H stretching frequency of acetone-butanol mixture.

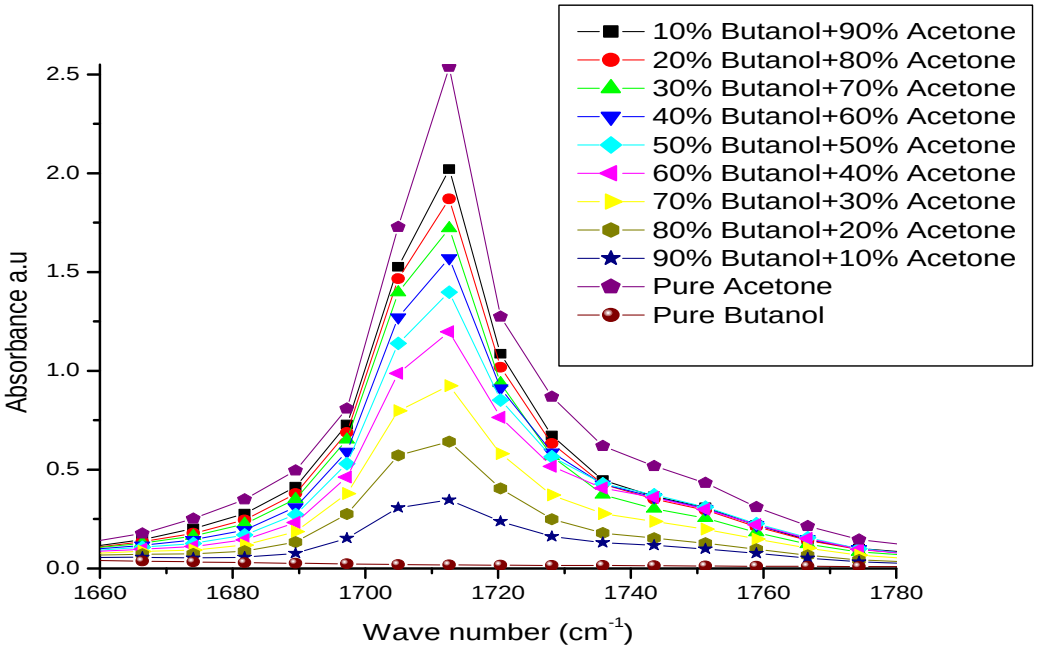

Figure 3.61: C=O stretching frequency of aniline-butanol mixture.

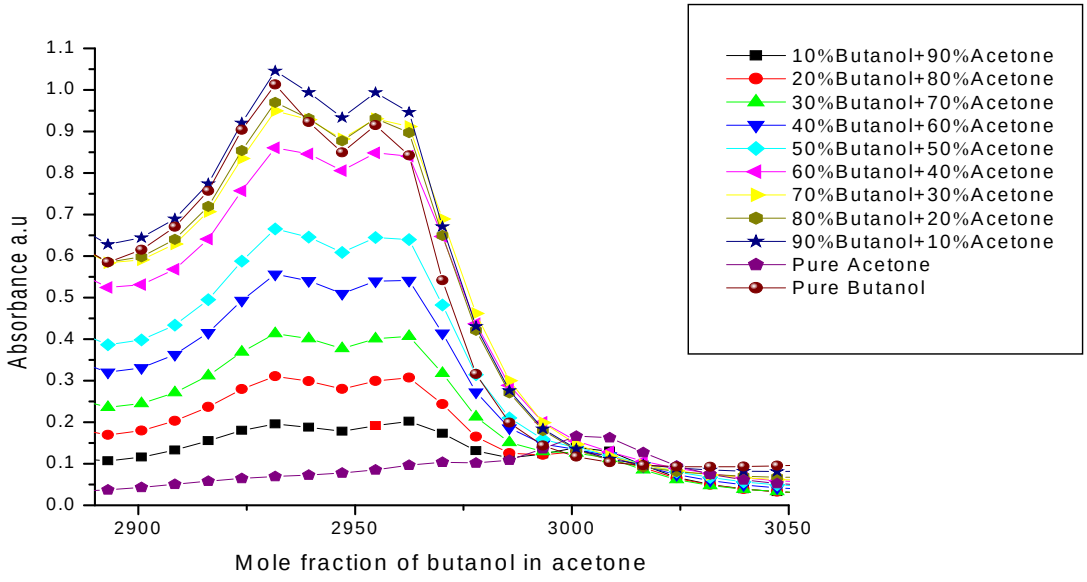

Figure 3.62: C-H stretching frequency of acetone-butanol binary mixture**.**

3.4.4.4 Wetting studies

The contact angle made by the acetone-butanol binary is shown in fig. 3.63 along with the corresponding surface tension in fig.3.64, which again follows the same trend as that of the previous system.

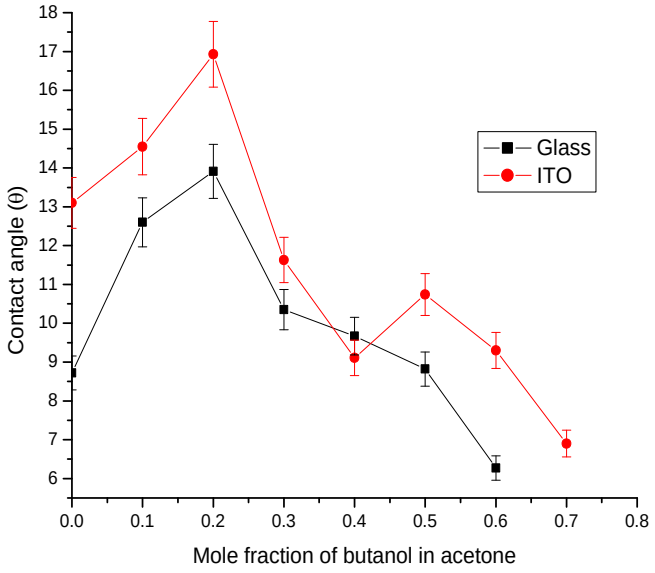

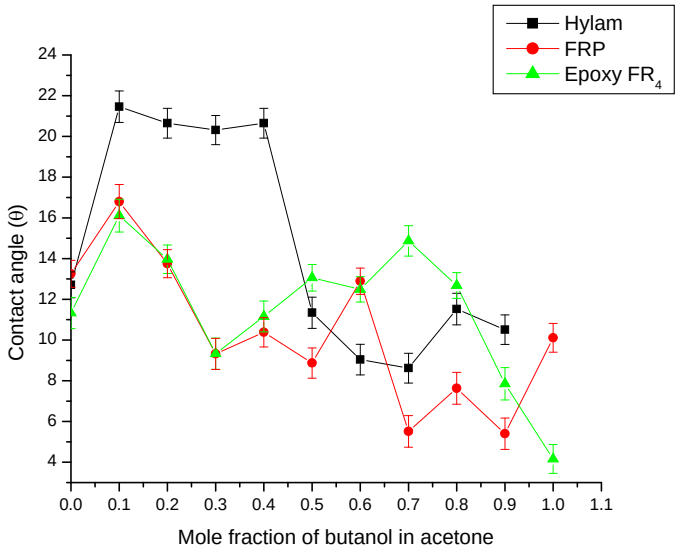

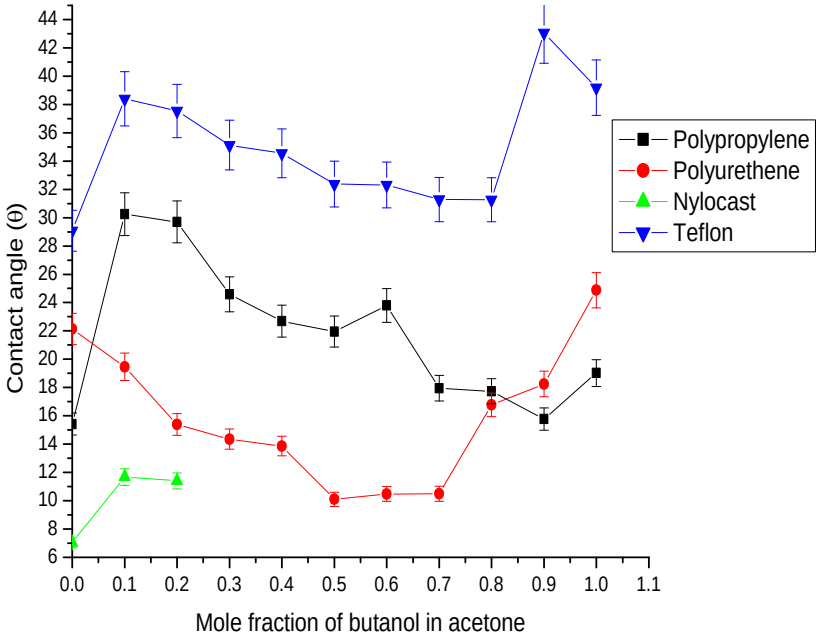

Figure 3.63: Variation of contact angle with mole fraction of butanol in acetone over different substrates.

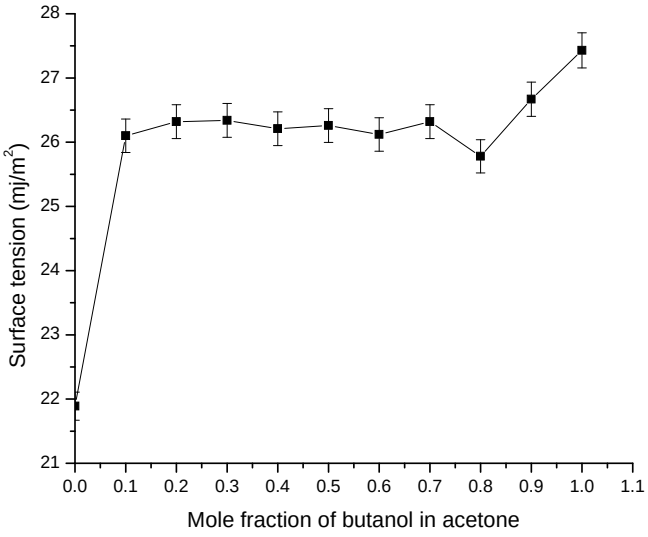

Figure 3.64: Variation of surface tension of mole fraction of butanol in acetone.

3.4.5 Binary mixture of Acetone-Hexanol

Long chain alcohol hexanol is also expected for forming hydrogen bond of the type C=O--H with acetone,is taken for the present studies. Not much of literature is available in respect of this system. From the studies of ultrasonic velocity, viscosity and density of binary mixture of dimethylsulphoside (DMSO)+1-hexanol, that the structure breaking effect of these moieties is seen to be overestimated although the interaction exist between them exists (*Ali et al.*, 2000).

3.4.5.1 Computational analysis

Among the three conformer in acetone-hexanol binary mixture as shown in fig. 3.65, the most stable conformer is the one given in fig.3.65(2). The corresponding data of the three conformers are shown in table 3.42.

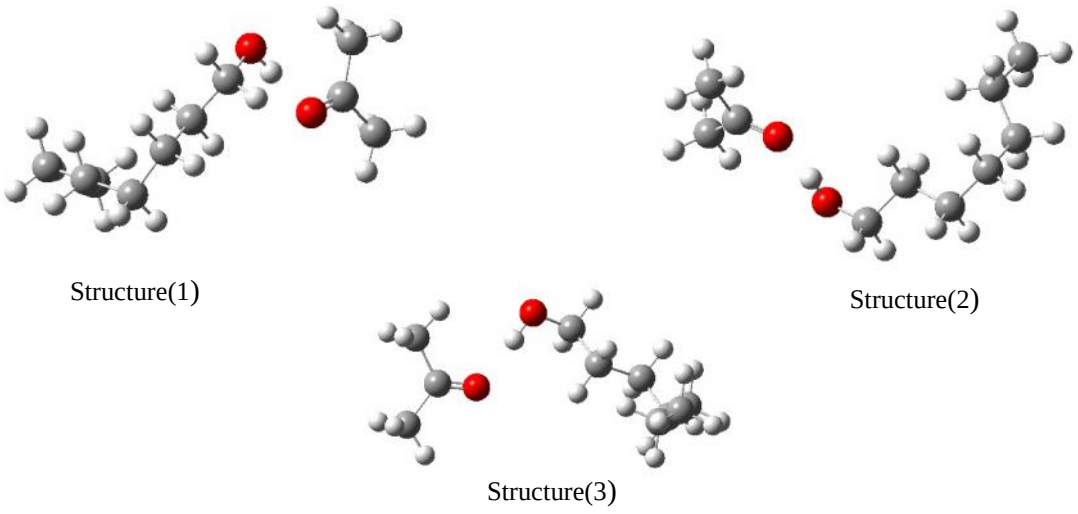

Figure 3.65: Three conformation of acetone-hexanol 1:1 binary.

Table 3.42: Computational modeling data of acetone-hexanol 1:1 binary structure shown in fig. 3.65.HF energy (hartree) and dipole moment (debye).

Basis	Parameter	Acetone	Hexanol	Structure 1	Structure 2	Structure 3
STO-3G	HF Energy	-189.536032779	-345.028454931	-534.571304084	-534.571304085	-534.571304084
	Dipole Moment	1.9186	1.5178	2.9379	2.4317	1.9739
6-31G	HF Energy	-191.875161568	-349.099466546	-540.986639493	-540.986639386	-540.986639412
	Dipole Moment	3.6072	2.2904	3.6132	4.0036	2.6564
6-31G(d)	HF Energy	-191.962236330	-349.243153788	-541.215290807	-541.215290773	-541.215290760
	Dipole Moment	3.1188	1.8703	3.7682	3.7099	2.6063
6-31G(d,p)	HF Energy	-191.972071644	-349.272735062	-541.179659418	-541.254674429	-541.254674411
	Dipole Moment	3.1406	1.8439	3.3250	2.9605	2.6392

It appears from the data in table 3.43 that acetone and hexanol rich region show a change on solvation by the other component.

Table 3.43: Solvation modeling data of three acetone-hexanol 1:1 binary structure shown in fig. 3.65.HF energy (hartree) and dipole moment (debye).

Basis	Parameter	Acetone rich region	Hexanol rich region
STO-3G	HF Energy	-189.536471370	-345.029178401
	Dipole Moment	1.7215	1.7272
6-31G	HF Energy	-191.877051288	-349.101384483
	Dipole Moment	4.2023	3.0066
6-31G(d)	HF Energy	-191.963603956	-349.244354702
	Dipole Moment	3.8878	2.4235
6-31G(d,p)	HF Energy	-191.973350855	-349.273751130
	Dipole Moment	3.8826	2.3327

The hydrogen bond energy of acetone-hexanol binary system is shown in table 3.44, and the average is approximated to be -6kcal/mol.

Table 3.44: Hydrogen bond energy of three acetone-hexanol 1:1 binary.

Basis set	Structure1 (kcal/mol)	Structure2 (kcal/mol)	Structure3 (kcal/mol)
STO-3G	4.277343	4.277343	4.277343
6-31G	7.53726	7.537193	7.53721
6-31G(d)	6.212781	6.21276	6.212752
6-31G(d,p)	6.192068	6.192095	6.192084

Hydrogen bond distance between oxygen of C=O acetone and hydrogen of O-H of hexanol are 1.81899 $\mathring{A}$ for structure 1, 1.81904 $\mathring{A}$ for structure 2 and 1.81904 $\mathring{A}$ for structure 3. Second weak hydrogen bond between oxygen of O-H and hydrogen attached to side chain of acetone are 2.90778 $\mathring{A}$, for structure 1, 2.90861 $\mathring{A}$ for structure 2 and 2.90851 $\mathring{A}$ for structure 3.

3.4.5.2 Dielectric studies

Dipole moment of 1:1 binary liquid of acetone-hexanol binary mixture is determined and the results are shown in table 3.45 and fig. 3.66.

Table 3.45: Dielectric data of acetone-hexanol 1:1 mixture in benzene solution

Concentration (mol/cc)	£$_{12}$	n_{12}^2	¢
0.000100	2.23	2.24	-0.031003
0.000200	2.30	2.24	0.041992
0.000301	2.39	2.24	0.134985
0.000401	2.48	2.24	0.218997
0.000501	2.54	2.24	0.284985
0.000601	2.65	2.23	0.400965
0.000702	2.76	2.23	0.516937
0.000802	2.81	2.24	0.557976
0.000902	2.94	2.22	0.702901
0.001002	3.03	2.22	0.789920

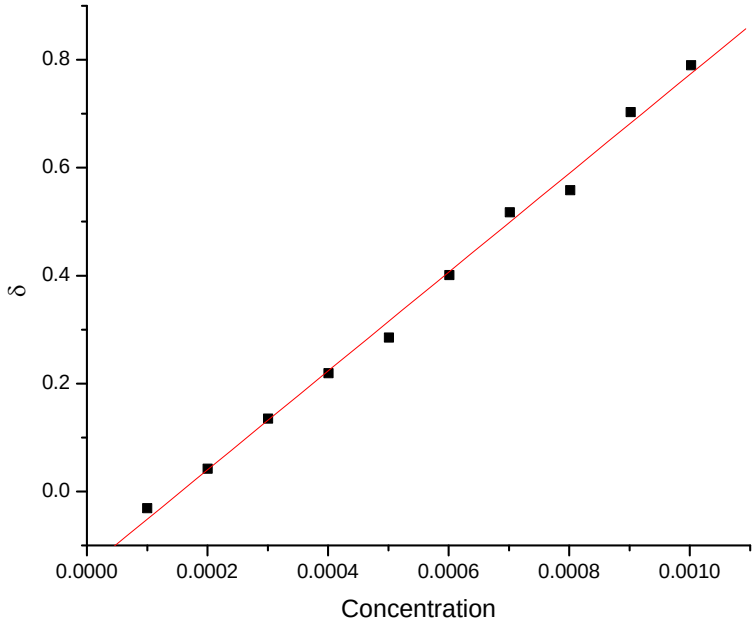

Figure 3.66: δ vs. concentration of the binary system used to determine the experimental dipole moment.

The experimentally determined dipole moment $\vec{\mu}$ =2.8D compared well with the simulations result of 1:1 conformer in table 3.42.

3.4.2.3 FTIR studies

The IR spectrum of acetone-hexanol over the entire concentration is reported. The O-H peak in fig. 3.67 shows a red shited hydrogen bonding. The C=O stretching shown in fig. 3.68 and C-H in fig.3.69 show a blue shifting hydrogen bond formation.

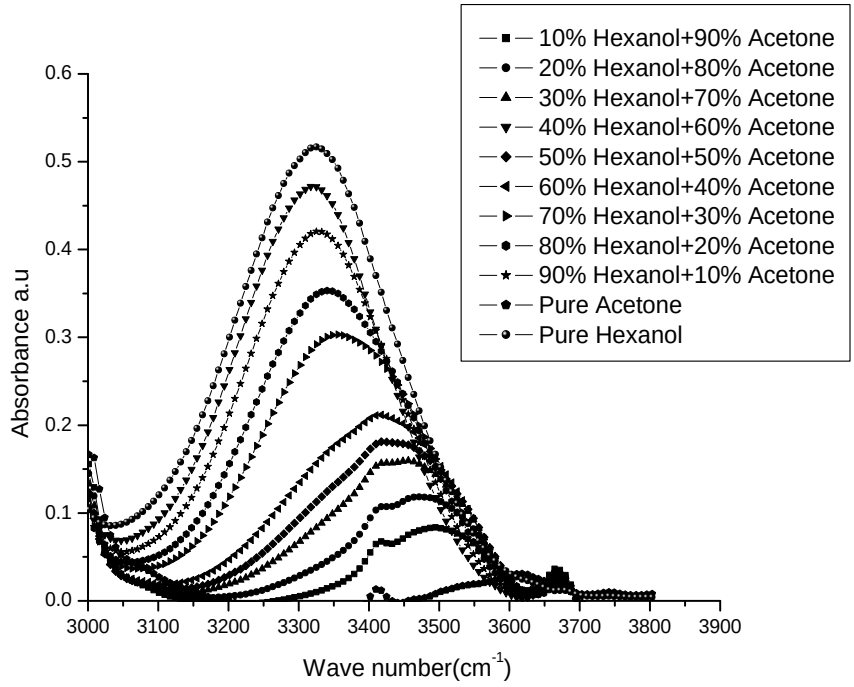

Figure 3.67: O-H stretching frequency of acetone-hexanol mixture.

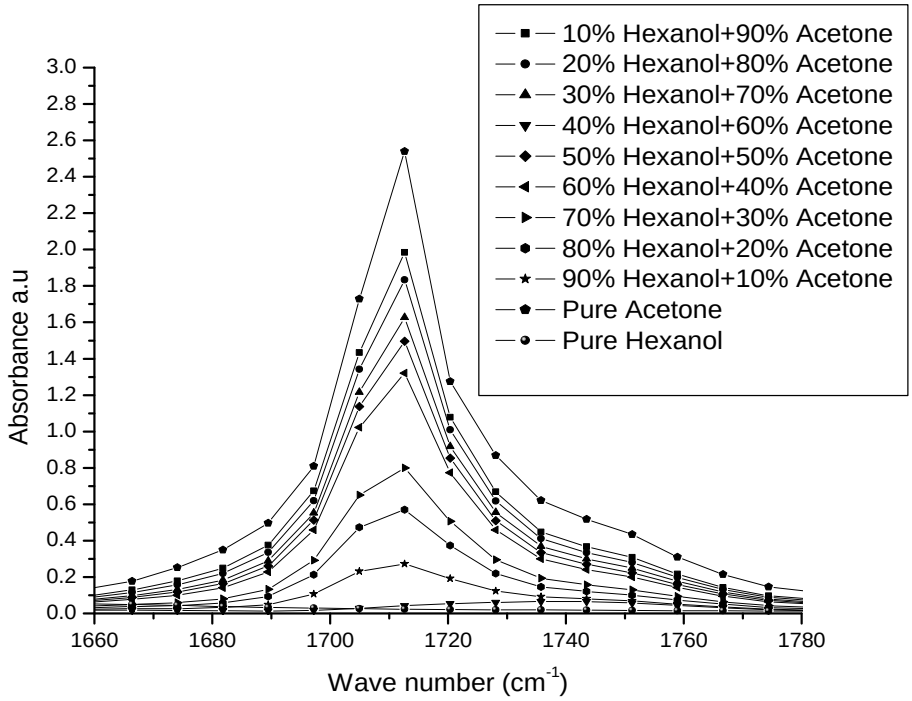

Figure 3.68: C=O stretching frequency of acetone-hexanol binary mixture

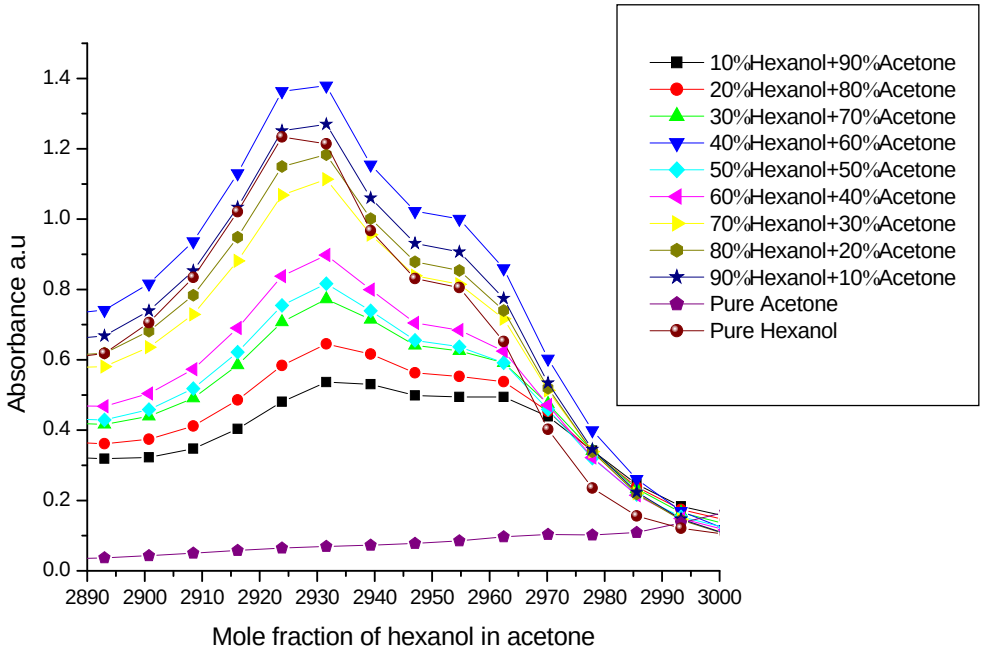

Figure 3.69: C-H stretching frequency of acetone –hexanol binary mixture**.**

3.4.5.4 Wetting studies

Contact angle of binary mixture of acetone-hexanol binary system is shown in fig. 3.70 along with the surface tension in fig.3.71.

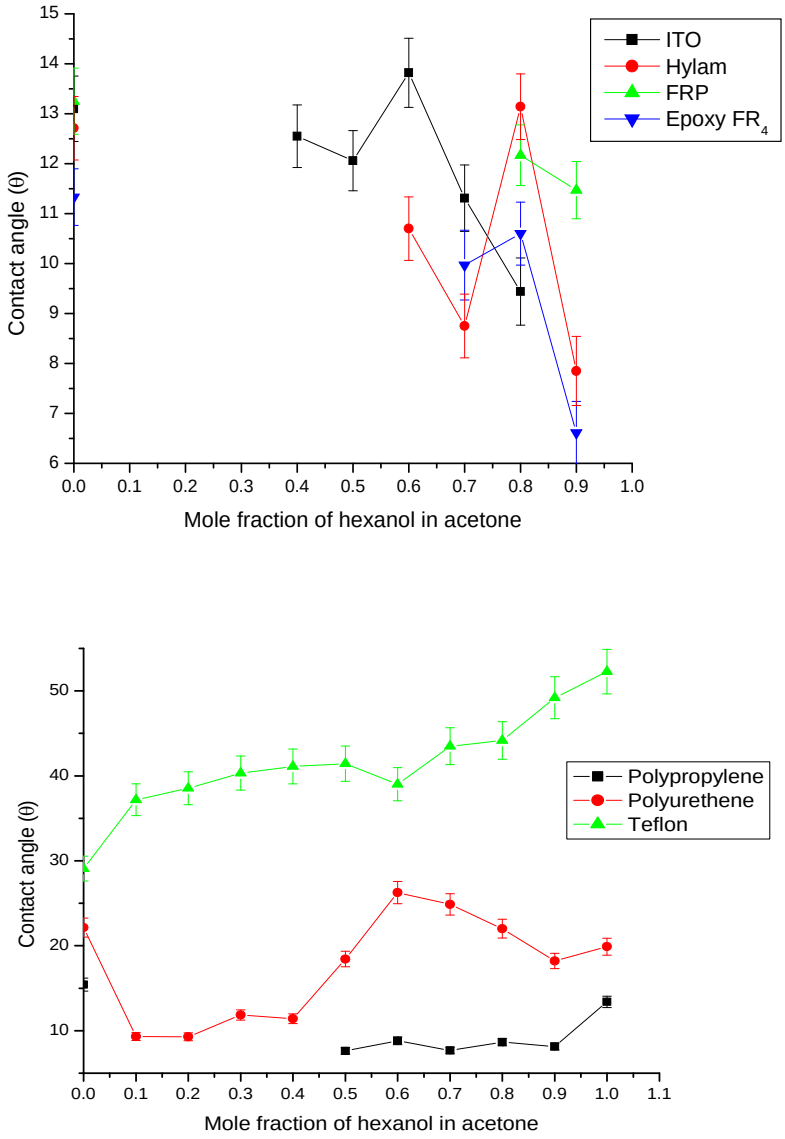

Figure 3.70: Variation of contact angle with mole fraction of hexanol in acetone over different substrates

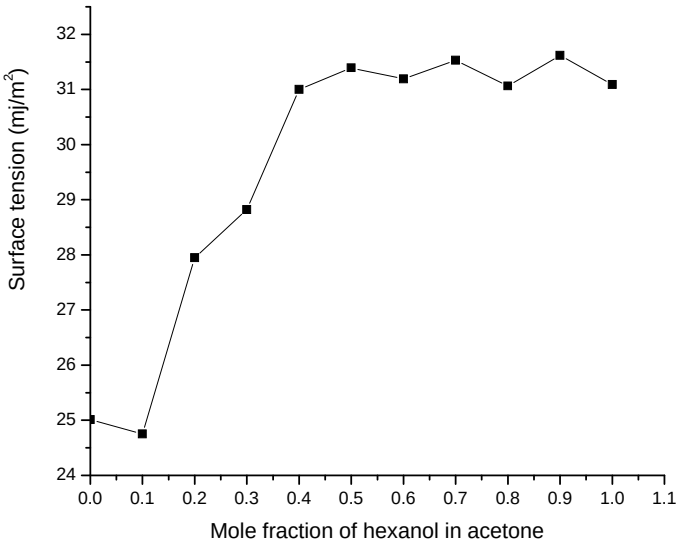

Figure 3.71: Variation of surface tension with mole fraction of hexanol in acetone

3.4.6 Binary mixture of Acetone-Octanol

Octanol being a long chain molecule, the interactions of the type discussed in the case of acetone-hexanol are also expected in this system. Molecular interaction between dimethylsulphoxide+1-octanol is observed by Ali et al (Ali et al., 2000), from ultrasonic velocity, viscosity and density studied. Studies on this binary system are rare till today.

3.4.6.1 Computational analysis

In this system of acetone-octanol system the three conformers is shown in fig. 3.72, among which the conformer shown in figure 3.72 (2) having the most stable is taken for the present studies. The data for the three conformations are shown in table 3.46.

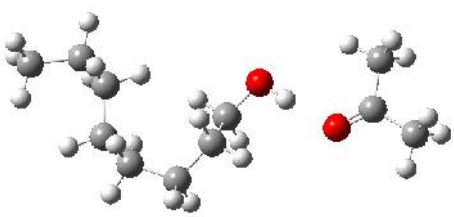

Structure (1)

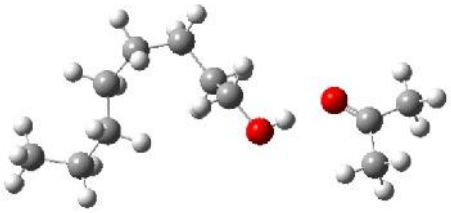

Structure (2)

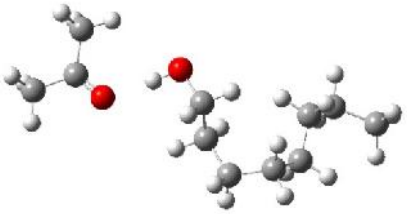

Structure (3)

Figure 3.72: Three conformationsof acetone-octanol 1:1 binary.

Table 3.46: Computational modeling data of acetone-octanol 1:1 binary structure shown in fig. 3.72.HF energy (hartree) and dipole moment (debye).

Basis	Parameter	Acetone	Octanol	Structure 1	Structure 2	Structure 3
STO-3G	HF Energy	-189.536032779	-383.605075453	-573.148240821	-573.148240822	-573.148239171
	Dipole Moment	1.9186	1.4209	2.9751	2.9748	2.9642
6-31G	HF Energy	-191.875161568	-388.115036549	-580.001745050	-580.001692484	-580.001692485
	Dipole Moment	3.6072	2.0199	3.6199	3.6117	3.6112
6-31G(d)	HF Energy	-191.962236330	-388.274454112	-580.246455603	-580.246369058	-580.246455604
	Dipole Moment	3.1188	1.6896	3.7470	3.5740	3.7468
6-31G(d,p)	HF Energy	-191.972071644	-388.307067725	-580.288437289	-580.288795797	-580.288795817
	Dipole Moment	3.1406	1.6525	4.0193	3.5307	3.5296

Solvation data of acetone-octanol system is shown in table 3.47

Table 3.57: Solvation modeling data of three acetone –octanol 1:1 binary structure shown in fig. 3.72.HF energy (hartree) and dipole moment (debye).

Basis	Parameter	Acetone rich region	Octanol rich region
	HF Energy	-189.536340864	-383.606132213
STO-3G	Dipole Moment	1.7032	1.6292
	HF Energy	-191.876256500	-388.116459919
6-31G	Dipole Moment	4.0768	3.2940
	HF Energy	-191.962944131	-388.275525613
6-31G(d)	Dipole Moment	3.7571	2.7558
	HF Energy	-191.972824421	-388.307957459
6-31G(d,p)	Dipole Moment	3.7784	2.6563

Hydrogen bond distance between oxygen of C=O acetone and hydrogen of O-H of hexanol are 1.82050 $\overset{o}{A}$ for structure 1, 1.82054 $\overset{o}{A}$ for structure 2 and 1.82048 $\overset{o}{A}$ for structure 3. Second weak hydrogen bond between oxygen of O-H and hydrogen attached to side chain of acetone are 2.90786 $\overset{o}{A}$, for structure 1, 2.90779 $\overset{o}{A}$ for structure 2 and 2.90905 $\overset{o}{A}$ for structure 3.

The calculated hydrogen bond energy is shown in table 3.48

Table 3.48: Hydrogen bond energy of three acetone-octanol 1:1 binary.

Basis set	Structure1 (kcal/mol)	Structure2 (kcal/mol)	Structure3 (kcal/mol)
STO-3G	4.475771	4.475772	4.474736
6-31G	7.245816	7.212830	7.212831
6-31G(d)	6.127736	6.073428	6.127737
6-31G(d,p)	5.834538	6.059505	6.059518

3.4.6.2 Dielectric studies

Dipole moment of 1:1 binary liquid of acetone-octanol binary mixture is determined and the result are shown in table 3.49 and fig. 3.73. The experimentally determined dipole moment « =2.9D compared well with the simulation result of 1:1 conformer in table 3.56.

Table 3.49: Dielectric data of acetone-hexanol 1:1 mixture in benzene solution

Concentration (mol/cc)	£$_{12}$	n_{12}^2	¢
0.000086	2.34	2.25	0.076000
0.000172	2.39	2.24	0.128997
0.000258	2.47	2.24	0.211992
0.000345	2.56	2.24	0.307976
0.000431	2.66	2.24	0.404985
0.000517	2.77	2.23	0.523952
0.000603	2.81	2.24	0.557976
0.000689	2.89	2.23	0.646937
0.000775	2.93	2.22	0.683952
0.000862	3.02	2.23	0.773952

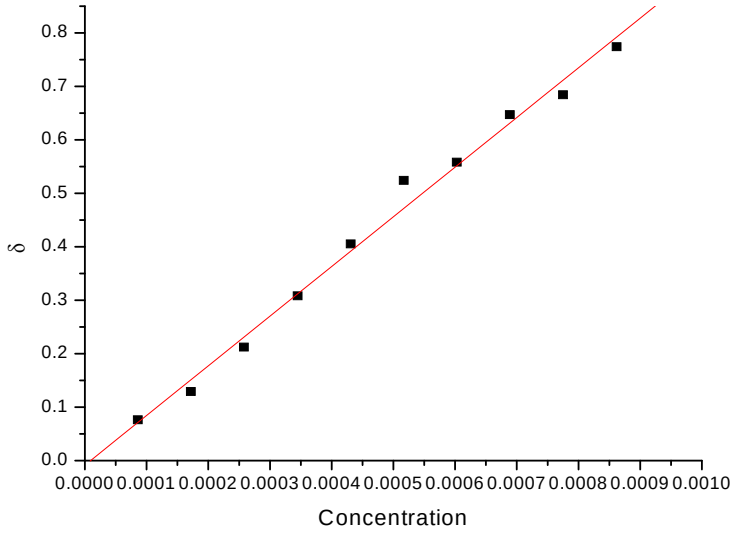

Figure 3.73: δ vs. concentration of the binary system used to determine the experimental dipole moment.

3.4.6.3 FTIR studies

The IR spectrum of acetone-octanol over the entire concentration is reported. The O-H peak in fig. 3.74 shows a red shifted hydrogen bonding and C=O shows a blue shifting hydrogen bond in fig.3.75 and similarly for C-H stretching frequency in fig.3.76.

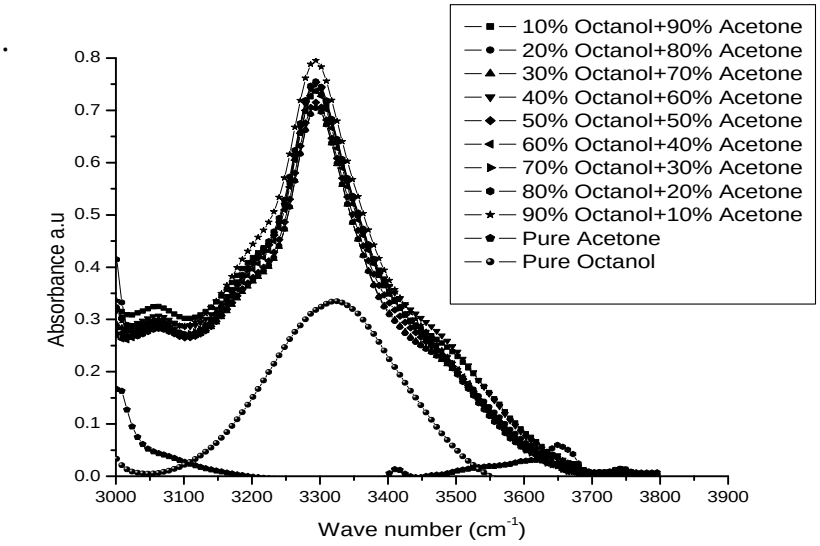

Figure 3.74: O-H stretching acetone-octanol mixture.

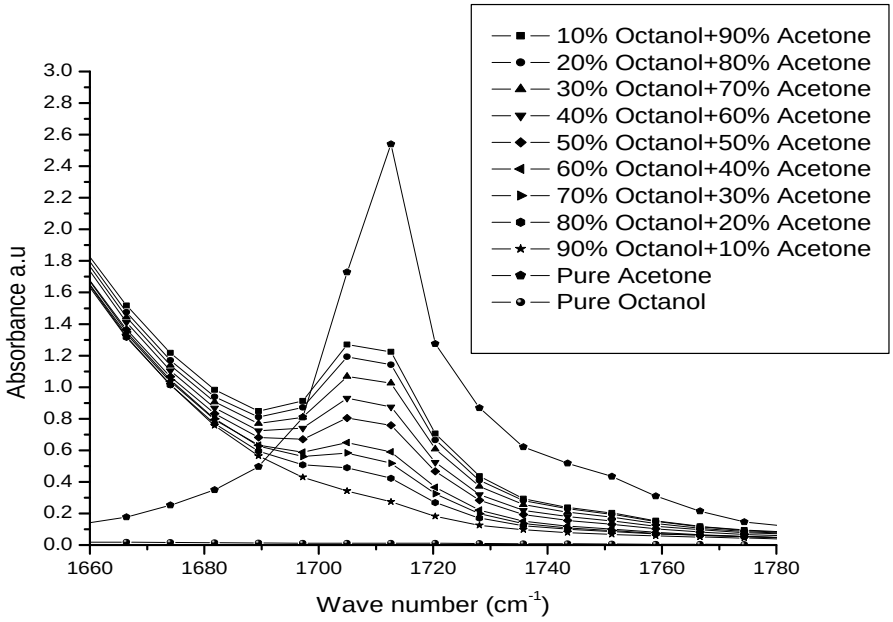

Figure 3.75: C=O stretching frequency of acetone-octanol mixture.

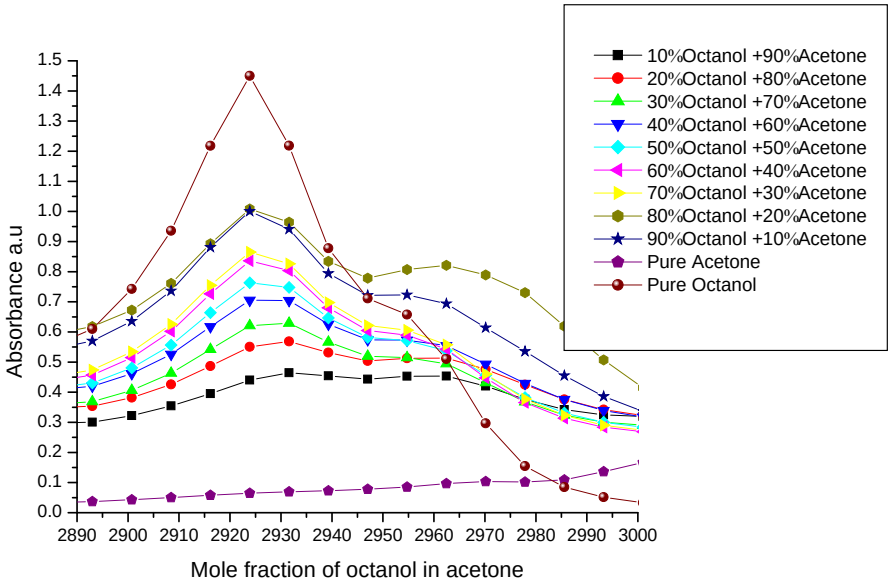

Figure 3.76: C-H stretching frequency of acetone-octanol binary mixture.

3.4.3.4 Wetting studies

Variation of contact angle of binary mixture of acetone-hexanol binary system for the enire concentration range is shown in fig.3.77 along with the corresponding surface tension in fig. 3.78.

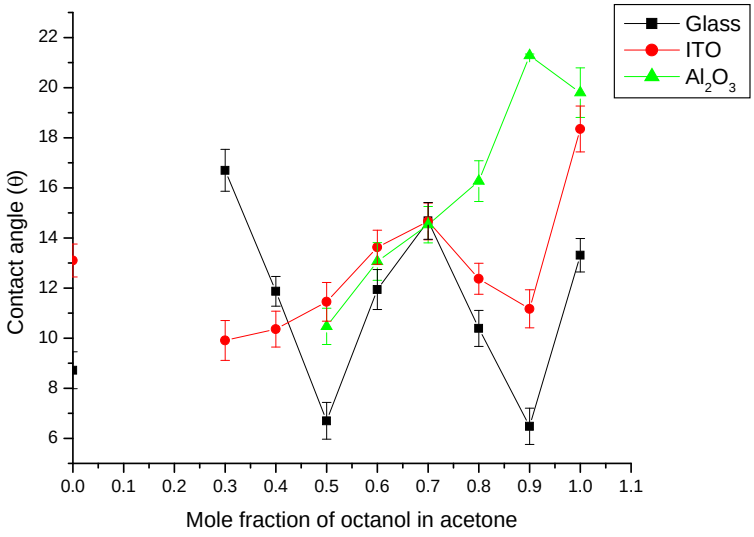
Glass
ITO
Al_2O_3
Contact angle (θ)
Mole fraction of octanol in acetone

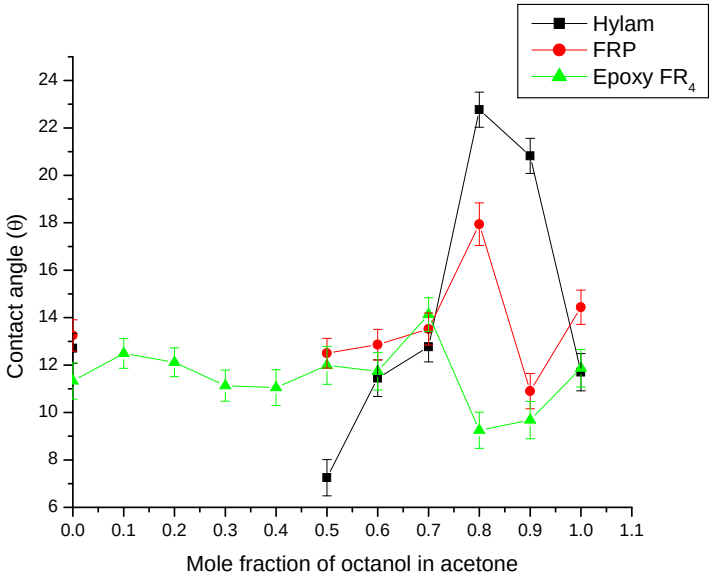
Hylam
FRP
Epoxy FR_4
Contact angle (θ)
Mole fraction of octanol in acetone

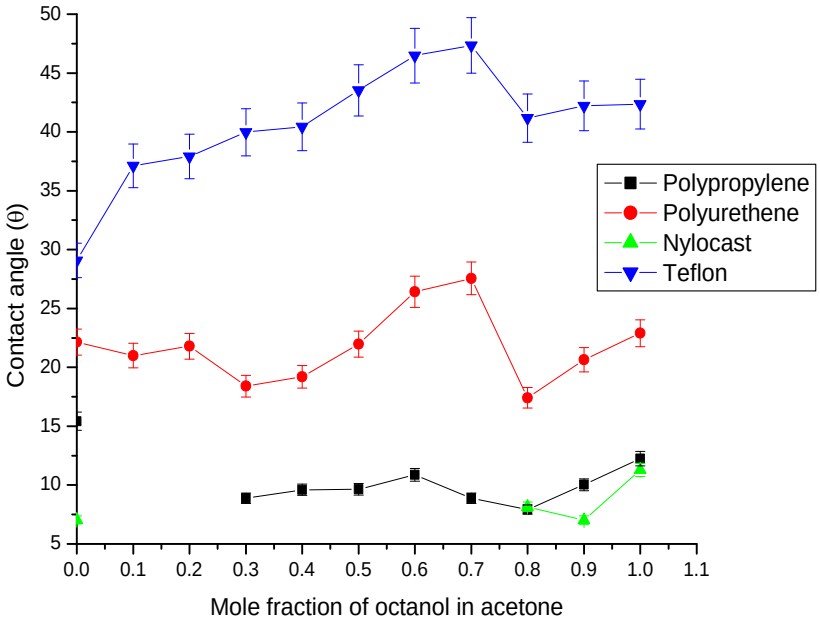

Figure3.77: Variation of contact angle with mole fraction of octanol in acetone over different substrates.

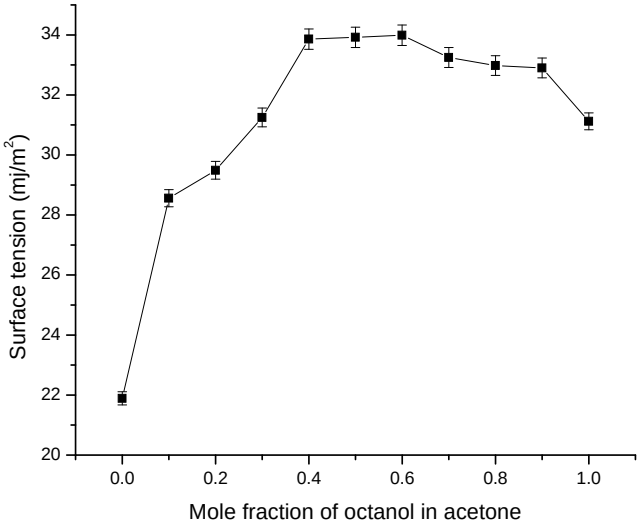

Figure 3.78: Variation of surface tension with mole fraction of octanol in acetone

Overall summary

For aniline-alcohols binary mixtures, six systems namely - aniline-methanol, aniline-ethanol, aniline-isopropanol, aniline-butanol, aniline-hexanol and aniline-octanol have been analyzed in this studies. Moreover,the mode of interaction between the two moieties is observed through wetting studies, FTIR studies, dipole moment calculation and computational conformational analysis. All studies show interaction of the type N-H--O hydrogen bonding. At about 10%-40% aniline concentration clusters of alcohol clusters are broken by aniline. Although literature suggests a secondary weak interaction the present studies do not show any secondary hydrogen bond. Since aniline chemically reacts with polymer a few substrates are taken for the present studies.

For the second system, acetone-methanol, acetone-ethanol, acetone-isopropanol, acetone-butanol, acetone-hexanol and acetone-octanolare studied. All the systems show ring like structure with a second weak hydrogen bond exist in acetone alcohols system. Solvation analysis is good for acetone rich region but is inadequate for the highly hydrogen bonded methanol rich region. Experimentally determined dipole moment is adequate to describe 1:1 structure. IR spectra show the characteristic red shift of OH peak and blue shift in CH indicating the formation of C-H--O peak for higher concentration of alcohol. Contact angle data indicates the breaking of HB on addition of acetone to alcohols. This is seen in the reduction of surface tension of the binary liquid and also in the decrease in contact angle. The formation of ring like conformer also contributes to the larger $\bar{}$ value compared to the low alcohol concentration. The contribution of side chain length is seen mainly at the C-H peak position of aniline-acetone binary mixture.

Aniline-alcohol systems show maximum interaction in the 10%-40% concentration of aniline whereas acetone-alcohol system shows maximum interaction around 50% concentration. Aniline-alcohols systems interact by mean of a single hydrogen bond, where as acetone-alcohol system exhibit two hydrogen bonds-one strong and one weak. The contact angle made by C=O--H complexes is seen to be far less than that made by N-H--O complexes. This is in agreement with the corresponding electro-negativity of the N and O.

CHAPTER- 4

Adhesion of Bio-Molecules to Substrates

Chapter 4
Adhesion of Bio-Molecules to Substrates

Introduction

The adhesion of bio molecules to various substrates is the topic of study of this chapter. Interaction of amino acids and two proteins namely Bovine Serum Albumin (BSA) and Ubiquitin are chosen for the present study. The substrates chosen are glass and indium tin oxide (ITO). The list of all substrates is given in table 4.1. In addition amino acids and proteins are coated on glass substrate layer by layer and their wetting properties are studied. The details are presented at the respective sections.

Biomolecules interact among themselves in a highly specific manner (Nussinov *et al*., 2011). They are able to selectively bind to other molecules by recognizing a specific site among many others that are available. This recognition has to be rapid and is usually dictated by long-range electrostatic interactions (Zhang *et al*., 2011).

Proteins are important components of all living cell (Alberts *et al*., 2004). Protein-protein interactions are interactions that help different proteins to bind together to form protein complexes. These complexes perform specific biological function such as DNA replication. Protein-protein interactions are mainly governed mostly by hydrophobic interactions, hydrogen bonding and Vander Waals interactions. Hydrophobic interactions are entropic in nature. They arise out of the breaking of hydrogen bonds in water by non-polar solute. The protein-protein interactions have two components-the transportation and the

reaction steps (Schluttig *et al*., 2010). In the present study, only the reaction step is considered.

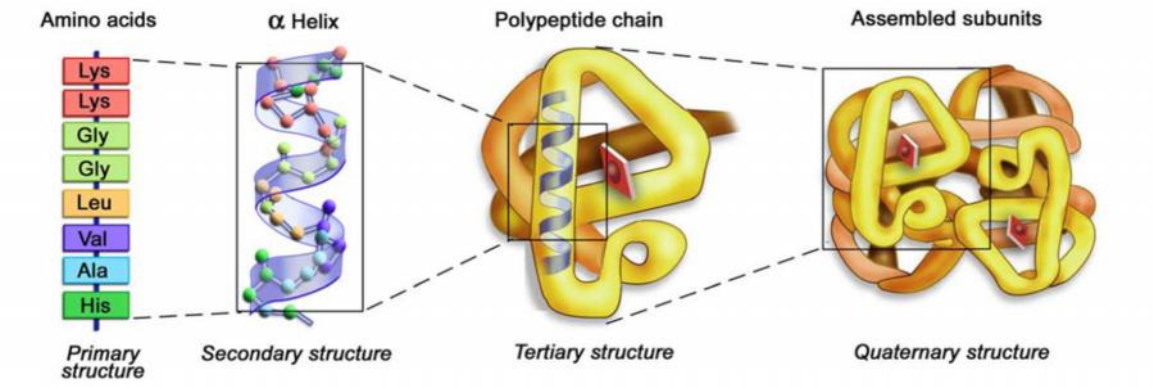

Figure 4.1: Structure of biomolecules (Lehninger *et al*., 2003)

Proteins (polypeptides) can transform their conformation through various mechanisms due to change in temperature, pH, and environment and also through adsorption on surfaces. While protein adsorption is very quick (~ 1 sec), it takes a longer time (~ a few minutes) for a protein monolayer to be absorbed on almost any kind of surface.

Various *in vitro* (Howell *et al*., 2006), *in vivo* (Lleres *et al*., 2007), *in silico* (Matsuzaki *et al*., 2009); Current Medicinal Chemistry (Leis *et al*., 2010). *In silico* prediction of binding sites on proteins are used to study protein-protein interactions. Meirnyk and Thelen studies these interactions using a variety of biochemical techniques (Meirnyk and Thelen, 2008). Ruvisky et al studies the changes in the side chain conformation since they are helpful in development of better protein-protein docking methods. Longer side chains with three or more dihedral angles are seen to undergo

conformational changes in protein-protein interations where as smaller side-chains did not show such changes (Ruvinsky *et al*., 2011)

Hence, understanding protein-protein interaction is important for learning about cell function, to understand, an underlying molecular interactios is necessary (Talley *et al*., 2008; Jones and Thornton, 1996; Sheinerman *et al*., 2000)

Interaction of proteins with surfaces has been a topic of interest owing to their importance in development of biomaterial (Latour, 2005) and in nanoelectronics (Sarikaya *et al*., 2003). Proteins interact well with inorganic materials (Sarikaya., *et al* 2003). Ceramics, metals, polymers (both synthetic and natural) and composities are the various classes of material generally used. The study of protein-surface interactions arises from their ability to modify cell adhesion, trigger biological cascade response for implants and also initiate other bio-adhesion such as marine fouling and bacterial adhesion. Experiments to determine the exact nature of protein-surface interaction are extremely challenging as these interactions involve probing of solid-biomolecular interactions in a liquid environment. Proteins adsorb on a surface only when the change in Gibb's free energy (G) of the system is

$$\Delta_{ads}G = \Delta_{ads}H - T\Delta_{ads}S < 0$$

H= enthalpy
S=entropy
T= Temperature

Here, system refers to the combined (protein+liquid+surface)

This case is similar to a drop of protein liquid placed as a sessile drop over a substrate. The equilibrium condition of such a drop can be explained either in term of the thermodynamic minimization of energy or in term of a mechanical equilibrium of forces (De-Genes and

Brocharel-Wyart, 2004). The later interpretation is simpler and gives an understanding of the equilibrium, which is commensurate with the result from thermodynamic interpretation. Hence, in the present work, interaction of amino acids and proteins with various substrates is probed through contact angle studies.

4.1 Wetting of amino acid surfaces.

As with chapter 3, smaller molecules are taken up as a simple model system in order to understand the interactions that exist in larger (polypeptides) proteins. In this part, the interactions of amino acids with surfaces through contact angle studies are taken up. The list of amino acids taken up for the present study along with their properties pertinent to the work is given in table 1 and fig 4.2.

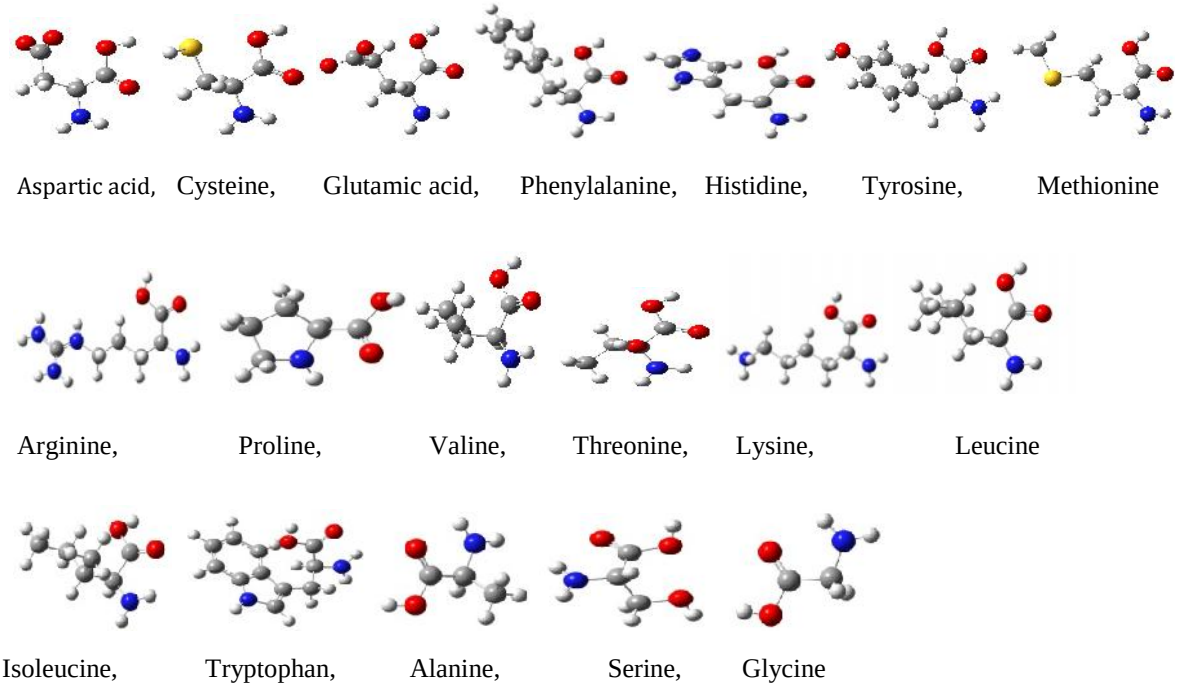

Figure 4.2: Structures of amino acids.

Table 4.1: Amino acids chosen for the present study and their properties.

Amino acids	Acid/Basic /Neutral*	Designation (BMS.data bank)	Polar.energy (mj/m^2)	Dispersive energy (mj/m^2)	Total.energy (mj/m^2)
Aspartic acid	Acid/Polar	W	26.97	40.52	67.49
Cysteine	Neutral/Slightly polar	L	27.00	38.63	65.63
Glutamic acid	Acidic/Polar	W	29.90	29.43	59.34
Phenylalanine	Neutral/Non-polar	L	35.11	24.02	59.13
Histidine	Basic/Polar	N	33.91	21.71	55.63
Tyrosine	Neutral/Polar	N	27.90	27.95	55.85
Methionine	Neutral/Non-polar	L	24.65	27.97	52.62
Arginine	Basic/Polar	W	24.54	27.47	52.01
Proline	Neutral/Non-polar	W	12.85	38.02	50.87
Valine	Neutral/Non-polar	L	31.55	18.94	50.49
Threonine	Neutral/Polar	W	25.51	21.25	46.76
Lysine	Basic/Polar	W	13.85	27.76	41.61
Leucine	Neutral/Non-polar	L	7.69	32.50	40.18
Isoleucine	Neutral/Non-polar	L	05.10	35.04	40.14
Tryptophan	Neutral/Slightly polar	L	6.10	33.97	40.07
Alanine	Neutral/Non-polar	N	12.30	27.42	39.72
Serine	Neutral/Polar	W	05.41	33.47	38.89
Glycine	Neutral/Non-polar	W	08.06	30.58	38.64
Bovine serum albumin	Polar	-	4.76	34.89	39.64
Ubiquitin	Polar	-	34.29	22.91	57.20
W=Hydrophilic	L=Hydrophobic	*Amino acids wikipedia			

The polar, dispersive and total surface energies reported in table 4.1 are determined using the multi-liquid tool discussed in chapter 2.

This part of the work consists of four parts (a) interaction of test liquids with amino acid substrates (b) variation of contact angle with time (c) interaction of amino acids with glass and ITO substrates and (d) thickness induced wetting transition in amino acids.

4.1.1 Interaction of test liquids with amino acids

Supersaturated solutions of amino acids in water are prepared and are deposited on glass substrates using a simplified spin-coating method discussed in chapter 2. A 6 «*l* drop of the supersaturated solution is placed on the spin coater where the glass slide is kept and dried first at room temperature. The contact angles made by three reference liquids, water, diiodomethane and glycerol, are measured and are shown in fig. 4.3.

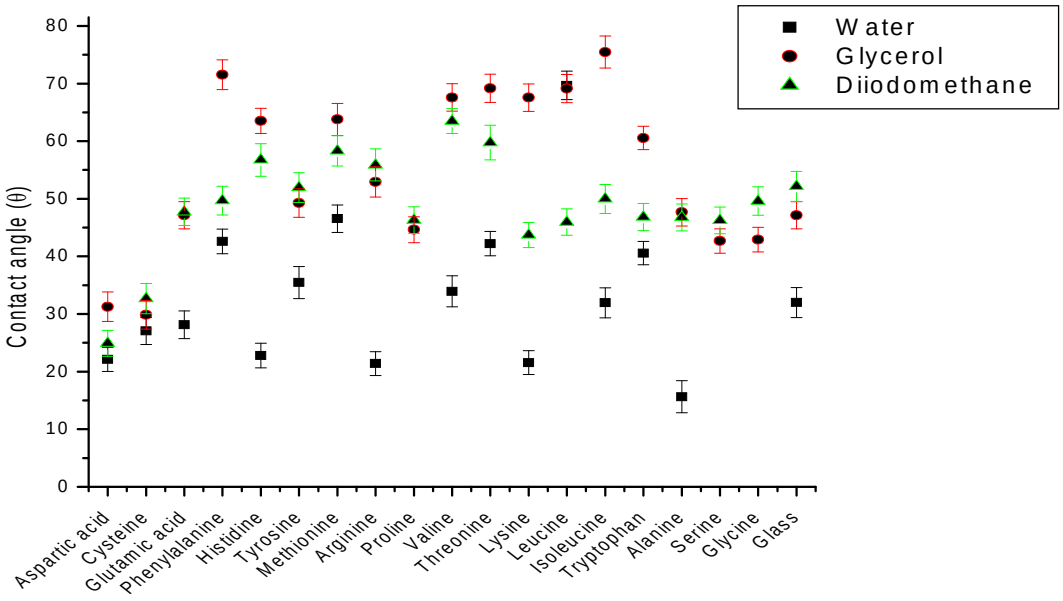

Figure: 4.3.Static contact angle of amino acids coated on glass by water, diiodomethane and glycerol.

As expected the contact angle of water for the three hydrophobic amino acids, namely phenylalanine, isoleucine and tryptophan is greater than the rest of the amino acids, while the data of diiodomethane and glycerol show similar trends.

4.2 Variation of contact angle with time measurement

The dynamic studies measured and contact angles of diiodomethane and glycerol over amino acids coated substrates are given in fig. 4.4. The contact angle of diiodomethane is constant with respect to time indicating a stable molecular interaction between diiodomethane and the amino acids. Glycerol drops show rapid decrease of contact angle (~ 15^{o}) for the initial 40 second, followed by linear decrease in contact angle. This is attributed to higher viscosity of glycerol. Higher viscosity requires a longer time to attain equilibrium. Hence diiodomethane is chosen as the test liquid in the next part of experiment.

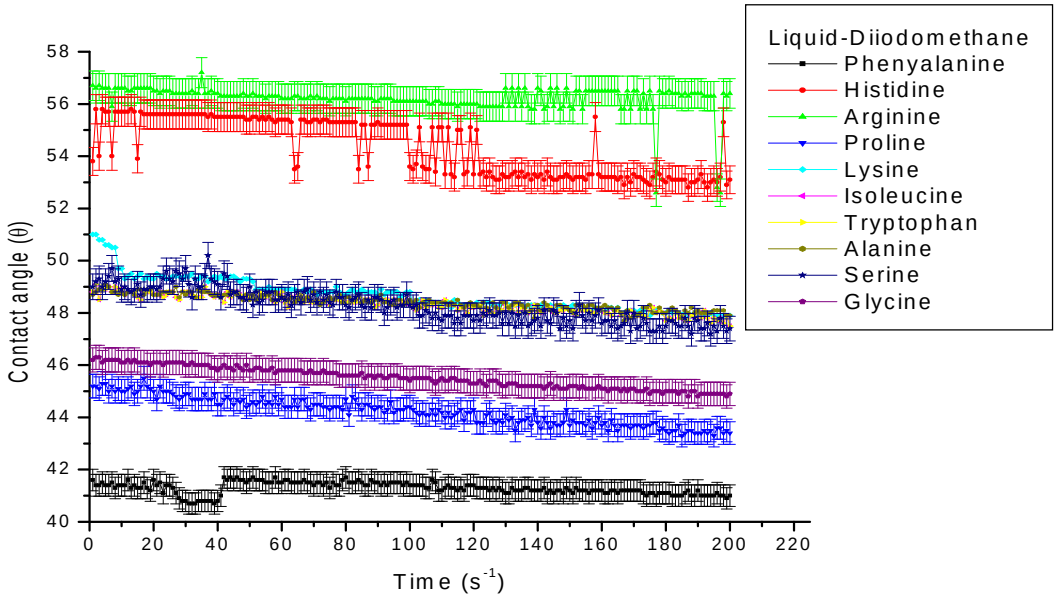

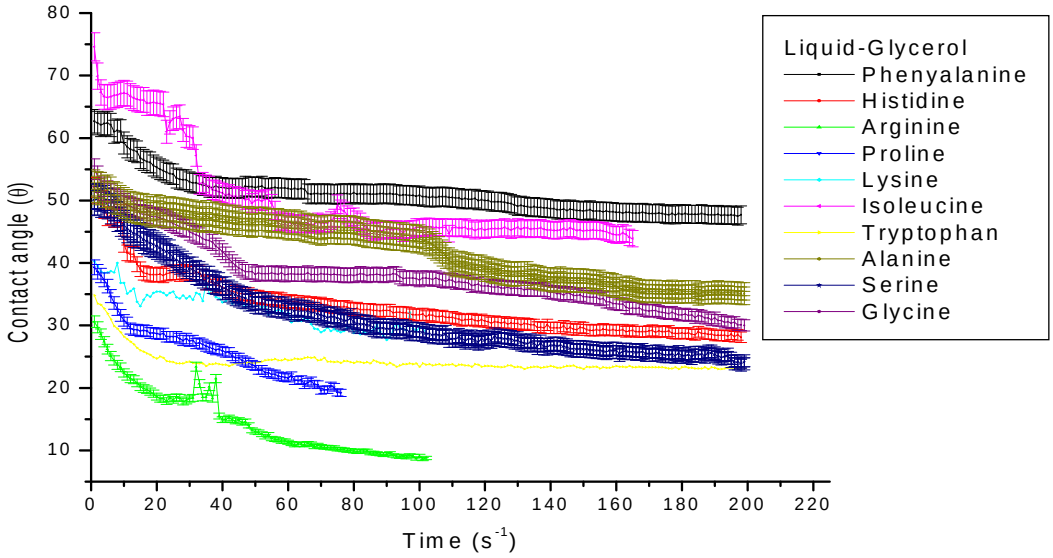

Figure 4.4: Variation of contact angle with time for amino acids coated on glass by diiodomethane and glycerol.

Since water interacts with amino acids extensively, the contact angles made by diiodomethane/glycerol are taken up for further studies, having observed that their contact angles on amino acids are similar to that of water, as seen from fig. 4.3.

The variation of contact angle with time for diiodomethane and glycerol over various amino acid substrates are shown in fig. 4.4. While the interaction of diiodomethane with amino acids exhibits a constant angle profile with respect to time, the contact angle of glycerol shows a rapid decrease for the first 40-60 second followed by a linear variation. From fig. 4.3 it is apparent that all three liquids show a mere or less similar interaction with the amino acids. Hence, the rapid decrease in contact angle seen in the case of glycerol is attributed to its high viscosity and density. For the same volume, a drop of glycerol is heavier than a drop of diiodomethane. Therefore as soon as a drop of glycerol is placed, it spread due to gravity, leading to a rapid decrease in the contact angle. After the initial spread, the rest of the

wetting process proceeds similar to that of diiodomethane. Since diiodomethane shows a stable $\bar{}$ vrs t graph, hence it is taken up for further studies.

4.3 Interaction of amino acids with surfaces

Study of interaction of amino acids with various substrates is of current interest (Paszti *et al.,* 2008). These studies are important in understanding the nature of interaction as well as for their potential application to bio medical devices such as bio MEMS. Adsorption of leucine on hydrophilic and hydrophobic surfaces has been reported through molecular dynamics simulation studies (Trudeau and Hore, 2010). Leucine is seen to adsorb on hydrophobic surfaces with its non-polar end towards the surface and when it is adsorbed on hydrophilic surfaces the attachment is through two orientations – one similar to the hydrophobic surface with the non-polar end towards the surface and the other with the entire molecule aligned flat on the surface. In the first case, there are reactive atoms available for the next layer whereas in the second case, no reactive site is available Adsorption of leucine on polystyrene surfaces has been reported by Hall *et al* (Hall *et al.,* 2011) using a combination of experimental and computational techniques.

From the above studies the conformation of adsorbant is appeared to be dependent on the nature of the substrate on to which the amino acid is adsorbed. This is verified through sum-frequency generation IR spectra of some amino acids on fused silica that did not show any ordered adsorbant layer, regardless of the kind of amino acid. On the other hand the adsorbant layer showed the formation of crystallites on drying of the layer, while on TiO_2 they showed an ordered layer (Pastzi *et al.,* 2008).

In most cases, the interaction between the amino acid and the surface can be understood in terms of the surface charges of the substrate and the net charge of the amino acid, in what is called the "lure and lock" model. Electrostatic interactions first lure the amino acid to the surface and then local interactions lock the molecules of the two systems together through weak, local interactions(Cruceanu *et al*., 2006).

The contact angle made by solution of amino acids on the substrates is given in table 4.2.

Table 4.2: Contact angle of amino acids on different substrates with their surface energy.

Substrates	Surface Energy (mj/m^2)			Contact Angle(θ)									
	Polar	Dispersive	Total	Arginine	Histidine	Lysine	Tryptophan	Isoleucine	Serine	Glycine	Phenylalanine	Alanine	Proline
Glass	29.22	26.52	55.74	15.20	18.25	19.46	32.58	36.99	37.92	38.63	42.59	45.35	45.43
ITO	0.46	30.60	31.06	45.4	42.01	49.79	96.57	98.18	90.62	91.3	65.73	94.00	94.08

The data in table 4.2 clearly indicate a lower contact angle of lysine, arginine and histidine which is lower than that of all other amino acids. The surface of borosilicate glass is negatively charged due to of alkali ions modifiers that break the Si-O network, leaving oxide ions on the surface. The three amino acids that exhibit low contact angle are positively charged (Betts *et al*., 2003) It is hence deduced that the interaction between glass and the amino acids is based on electrostatic interactions between the two.

Indium Tin Oxide (ITO) films have been used as novel membrane exchange sensors on deposition of cellulose + insulating polymer layers (Hillebrandt *et al.*, 2002). Their

optical transparency is very useful in the fabrication of capacitance cells and bioMEMS. From table 4.2 it is seen that the contact angle of the test liquids over ITO is similar to that over glass in that the lowest contact angles are made by the positively charged three amino acids namely arginine, histidine and lysine. Thus, it is expected that the surface of ITO is negatively charged, like glass. It can hence be concluded that the measurement of contact angle made by the saturated solutions of various amino acids can be used to predict the surface charge of inorganic surfaces.

4.4 Thickness dependent wetting.

Contact angle made by diiodomethane on dried amino acid layers on glass of varying thickness is observed, and is reported in fig. 4.5. Each layer is deposited on glass by placing 6µl of saturated solution of amino acid in water using spin coating and drying technique. A second layer is deposited only after the previous layer has dried.

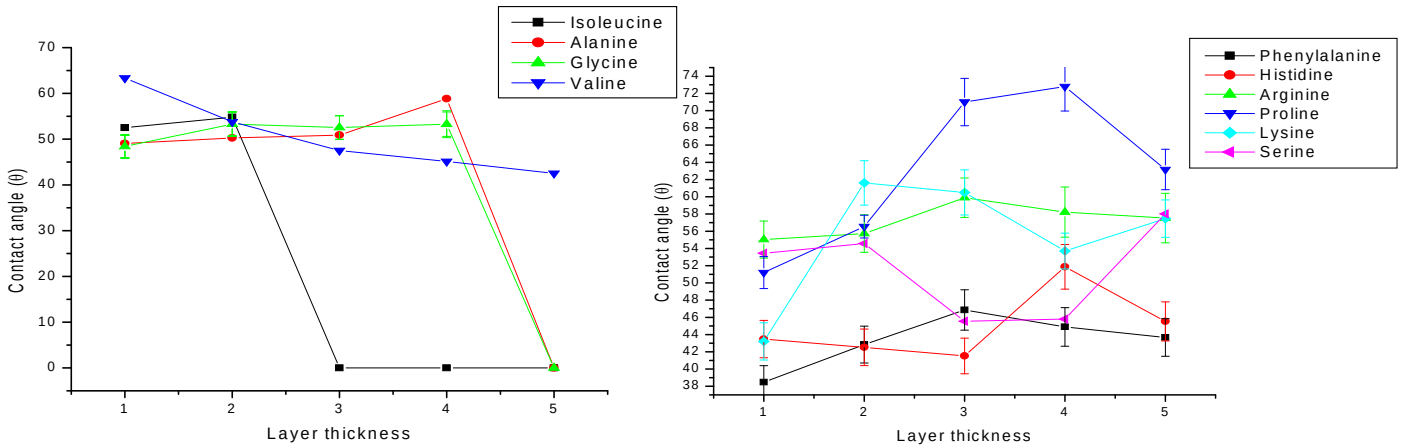

Figure 4.5: Contact angle of diiodomethane on layers of amino acids.

Glycine, alanine and isoleucine show a transition in contact angle from ~ 55^o to almost 0^o for different layer thickness. Other amino acids show a more-or-less constant contact angle for various thicknesses. It is evident from fig.4.5 that these three amino acids have a non-polar side group R and form a homologous series. The presence of a polar R is seen to cause the amino acid layer to be lyophobic while a non-polar R causes the amino acid to undergo a contact angle transition from about 50^o to 0^o. It is interesting to note from table 4.1 that in the pure form glycine is hydrophilic, alanine is neutral and isoleucine is hydrophobic. That is clear that depending on the polarity of R group and the thickness of layer deposited, a contact angle transition can be induced, turning a wetting surface to a non-wetting surface.

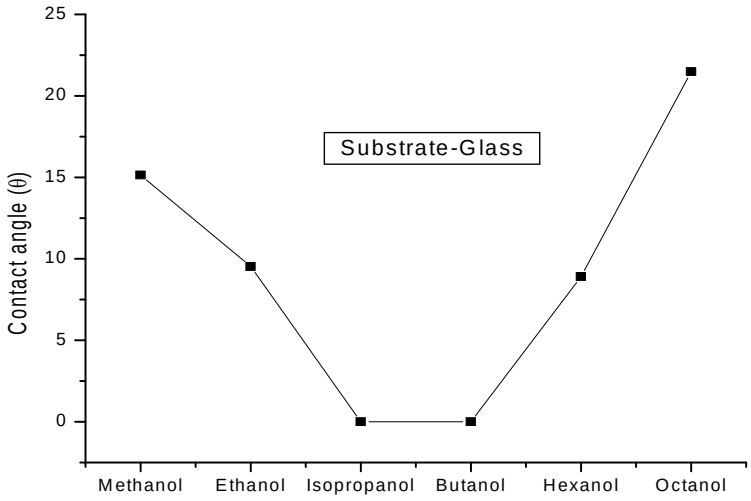

Figure 4.6: Chain length effect in contact angle.

As reported in chapter 3, fig. 4.6 shows that increase in the chain length of the alkyl R group has distinct interaction. When a comparison is made with biomolecules, their respective R group shows a peculiar behavior and it appear that the binding of amino acid to protein is also governed by the alkyl chain length as observed in this chapter.

Summary.

To summarize, it is seen that the interaction between an amino acid and a surface depends, not only on the nature of the amino acid but also on the nature of charges on the surface. Since water interacts with the amino acids and glycerol shows viscosity effects, diiodomethane is chosen as the test liquid, since its contact angle over amino acids is similar to that of water. Positively charged amino acids namely arginine, lysine and histidine are seen to adsorb preferentially on negatively charged surfaces such as borosilicate glass. The contact angles over ITO show trends similar to that of glass and hence it is concluded that ITO is negatively charged on the surface. Hence it is concluded that contact angle measurements can be used a tool to qualitatively determine the charge of a surface. Thickness dependent wetting transition is observed in the case of amino acid with alkyl side chains. The chain length dependent wetting trend is identical to that seen in the case of the interaction of alcohols over various substrates, as seen in chapter 3.

4.5 Interaction of Proteins with Surfaces

In the field of biomaterials, the first step is considered to be the adsorption of proteins on surfaces (Horbett, 2003). Protein adsorption on surfaces is important in the construction of micro and nano sensors and other such devices based on self-assembly and bio nano assembly techniques (Texter and Tirrell, 2001). Wetting studies performed for two proteins -BSA and ubiquitin, are presented here. Both proteins are globular but are vastly different in their sizes. Also, ubiquitin is known for its preferential binding to amino acids, as compared to BSA.

The motivation for the study of interactions of proteins with surfaces through contact angle studies is the following. Although there are many studies on such interactions, they are

fairly complex experiments. Some of the experimental techniques used to study protein-surface interactions are solution-depletion method (Noh and Vogler, 2007), radiolabelling (Moulton *et al*., 2003),enzyme-linked immunosorbent assay (ELISA) (Weber *et al*.,2002), ellipsometry (Seitz *et al.*, 2005), total internal reflection fluorescence (TIRF) (Toscano and Santore, 2006), optical waveguide light-mode spectroscopy (OWLS) (Ngankam *et al*., 2004) surface plasmon resonance (SPR) (Evans *et al*., 2006) neutron reflectivity (NR) (Forciniti and Hamilton, 2005),Electrochemical quartz crystal nanobalance (EQCN) (Cosman and Roscoe, 2004) and quartz crystal microbalance (QCM) (Hemmersam *et al*.,2005) X-ray photoelectron spectroscopy (XPS) (Ithurbide *et al*., 2007) surface matrix assisted laser desorption ionization time-of-flight mass spectroscopy (surface-MALDI-TOF-SIMS) (Ademovic *et al*., 2002) scanning tunneling microscopy (STM) (Li *et al*., 2003) have been used. Atomic force microscopy (AFM) and scanning electron microscopy (SEM) have been used to observe the conformation of surface adsorbed proteins (Pasche *et al*., 2005; Tunc *et al*., 2005). A detailed discussion about the experiments used is discussed by Ahmed and Omanovic (Ahmed and Omanovic, 2011)

As explained earlier, since the equilibrium conditions of interaction are similar to that of a sessile drop on a surface, the current work is taken up to see if contact angle measurements can be used as a qualitative first step towards understanding the interactions.

4.5.1 Bovine serum albumin (BSA)

Bovine serum albumin (BSA), as the name suggests, is a serum albumin derived from cows. It is made of 607 amino acids of which 18 are what are called signal peptides that are useful in the transportation of peptides. BSA is added in DNA fragmentation reactions to reduce the adhesion of enzymes used to pipettes etc. (Szabo *et al.,* 2002). Adhesion forces are usually measured using Atomic Force Microscopy techniques (Anand *et al.,* 2011). The effect of surface charge of a cationic monolayer on the adsorption of BSA is studied using ellipsometery methods (Watenabe *et al.*, 1986). The adsorption of BSA on hydroxyapatite ceramic is probed by measuring the zeta potential of the hydroxyapatite surface and by varying the pH of the BSA solution (Zhu *et al*, 2007).

The adsorption of BSA on titania as a function of ion concentration has been reported by de Serro *et al* (Serro *et al.*,1999). The presence of calcium and phosphate ions caused an increase in the hydrophllicity of the substrate by rapid adsorption of BSA. Also, the adsorption of only a small fraction of BSA on titania is attributed to electrostatic and/or conformational effects. The decrease in Y_{sl} with time for water/diiodomethane over titanium substrates pre-incubated in Hank's balanced salt solution and BSA has been observed and attributed to protein desorption form the substrate (Serro, 1997).

Adsorption and desorption of BSA on various polymers is studied using dynamic contact angle hysteresis using the Wilhelm plate method by Ueda *et al* (Ueda *et al*., 1995) and it is concluded that a faster desorption rate from some of the polymers is due to the poor interaction between BSA and the polymer. Adsorption of BSA from an aqueous solution on

silicon dioxide and silicon substrates is studied using in situ ATR-IR spectroscopy. Contact angle of water over monolayer BSA is found to be 53 ± 1^{o} and the film thickness to be 2.0-3.8 nm, assuming that the film is as thick as the bulk protein. BSA is seen to adsorb as a side-on monolayer with flattening of the protein due to denaturing. Furthermore protein unfolding is seen on hydrophobic surfaces compared to hydrophilic surfaces, with the contact angle being the same (Mc Clellan and Franses, 2005).

Stronger adhesion of BSA is seen on substrates that exhibited a water contact angle > 60^{o}-65^{o} where as the adhesion is poor for substrates with water contact angle $<60^{o}$ (Xu and Siedlecki, 2007). Adsorption of BSA on model hydrophilic (OH) and hydrophobic (CH_3) surfaces from quartz crystal microbalance studies and grazing angle infra red studies show that adsorption of BSA is a single step process and has a stronger affinity to CH3 compared to OH (Roach *et al.*, 2005). While the adsorption of BSA on hydrophilic and hydrophobic substrates is due to different mechanisms, the result is the passivation of the outer layer, identical for both the cases (Swerdyda *et al*., 2004). In both cases adsorption occurs until passivation of the outer layer as exhibited by a similar contact angle. Water content near the surface is found to be of importance in the desorption of BSA from metal surfaces (Anand *et al*., 2011).

The surface energy of amino acids and surface tension of the three liquids are given in table 4.1 and table 4.3 respectively. The contact angle made by the three test liquid on a substrate of BSA are shown in fig4.8, the contact angle show the expected trend. There is no variation of $\bar{}$ with time as in the case of amino acid, as seen from fig 4.9. Hence, no active adsorption or desorption from the surface is expected for these test liquids and the given substrates.

However, the contact angles made by the saturated aqueous amino acid drop on BSA surface show interesting results. The data are given in fig.4.9, while the contact angle made by most of amino acids is in the range of 70-80^{o}. The $\bar{}$ value for lysine is ~ 35^{o}. By looking into table 4.1 no specific reason for the anomalous value can be found.

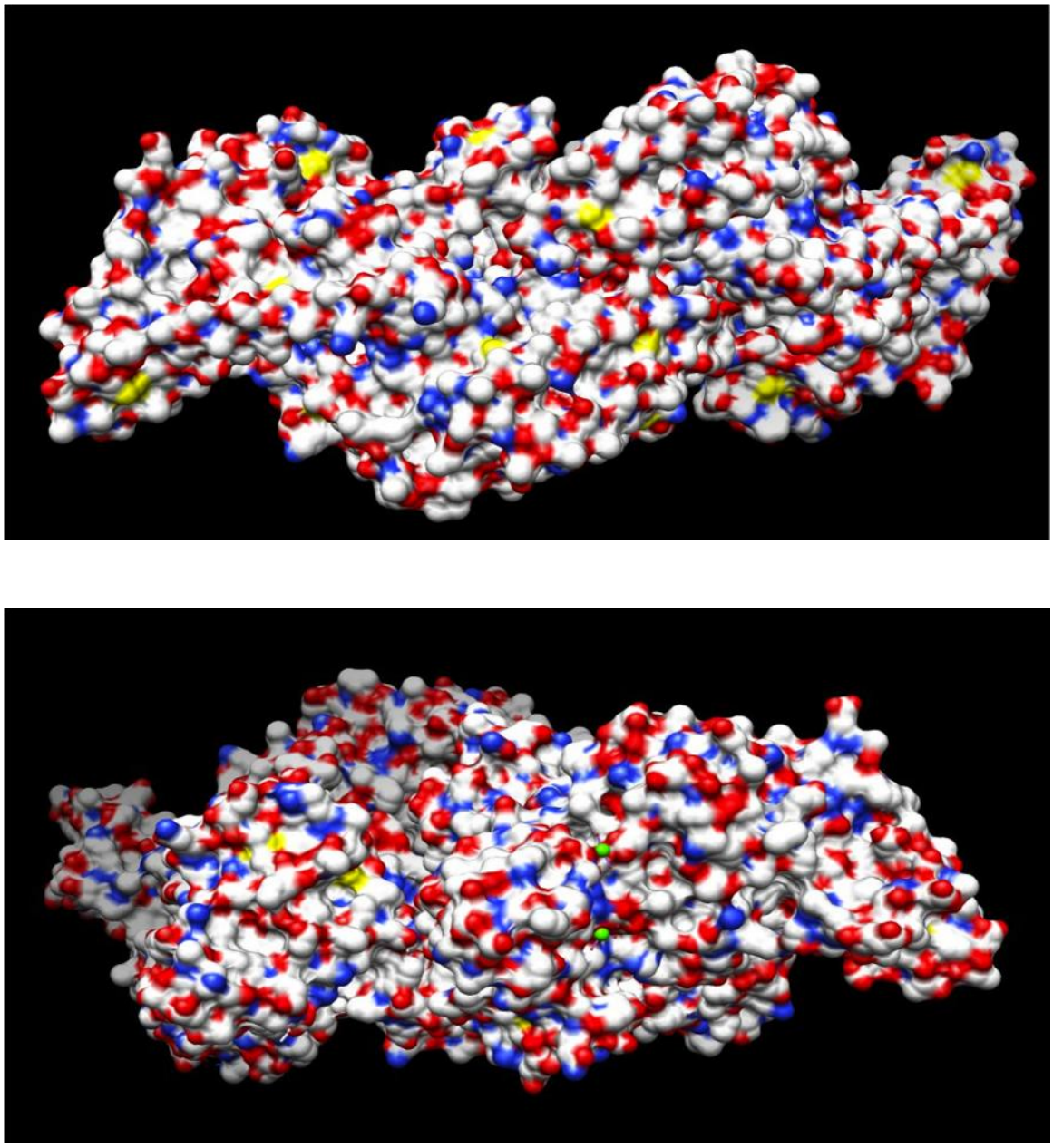

Figure 4.7: Bovine serum albumin structure.

Table 4.3: Surface tension of test liquids.

Test liquids	Surface tension (mj/m^2)
Water	72.46
Glycerol	63.79
Diiodomethane	51.21

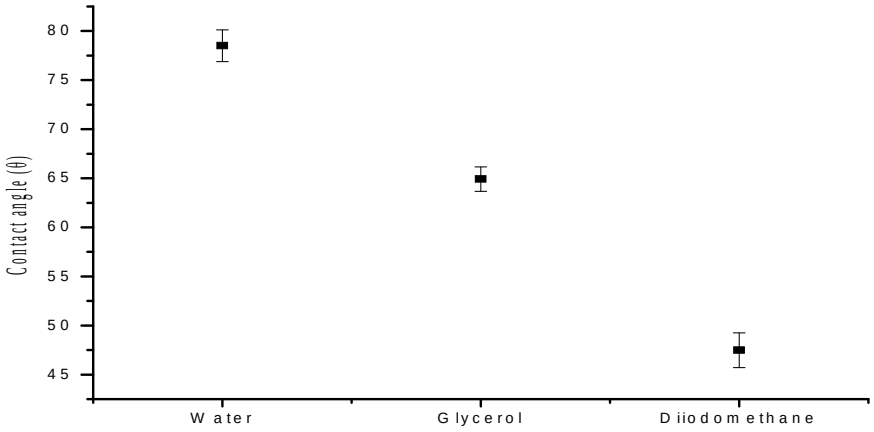

Figure 4.8: Contact angle of BSA on glass with water, diiodomethane and glycerol.

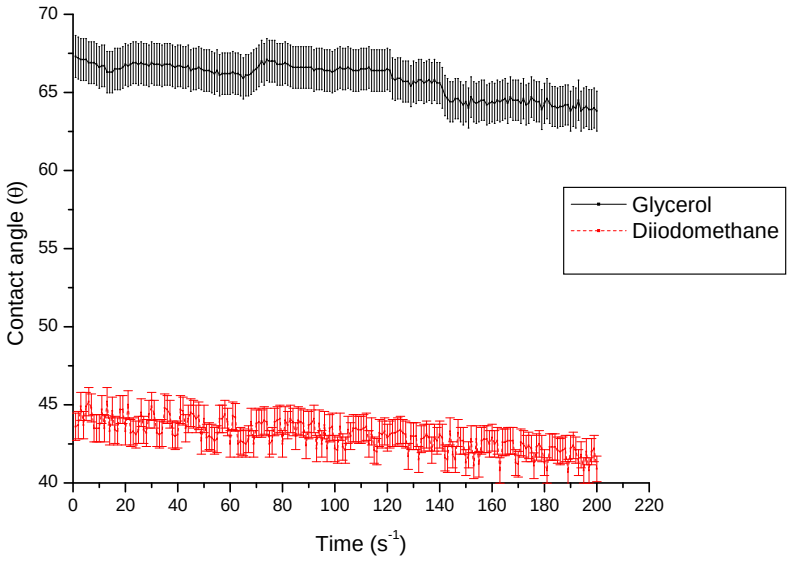

Figure 4.9: Contact angle of BSA on glass with diiodomethane and glycerol, time variation.

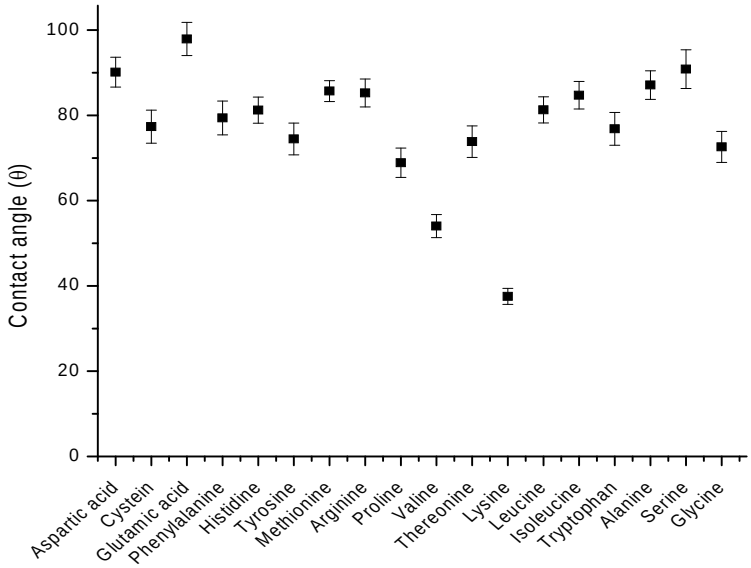

Figure 4.10: Contact angle of amino acids solution on BSA coated on glass.

The contact angles made by solutions of amino acids over BSA coated over glass surfaces is reported in fig. 4.10. The contact angle made by most amino acids is in the range of 70-80^{o} except for lysine where it is ~ 30^{o}. These results can be understood in terms of the surface charges present on BSA, as shown in fig.4.7. The two figures show the surface charges on either side of the protein structure (Majorek *et al*., 2011). The charges are obtained from the pdb database. As seen from the surface of BSA is predominantly negatively charged (red) or neutral (white) with a few parts of positively charged areas. Since, there is a dominance of negative charges on the surface, BSA binds readily to positively charged lysine and show a large contact angle for the negatively charged asparitic acid and glutamic acid. The large neutral surface charge is indicated in the lower contact angle of neutral amino acid valine. Since BSA protein has a large size and significant parts

of surface that are positive/negative/neutral charged, most amino acids, other than those discussed above, display contact angles between 70-80^{o}.

4.5.2 Ubiquitin

Ubiquitin consists of 76 amino acids and is among the smaller proteins exist in nature. Ubiquitin is a well-conserved protein meaning that its amino acid sequence is almost the same in all organisms. It is found throughout the cell and this ubiquitous existence gives it the name ubiquitin. It is a heat stable protein that folds up into a globular structure that is compact. It can exist either in the free form or as a complex with other proteins. When it forms a complex with other proteins the attachment is through the glycine on the end of ubiquitin and the lysine side chains of other proteins. It plays an important role in protein disposal and in transport of proteins in and out of cells. This is through covalent link to a target protein and this linkage is called ubiquitination. The selective transportation displayed by ubiquitin involves its specific binding to selective amino acids. Ubiquitin act as a marker for protein degradation (Sutovsky *et al*., 1999). Ubiquitin is altered at the initiation and progress of cancer (Hoelle and Dikic, 2009). Ubiquitin binds tightly to surfaces that contain propyl or hexyl groups in the correct concentration and are desorbed slowly over a period of 24-100 days (Chatzinikolaidou *et al.,* 2002).

As in the case of BSA, the surface charges of ubiquitin as determined from the pdb database structure (Vijay-Kumar *et al*., 1987) shown in fig. 4.11.Ubiquitin contain seven lysine residue at position 6, 11, 27, 29, 33, 48 and 63 through which it can be attached to the substrate or to one another (Wikipedia).

.

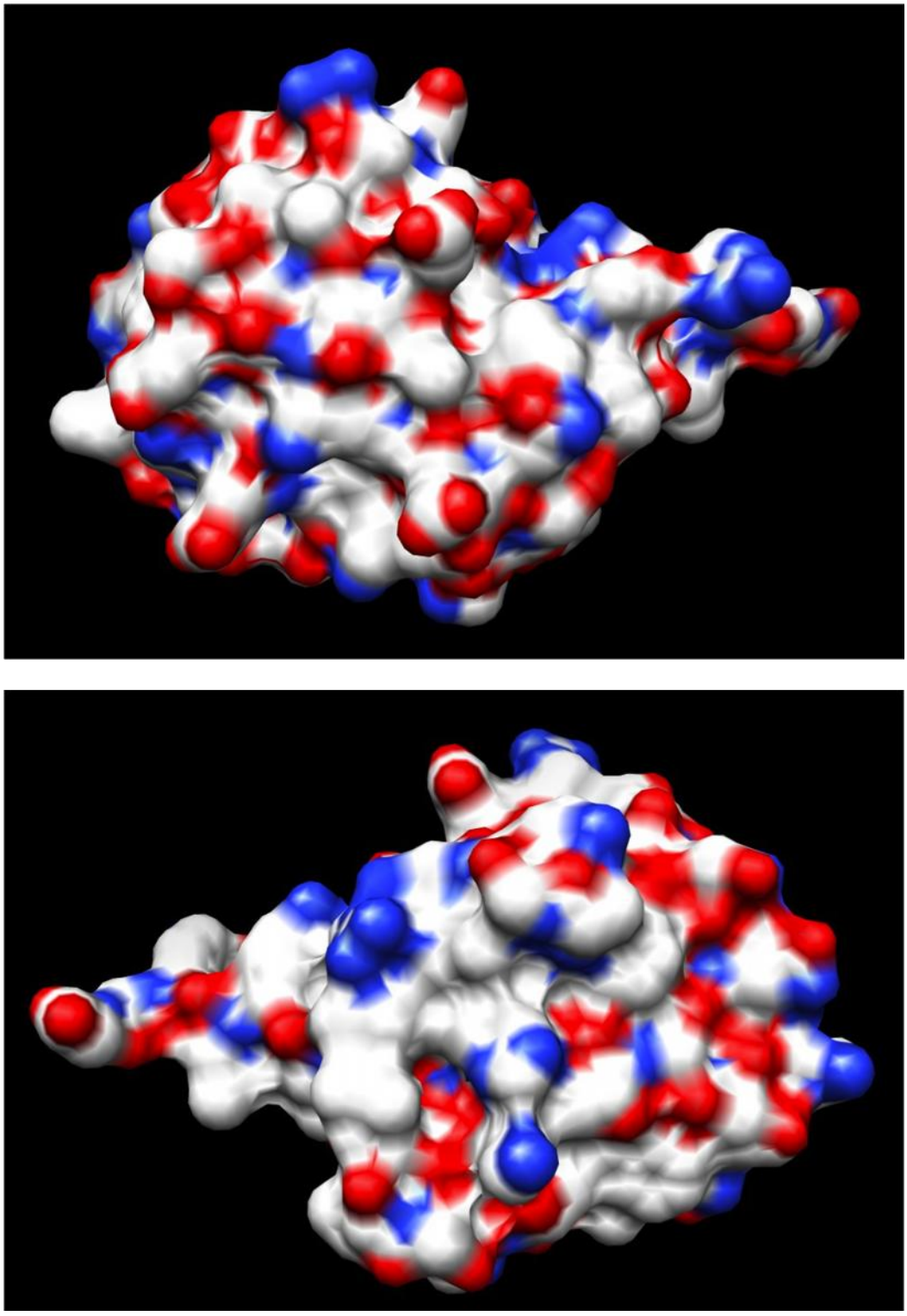

Figure 4.11: Ubiquitin structure.

Ubiquitin is characterized by its 6 lysine side chains in orange color, as shown in figure 4.12. Ubiquitin interacts predominantly through its lysine chains (Sundd *et al*., 2002; Saha *et al*., 2011)

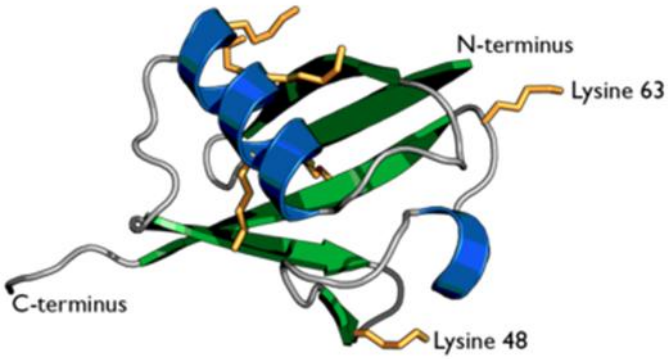

Figure 4.12: Ubiquitin link by lysine.

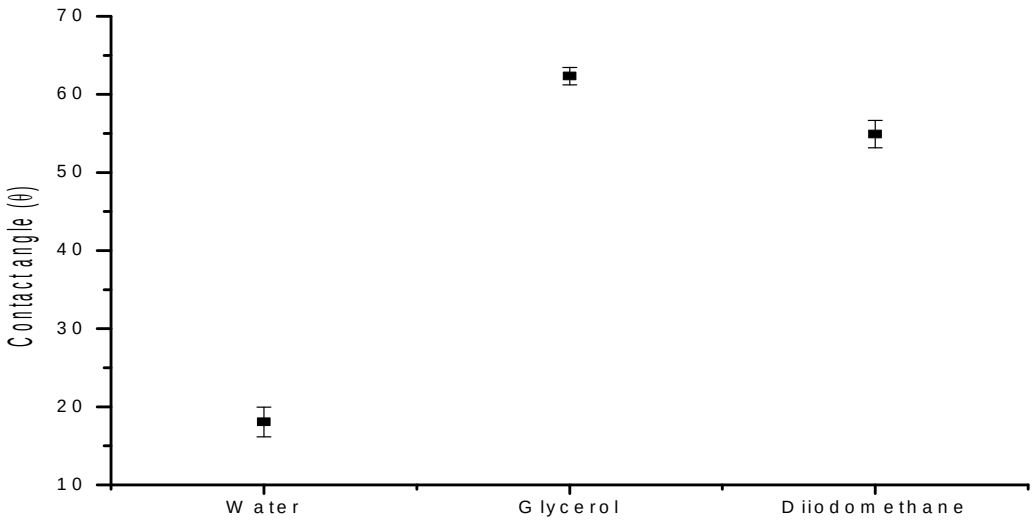

4.13: Ubiquitin on glass + water, diiodomethane and glycerol. Static

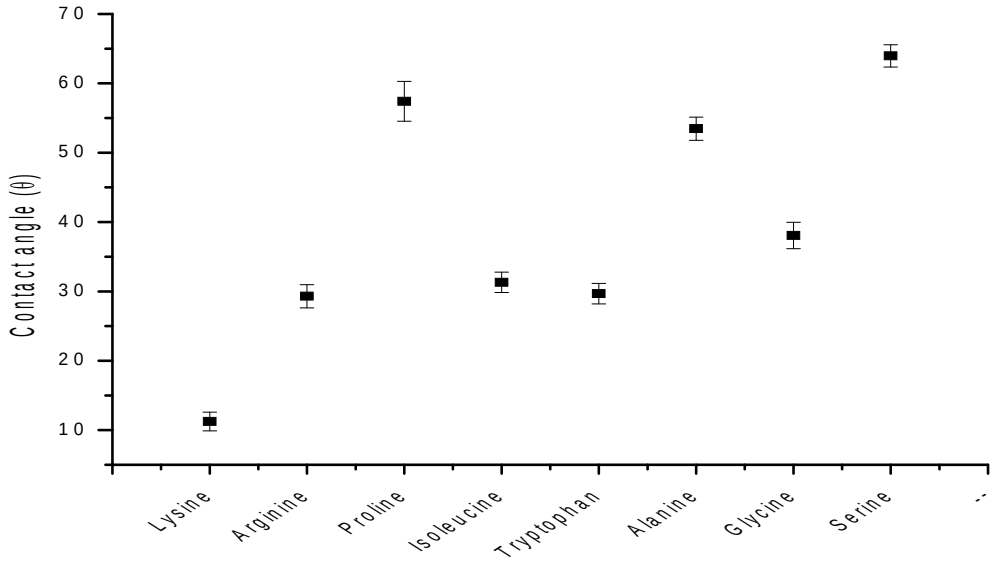

Figure: 4.14. Ubiquitin on glass with 8 Amino Acids

The contact angles made by solutions of amino acids over ubiquitin coated on glass surfaces is reported in fig. 4.14. Lysine has the lowest contact angle (~10^{o}) followed by arginine. The low contact angle with lysine is consistent with the known interaction of ubiquitin through lysine linkages. Lysine and arginine are positively charged and they interact with the negative charges on ubiquitin molecule. The non-polar amino acids show a larger contact angle.

Summary and Conclusions

Wetting behavior of amino acids and two proteins is reported in this chapter. From the wetting studies of amino acids the primary conclusions drawn are (a) there is no active adsorption-desorption for the first three minutes (b) positively charged amino acids bind better to the negatively charged surfaces of borosilicate glass and ITO and (c) amino acids with alkyl side chains display a thickness dependent wetting.

BSA and ubiquitin display wetting characteristics that are consistent with their surface charges. BSA displays a preference in bonding to positively charged lysine, as seen by the small contact angle. Ubiquitin has a very low contact angle for lysine solution and this is consistent with the known interactions of ubiquitin through lysine linkages.

To the best of our knowledge, this is the first time that contact angle measurements are shown ablility to detect specific protein-protein interactions. Measurement of contact angle is a fairly simple experiment, although a lot of care must be taken to avoid erroneous results due to presence of contaminants etc. Hence measurement of contact angle can be treated as a first step in understanding protein-protein/surface interactions.

Further, membranes used for reverse osmosis and ultra-filtration are often fouled by solutes that are attached to the membrane by hydrophobic and or electrostatic attraction (Koo *et al*., 2003). Hence understanding the electrostatic attractions in biological systems, especially to surface, is useful with the fabrication of better filtration equipment. Serum albumin is a known binder for the transportation of metal ions (Balet *et al*., 1998). Hence by understanding the nature of binding of BSA to other amino acids, and hence altering the surface charge and structure, BSA can be used as a metal sensor.

CHAPTER- 5

Summary and Conclusions

Chapter5

Summary and Conclusions

Intermolecular interactions in molecules relevant to biological systems were taken up for the present studies. The main approach taken for the present study was through small molecule prototyping where similar interactions that are existences in smaller molecules are used to understand interactions in larger and complex molecules. The complex molecules chosen for the study are two proteins, namely, bovine serum albumin and ubiquitin. Interactions involving proteins are understood through similar studies in amino acids and in binary liquids. The interactions between all these systems and surfaces is of special interest.

Binary liquids were used to understand the C=O···H and N—H···O hydrogen bonds and correlate with similar bonds present in biomolecules. For this, the liquids used are water, glycerol, diiodomethane, alcohols, aniline and acetone. Eighteen amino acid namely aspartic acid, cystein, glutamic acid, phenylalanine, histidine, tyrosine, methionine, arginine, proline, valine, threonine, lysine, leucine, isoleucine, tryptophan, alanine, serine and glycine were the samples of choice.

Conformational analysis using Hartree Fock-Self Consistent Field method is applied for the molecular analysis. At the same time, experimental techniques like contact angle measurement using goniometer, dipole moment calculation using RLC meter and Abbe refractometer and spectroscopic studies using FTIR are employed.

The salient results of the studies are briefly discussed below.

Systems with $N—H\cdots O$ hydrogen bond do not show any concentration variation of contact angle where as $C=O\cdots H$ does. Binary systems with aniline are not as conducive to the presence of a secondary weak hydrogen bond as binary systems containing acetone and alcohol. Weak hydrogen bonds are important for many biological systems.As for the interaction with the substrates is concerned, $N—H\cdots O$ shows a higher contact angle than $C=O\cdots H$. This trend is seen in the case of interactions of proteins where BSA, which contains larger percentage of nitrogen, displays a larger contact angle for the same liquid as compared to ubiquitin.

Contact angle of water on amino acid coated over glass reflected the hydrophobic/ hydrophilic nature of amino acids

When the amino acids are coated one layer after the other, three amino acids with alkyl ‘R’ group namely glycine, alanine and isoleucine showed a marked transition in the contact angle of diiodomethane from ~40^o to 0^o on increasing the number of layers (and hence the thickness of coating). The point of transition to complete wetting is when the chain length of alkyl chain is between 3 and 4 and this is similar to the effect seen in the case of alcohols with varying chain length.

There was no variation of contact angle with respect to time for water and diiodomethane. In the case of glycerol, the contact angle fall sharply for the few seconds and then reached an equilibrium. This is attributed to the high viscosity of glycerol and its density.

Contact angle of amino acids over two protein coated glass surfaces showed interesting results. The contact angle made by a drop of aqueous amino acid solution did not show any trend. However, certain amino acids such as lysine over BSA and isoleucine, tryptophan and glycine over ubiquitin displayed a very low contact angle compared to the other amino acids indicating specific amino acid protein interactions. The preference to certain amino acids is attributed to the electrostatic surface charges present on the protein and amino acid. Similar results were observed in the case of interactions of amino acids with glass and ITO surfaces.

It is evident that the interaction between glass and ITO with amino acids is different from the interaction of BSA and ubiquitin with amino acids. In the former case, the interactions can be explained purely based on electrostatic attraction between the two materials. Whereas, in the later in addition to a general electrostatic attraction, there are also specific steric interactions that cause lysine to bind strongly to proteins but not other positively charged amino acids like Arginine and histidine.

Hence it is possible to apply contact angle measurement as a qualitative tool to understand and predict specific biomolecular interactions. To the best of our knowledge, this is the first time that such a study has been undertaken

Such intermolecular hydrogen bond studies will shed a light in research and industrial purpose, and it will lead to the better fabrication of bio-devices like lab-on-chip, micro fluidic, biosensor and the beneficiary goes to rheological devices.

References

References

Ademovic, Z., Klee, D., Kingshott, P., Kaufmann, R. and Hocker, H. (2002). Minimization of protein adsorption on poly(vinylidene fluoride). *Biomol. Eng*.,**19**: 177-182.

Adya, A.K., Bianchi, L. and Wormald, C.J. (2000). The structure of liquid methanol by H/D substitution technique of neutron diffraction. *J. Chem. Phys*., **112**: 4231-4241.

Ahmed, K.H. and Omanovic, S. (2011). The Influence of Surface Potential on the Kinetics of Bovine Serum Albumin Adsorption on a BiomedicalGrade 316LVM Stainless Steel Surface. *World. Acad. Sci. Eng. Technol*., **77**: 491-497.

Alberts, B., Bray, D., Lewis, J., Raff, M., Roberts, K. and Watson, J.D. (1994). *Molecular biology of the cell*. Garland Publishing, New york., pp.3-11.

Ali, A., Tewari, K., Nain, A.K and Chakravortty, V. (2000). Study of Intermolecular Interaction in Dimethylsulphoxide+ 1-Alkanols (1-Butanol, 1-Hexanol, 1-Octanol). *Phys. Chem. Liq*., **38**: 459-473.

Anand, G., Zhang, F., Linhardt, R.J. and Belfort, G. (2011).Protein-associated water and secondary structure effect removal of blood proteins from metallic substrates. *Langmuir*., **27**:1830-1836.

Arunan, E., Desiraju, G.R., Klein, R.A., Sadlej, J., Scheiner, S., Alkorta, I., Clary, D.C., Crabtree, R.H., Dannenberg, J.J., Hobza, P. and others . (2011). Definition of the hydrogen bond (IUPAC Recommendations 2011). *Pure Appl. Chem*., **83**: 1637.

Atkins, P.W., Friedman, R.S. and Net Library, Inc. (1997*). Molecular quantum mechanics* (3th ed). Oxford University Press, Oxford.

Automatic RCL meter PM6303A user manual. (2005). Fluke corporation, Germany.

Autumn, K., Sitti, M., Liang, Y.A., Peattie, A.M., Hansen, W.R., Sponberg, S., Kenny, T.W., Fearing, R. and Israelachvili, J.N. (2002). Evidence for van der Waals adhesion in gecko setae. *Proc. Nat. Acad. Sci*., **99**: 12252-12256.

Bal, W., Christodoulou, J., Sadler, P.J. and Tucker, A.(1998).Multi-metal binding site of serum albumin. *J. Inorg. Biochem*., **70**: 33-39.

Benmore, C.J. and Loh, Y.L. (2000). The structure of liquid ethanol: A neutron diffraction and molecular dynamics study. *J. Chem. Phys*., **112**: 5877-5883.

Betts, M.J. and Russell, R.B. (2003). Amino-acid properties and consequences of substitutions. Bioinformatics for geneticists: In a bioinformatics primer for the analysis of genetic data, M.R.Barnes,(eds). John Wiley & Sons Limited, Chichester, UK, pp. 311-342.

Burton, C.J. (1948). A study of ultrasonic velocity and absorption in liquid mixtures. *J. Acoust. Soc. Am*., **20**: 186-199.

Carre, A. (2007). Polar interactions at liquid/polymer interfaces. *J. Adhes. Sci. Technol*., **21**: 961-981.

Chatzinikolaidou, M., Laub, M., Rumpf, H. and Jennissen, H.P. (2002). Biocoating of Electropolished and Ultra-Hydrophilic Titanium and Cobalt Chromium Molybdenum Alloy Surfaces with Proteins. *Materialwiss. Werkstofftech.,* **33**:720-727.

Chaudhari, A. and Mehrotra, S.C. (2002). Dielectric relaxation study of pyridine-alcohol mixtures using time domain reflectometry. *Mol. Phys*., **100**: 3907-3913.

Chen, B., Siepmann, J.I. and Klein, M.L. (2002). Vapor-liquid interfacial properties of mutually saturated water/1-butanol solutions. *J. Am. Chem. Soc*., **124**:12232-12237.

Cosman, N.P. and Roscoe, S.G. (2004). Electrochemical quartz crystal nanobalance (EQCN) studies of protein interfacial behavior at Pt. *Langmuir*., **20**:1711-1720.

Coutinho, K., Saavedra, N. and Canuto, S. (1999). Theoretical analysis of the hydrogen bond interaction between acetone and water. *J. Mol. Struc: THEOCHEM*., **466**: 69-75.

Cruceanu, M., Urbaneja, M.A., Hixson, C.V., Johnson, D.G., Datta, S.A., Fivash, M.J., Stephen, A.G., Fisher, R.J., Gorelick, R.J., Casas-Finet, J.R. and others . (2006). Nucleic acid binding and chaperone properties of HIV-1 Gag and nucleocapsid proteins. *Nucleic. Acids. Res*., **34**: 593-605.

De Genes, P.G. and Brochard-Wyart, F. D. (2004). Capillarity and Wetting Phenomena, ISBN 978-0-387-00592-8. *Springer.*, pp. 291.

DeBolt, S.E. and Kollman, P.A. (1995). Investigation of structure, dynamics, and solvation in 1-octanol and its water-saturated solution: molecular dynamics and free-energy perturbation studies. *J. Am. Chem. Soc*., **117**: 5316-5340.

Deshpande, D.D., Bhatgadde, L.G., Oswal, S. and Prabhu, C.S. (1971). Sound velocities and related properties in binary solutions of aniline. *J. Chem. Eng. Data*., **16**: 469-473.

Do Serro, A.P.V.A., Fernandes, A.C., Saramago, B.J.V. and Norde, W. (1999) Bovine serum albumin adsorption on titania surfaces and its relation to wettability aspects. *J. Biomed. Mater. Res*., **46**: 376-381.

Ellena, J., Goeta, A. E., Howard, J. A. K., Wilson, C. C., Autino, J. C. and Punte, G. (1999). Experimental evidence for the amino-group non-planarity in nitroanilines: neutron diffraction study of 2-methyl-5-nitroaniline at 100K. *Acta. Cryst*., **B55**: 209-215.

Evans-Nguyen, K.M., Fuierer R.R., Fitchett. B.D., Tolles. L.R., Conboy. J.C. and Schoenfish, M.H. (2006). Changes in adsorbed fibrinogen upon conversion to fibrin. *Langmuir*., **22**: 5115-5121.

Fattepur, R.H., Hosamani, M.T., Deshpande, D.K. and Mehrotra, S.C. (1994). Dielectric relaxation and structural study of aniline-methanol mixture using picosecond time domain reflectometry. *J.Chem.Phys*., **101**:9956-9960.

Forciniti, D. and Hamilton, W.A. (2005). Surface enrichment of proteins at quartz/water interfaces: A neutron reflectivity study. *J. Colloid Interface Sci*., **285**: 458-468.

Forlani, L. (2007). *Hydrogen bonds of anilines' in the chemistry of anilines*, Z.R.Wiley (eds). An interscience publication, Jerusalem, pp.407-449.

Frisch, M. J., Trucks, G.W., Schlegel, H., Scuseria, G.E., Robb, M.A., Cheeseman, J.R., Montgomery, Jr J.A., Vreven, T., Kudin, K.N., Burant, J.C., Millam, J.M., Iyengar, S.S., Tomasi, J., Barone. V., Mennucci, B., Cossi, M., Scalmani, G., Rega, N., Petersson., G.A., Nakatsuji, H., Hada, M., Ehara, M., Toyota, K., Fukuda, R., Hasegawa, J., Ishid, M., Nakajim, T., Honda, Y., Kitao, O., Nakai, H., Klene, M.,

Li, X., Knox, J.E., Hratchian, H.P., Cross, J.B., Adamo, C., Jaramillo, J., Gomperts, R., Stratmann, R.E., Yazyev, O., Austin. A, J., Cammi, R., Pomelli, C., Ochterski, J. W., Ayala, P.Y., Morokuma, K., Voth, G.A., Salvador, P., Dannenberg, J.J., Zakrzewski, V.G., Dapprich, S., Daniels, A.D., Strain, M.C., Farkas, O., Malick, D. K., Rabuck, A.D., Raghavachari, K., Foresman, J.B., Ortiz, J.V., Cui, Q., Baboul, A.G., Clifford, S., Cioslowski, J., Stefanov, B.B., Liu, G., Liashenko, A., Piskorz, P., Komaromi, I., Martin, R.L., Fox, D.J., Keith, T., Laham, M.A.A., Peng, C.Y., Nanayakkara, A., Challacombe, M., Gill., P.M.W., Johnson B., Chen, W., Wong, M.W., Gonzalez & C., Pople,J.A. (2003).Gaussian *03.*, Revision B.03., Gaussian., Inc., Pittsburgh PA.

Gallant, M., Tan, P.V.M. and Wuest, J.D. (1991). Use of hydrogen bonds to control molecular aggregation. Association of dipyridones joined by flexible spacers. *J. Org. Chem*., **56**: 2284-2286.

Gray, J.J. (2004). The interaction of proteins with solid surfaces. *Curr. Opin .Struc.Biol*., **14**: 110-115..

Guardia, E., Marti, J., Garcia-Tarres, L. and Laria, D. (2005). A molecular dynamics simulation study of hydrogen bonding in aqueous ionic solutions. *J. Mol. Liq.*, **117**: 63-67.

Guggenheim, E.A. (1951). The computation of electric dipole moments. *Trans. Faraday Soc*., **47**: 573-576.

Hall, S.A., Jena, K. C., Trudeau, T.G. and Hore, D.K. (2011). Structure of Leucine Adsorbed on Polystyrene from Nonlinear Vibrational Spectroscopy Measurements,

Molecular Dynamics Simulations, and Electronic Structure Calculations. *J. Phys. Chem. C*., **155**: 11216-11225.

Han, S.W. and Kim, K. (1996). Infrared Matrix Isolation Study of Acetone and Methanol in Solid Argon. *J. Phys. Chem*., **100**:17124-17132.

Hansen, F.K. (2004).*The Measurement of surface energy of polymer by means of contact angles of liquids on solid surfaces.A short overview of frequently used methods*. University of Oslo, Oslo, pp. 1-12.

Hemmersam. A.G., Foss, M., Chevallier, J. and Besenbacher, F. (2005). Adsorption of fibrinogen on tantalum oxide, titanium oxide and gold studied by the QCM-D technique. *Colloids. Surf. B*., 43: 208-215.

Hillebrandt, H., Tanaka, M. and Sackmann, E . (2002). A novel membrane charge sensor: Sensitive detection of surface charge at polymer/lipid composite films on indium tin oxide electrodes. *J. Phys. Chem. B*., **106**: 477-486.

Hirsch, T.K. (2003). *Computational-chemistry studies of hydrogen bonding networks in crystalline materials and liquid water*, ISBN: 91-7265-731-6. Stockholm University, Stockholm, pp 2-39.

Hoeller, D. and Dikic, I. (2009). Targeting the ubiquitin system in cancer therapy. *Nature*., **458**: 438-444.

Horbett, T, A. (2003). Biological activity of adsorbed proteins. *Surfact. Sci. Ser*., **110**:393-413.

Howell, J.M., Winstone, T.L., Coorssen, J.R. and Turner, R.J. (2006). An evaluation of in vitro protein--protein interaction techniques: Assessing contaminating background proteins. *Proteomics*., **6**: 2050-2069.

http://www.bmrb.wisc.edu/referenc/commonaa.php. Downloaded on 23th May 2012 at 3:30 Pm.

http://en.wikipedia.org/wiki/Amino_acid. Downloaded on 20th May 2012 at 4 Pm.

http://en.wikipedia.org/wiki/Ubiquitin. Downloaded on 20th May 2012 at 1:30 Pm.

Ithurbide. A., Frateur. I., Galtayries, A. and Marcus, P. (2007). XPS and flow-cell EQCM study of albumin adsorption on passivated chromium surfaces: Influence of potential and pH. *Electrochim. Acta*., **53**: 1336-45.

Ivanova, I. I., Pomakhina, E. B., Rebrov, A. I., Hunger, M., Kolyagin, Y. G. and Weitkamp, J. (2001). Surface Species Formed during Aniline Methylation on Zeolite H–Y Investigated by in Situ MAS NMR Spectroscopy. *J. Catal*., **203**: 375-381.

Ivanova, I.I., Pomakhina, E.B., Rebrov, A.I., Hunger, M., Kolyagin, Y.G. and Weitkamp, J. (2001). Surface species formed during aniline methylation on zeolite HY investigated by in situ MAS NMR spectroscopy. *J. Catal*., **203**:375-381.

Jakobsen, R.J. and Brasch, J. W. (1965). Far infrared studies of the hydrogen bond of phenols. *Spectrochim. Acta*., **21**: 1753-1763.

Jensen, F. and My Library.(1999). *Introduction to computational chemistry* (2nd ed). Wiley, New York.

Jiang, L. and Lai, L. (2002). CH--O hydrogen bonds at protein-protein interfaces. *J. Bio. Chem*., **277**: 37732-37740.

Jones, S. and Thornton, J. (1996). Principles of protein-protein interactions derived from structural studies. *Proc. Nat. Acad. Sci.,* **93**:13-20.

Jorgensen, W. (1986). Optimized Intermolecular Potential Function for Liquid Alcohol. *J. Phy. Chem*. **90**:1276-1284.

Kentsch, J. Breisch, S. and Stelzle, M. (2006). Low temperature adhesion bonding for BioMEMS. *J. Micromech. Microeng*., **16**: 802-807.

Koo, J. and Hong, S.P. and Hyung, H. and Kim, Y.H. and Yoon, S. and Kim, S.S. (2003). Fouling resistant reverse osmosis membranes. Copy right © 2003 American water work association: Membrane Technology Conference.

Kusalik, P.G., Lyubartsev, A.P., Bergman, D.L. and Laaksonen, A. (2000). Computer Simulation Study of tert-Butyl Alcohol. 2. Structure in Aqueous Solution. *J. Phys. Chem. B*., **104**: 9533-9539.

Lakshmanan, P. and Govindasamy, M. (2011). Molecular interaction studies in binary mixtures containing aniline, toluene and n-butanol. *Turk. J. Phys* **35**:303-310.

Latour, RA. (2005). Biomaterials: Protein-surface interactions. *Encyclopedia. Biomater. Biomedic. Engg*., 1: 270-278.

Lehninger, A. H., Nelson, D. L. and M M Cox. (2000). *Principles of biochemistry*. Fifth Edition (Freeman Publishers. New York. p, 171-184.

Leis, S., Schneider, S. and Zacharias, M. (2010). In silico prediction of binding sites on proteins. *Curr. Med. Chem*., **17**:1550-1562.

Li, L.Y., Chen, S.F. and Jiang, S.Y. (2003). Protein adsorption on alkanethiolate self assembled monolayers:Nanoscale surface structural and chemical effects. *Langmuir*., **19**: 2974-2982.

Lin, Y. and Mao, C. (2011). Bio-inspired supramolecular self-assembly towards soft nanomaterials. *Front. Mater. Sci*., 1-19.

Lleres, D.,Swift, S. and Lamond, A.I. (2007). Detecting protein-protein interactions in vivo with FRET using multiphoton fluorescence lifetime imaging microscopy (FLIM). *Curr. Protoc. Cytom*., **42**: 1-12.

Madhurima, V., Purkayastha, D.D. and Rao, N. V. S. (2011). Wettability, FTIR and dielectric studies of 1, 4-dioxane and water system. *J. Colloid Interface Sci*., **357**: 229-233.

Madhurima, V., Viswanathan, B. and Murthy, VRK. (2006). Effect of steric hindrance of ketones in the dielectric relaxation of methanol+ ketone systems. *Phys. Chem. Liq*., **44**: 563-569.

Mafun, F., Takeda, Y., Nagata, T. and Kondow, T. (1994). Inhomogeneous solvation in an aniline-ethanol solution studied by laser photoionization of a liquid beam. *Chem. Phys. Lett*., **218**:234-239.

Matsuura, H., Yoshida, H., Hieda, M., Yamanaka, S., Harada, T., Shin-Ya, K. and Ohno, K. (2003). Experimental evidence for intramolecular blue-shifting CH--O hydrogen

bonding by matrix-isolation infrared spectroscopy. *J. Am. Chem. Soc*., **125**: 13910-13911.

Matsuzaki, Y., Matsuzaki, Y., Sato, T. and Akiyama, Y. (2009). In silico screening of protein-protein interactions with all-to-all rigid docking and clustering: an application to pathway analysis. *J. Bioinformatics. Comput. Biol*., **6**: 991-1012.

McClellan, S.J. and Franses, E.I. (2005).Adsorption of bovine serum albumin at solid/aqueous interfaces. *Colloids Surf., A*., **260**:265-275.

Miernyk, J.A., Thelen, J.J. (2008). Biochemical approaches for discovering protein--protein interactions. *The Plant Journal*., **53**: 597-609.

Mohan, T.M., Sastry, S.S. and Murthy, V.R.K. (2011). Thermodynamic, Dielectric and Conformational Studies on Hydrogen Bonded Binary Mixtures of Propan-1-ol with Methyl Benzoate and Ethyl Benzoate. *J. Solution Chem*., **40**: 131-146.

Morokuma, K. (1971). Molecular Orbital Studies of Hydrogen Bonds. III. C [Double Bond] O··· H [Single Bond] O Hydrogen Bond in HCO··· HO and HCO··· 2HO. *J. Chem. Phys*., **55**:1236.

Moulton, S.E., Barisci, J.N., Bath, A., Stella, R. and Wallace, G.G . (2003).Investigation of protein adsorption and electrochemical behavior at a gold electrode. *J. Colloid Interface Sci.*, **261**: 312-319.

Musah, R.A. and Goodin, D.B. (1997). Introduction of novel substrate oxidation into cytochrome c peroxidase by cavity complementation: oxidation of 2-aminothiazole and covalent modification of the enzyme. *Biochem*. **36**:11665-11674.

Nagata, I. and Sano, M. (1992). Thermodynamics of associated solutions involving aniline and ethanol. *Thermochim. Acta*., **200:** 475-488.

Ngankam, A.P., Mao, G.Z. and Van-Tassel, P.R. (2004). Fibronectin adsorption onto polyelectrolyte multilayer films. *Langmuir*., **20**: 3362-3370.

Noh, H. and Vogler, E.A. (2007).Volumetric interpretation of protein adsorption: competition from mixtures and the Vroman effect. *Biomaterials*., **28**:405-422.

Novakovskaya, Y.V. (2012). Conjugation in hydrogen-bonded systems. *Struc. Chem.*, **23**:1-14.

Nussinov, R., Panchenko, A.R. and Przytycka, T. (2011). Physics approaches to protein interactions and gene regulation. *Phys. Biol*.,**8**: 030301.

Onsager, L.(1936). Electric moments of molecules in liquids. *J.Am. Chem. Soc*.,**58**: 1486-1493.

Owens, D. K. and Wendt, R. C. (1969). Estimation of the surface free energy of polymers. *J. Appl. Polym. Sci.,* **13** :1741-1747.

Paolantoni, M., Sassi, P., Morresi, A. and Cataliotti, R.S. (2005). Infrared study of 1-octanol liquid structure. *Chem. Phys*.,**310**:169-178.

Pasche, S. Voros, J., Griesser, H.J., Spencer, N.D. and Textor, M. (2005). Effects of ionic strength and surface charge on protein adsorption at PEGylated surfaces. *J. Phys. Chem. B.,109*: 17545-17552

Paszti, Z., Keszthelyi, T., Hakkel, O. and Guczi, L. (2008). Adsorption of amino acids on hydrophilic surfaces. *J. Phys. Condens. Matter*., **20**: 224014.

Patil, S.P., Chaudhuri, A.S., Lokhande, M.P., Lande, M.K., Shankarwar, A .G., Helambe, S. N., Arbad, B.R. and Mehrotra, S. C. (1999). Dielectric measurement of aniline and alcohol mixtures at 283, 293, 303 and 313 using the time domain technique. *J. Chem. Eng. Data*., **44**: 857-878.

Piehler, J. (2005). New methodologies for measuring protein interactions in vivo and in vitro. *Curr. Opin. Struc . Biol*., **15**: 4-14.

Popelier, P.L.A and Bader, R.F.W. (1992). The existence of an intramolecular C-H--O hydrogen bond in creatine and carbamoyl sarcosine. *Chem. Phys. Lett*., **189**: 542-548.

Rajagopal, K. and Chenthilnath, S. (2010). Excess thermodynamic studies of binary liquid mixtures of 2-methyl-2-propanol with ketones. *Indian J. Pure Appl. Phys*., **48**: 326-333.

Ramachandran, K., Sivagurunathan, P., Dharmalingam, K. and Mehrotra, S.C. (2007). Dielectric Relaxation Study of Amide-Alcohol Mixtures by Using Time Domain Reflectometry. *Acta. Physico-Chimica. Sinica*., **23**: 1508-1515.

Ray, N. and Bagchi, S. (2002). UV-Vis spectroscopic study of solvation in the ternary mixture methanol+ ethanol+ acetone. *Chem. Phys. Lett*., **364**: 621-627.

Roach, P., Farrar, D. and Perry, C.C. (2005).Interpretation of protein adsorption: surface-induced conformational changes. *J. Am. Chem. Soc*., **127**:8168-8173.

Roe, R.J., Bacchetta, V.L. and Wong, P.M.G. (1967). Refinement of pendent drop method for the measurement of surface tension of viscous liquid. *J. Phys. Chem*., **71**: 4190-4193.

Rojo, G., de la Torre, G., Garcia-Ruiz, J., Ledoux, I., Torres, T., Zyss, J. and Agullo-Lopez, F. (1999). Novel unsymmetrically substituted push-pull phthalocyanines for second-order nonlinear optics. *Chem. Phys*., **245**:27-34.

Ruvinsky, A.M., Kirys, T., Tuzikov, A.V. and Vakser, I.A. (2011). Side-chain conformational changes upon protein-protein association. *J. Mol. Biol*., **408:**356-365.

Saha, A., Lewis, S., Kleiger, G., Kuhlman, B. and Deshaies, R.J. (2011). Essential role for ubiquitin-ubiquitin-conjugating enzyme interaction in ubiquitin discharge from Cdc34 to substrate. *Mol cell*., **42**: 75-83.

Saha, R.P., Bahadur, R.P., Chakrabarti, P. (2005). Interresidue contacts in proteins and protein-protein interfaces and their use in characterizing the homodimeric interface. *J. Proteome. Res*., **4**:1600-1609.

Sahoo, A., Sarkar, S., Krishna, P.S.R., Bhagat, V. and Joarder, R. N. (2008). Molecular conformation and structural correlations of liquid D-1-propanol through neutron diffraction. *Pramana*., **71**:133-141.

Saiz, L., Padro, J. A. and Guardia, E. (1997). Structure and dynamics of liquid ethanol. J. *Phys. Chem. B*., **101**: 78-86.

Sarikaya, M., Tamerler, C., Jen, A.K.Y., Schulten, K., Baneyx, F. and others. (2003). Molecular biomimetics: nanotechnology through biology. *Nat. mater*., **2**: 577-585.

Sassi, P., Morresi, A., Paolantoni, M. and Cataliotti, R.S. (2002). Structural and dynamical investigations of 1-octanol: a spectroscopic study. *J. Mol. Liq*., **96**: 363-377.

Sathyan, N., Santhanam, V., Madhurima, V. and Sobhanadri, J. (1995). Conformational study on the binary mixture acetone-methanol involving H-bonding. *J. Mol. Struc: THEOCHEM*., **342**:187-192.

Scheiner, S., Kar, T. and Gu, Y. (2001). Strength of the C-H--O hydrogen bond of amino acid residues. *J. Biol. Chem*., **276**: 9832-9837.

Schluttig, J., Korn, C.B. and Schwarz, U.S. (2010). Role of anisotropy for protein-protein encounter. *Phys. Rev. E*., **81**: 030902.

Schmitz, D. (1972) Attenuated total reflection technique. *Pigm. Resin.Technol*., **1**: 29-32.

Seitz R., Brings, R. and Geiger R. (2005). Protein adsorption on solid-liquid interfaces monitored by laser-ellipsometry. *Appl. Surf. Sci*., **252**: 154-157.

Sheinerman, F., Norel, R. and Honig B. (2000). Electrostatics Aspects of Protein-Protein Interactions. *Curr. Opin. Struc. Biol.*, 10:153-159.

Sonar, A.N., Pawar, N.S. and Khairnar, M.D. (2011). Ultrasonic studies on molecular interaction of substituted heterocyclic compounds in acetone-water mixture at 303k . *Int. J. Appl. Biol. Pharm. Technol*., **2(3)**: 291-295.

Stokely, K., Mazza, M.G., Stanley, H.E. and Franzese, G . (2010). Effect of hydrogen bond cooperativity on the behavior of water. *Proc. Nat. Acad. Sci*., **107**: 1301-1306.

Strich, A. (1993). Quanta a handbook of concepts, By PW Atkins. *Int. J. Quantum Chem.*, **47**: 239-242.

Sundd, M., Iverson, N., Ibarra-Molero, B., Sanchez-Ruiz, J.M. and Robertson, A.D. (2002).Electrostatic interactions in ubiquitin: stabilization of carboxylates by lysine amino groups. *Biochem.*, **41**: 7586-7596.

Sutovsky, P., Moreno, R.D., Ramalho-Santos, J., Dominko, T., Simerly, C. and Schatten, G. (1999).Development: Ubiquitin tag for sperm mitochondria. *Nature*., **402**: 371-372.

Sweryda-Krawiec, B., Devaraj, H., Jacob, G. and Hickman, J.J. (2004). A new interpretation of serum albumin surface passivation. *Langmuir*., **20**:2054-2056.

Szabo, B., Siemes, S. and Wallmichrath, I. (2002). Short communication inhibition of gabaergic neurotransmission in the ventral tegmental area by cannabinoids. *Eur.J. Neurosci*., **15**: 2057-2061.

Talley, K., Ng, C., Shoppell, M., Kundrotas, P. and Alexov, E. (2008). On the electrostatic component of protein-protein binding free energy. *PMC. Biophys*., 1:2.

Tareste, D., Pincet, F., Lebeau, L. and Perez. (2007). Hydrophobic forces and hydrogen bonds in the adhesion between retinoid-coated surfaces. *Langmuir*., **23**: 3225-3229.

Texter, J. and Tirrell, M. (2001). Chemical processing by self-assembly. *AIChE. J.*, **47**:1706-1710.

Toscano, A.and Santore, M. M. (2006). Fibrinogen adsorption on three silica-based surfaces: Conformation and kinetics. *Langmuir*., **22**: 2588-2597.

Trudeau, T.G. and Hore, D.K. (2010). Hydrophobic Amino Acid Adsorption on Surfaces of Varying Wettability. *Langmuir*., **26**: 11095-11102.

Tsierkezos, N. G., Palaiologou, M. M. and Molinou, I. E. (2000). Densities and Viscosities of 1-Pentanol Binary Mixtures at 293.15 K. *J. Chem. Eng. Data*., **45**: 272-275.

Tunc, S., Maitz, M.F., Steiner, G., Vazquez, L., Pham. M.T. and Salzer, R. In situ conformational analysis of fibrinogen adsorbed on Si surfaces. *Colloids. Surf. B.*,**42**: 219-225

Ueda, T., Ishihara, K. and Nakabayashi, N.(1995).Adsorption-desorption of proteins on phospholipid polymer surfaces evaluated by dynamic contact angle measurement. *J. Biomed. Mater. Res*., **29**: 381-387.

Vijay Kumar, S., Bugg, C.E. and Cook, W.J. (1987). Structure of Ubiquitin refined at 1.8A resolution. *J. Mol. Biol*., **194**: 531-544.

Vijaya Krishna, T., Sreehari Sastry, S. and Murthy, V.R.K. (2001). Dielectric relaxation, thermodynamic and theoretical studies on hydrogen bonded polar binary mixtures of N-methyl aniline with propan-1-ol and isopropyl alcohol. *Indian. J. Phys*., **85**: 379-390.

Weber, N., Wendel, H.P. and Ziemer, G. (2002). Hemocompatibility of heparin-coated surfaces and the role of selective plasma protein adsorption. *Biomaterials*., **23**: 429-39.

Weizmann, C., Bergmann, E. and Hirshberg, Y. (1938). Photochemical interaction between ketones and alcohols. *J. Am. Chem. Soc*., **60**:1530-1533.

Watanabe, N., Shirakawa, T., Iwahashi, M., Ohbu, K. and Seimiya, T. (1986). Effect of surface charge on adsorption of bovine serum albumin as studied by ellipsometry 1. Adsorption on cationic monolayer. *Colloid. Polym. Sci* ., **264**: 903-908.

Wu, S. (1971). Calculation of interfacial tension in polymer systems. *J. Polym. Sci. Pol. Sym*., 34:19-30.

Xia,Y., Qin, D. and Yin, Y. (2001). Surface patterning and its application in wetting or dewetting studies. *Curr. Opin. Colloid. in*., **6**: 54-64.

Xu, L.C. and Siedlecki, C.A. (2007).Effects of surface wettability and contact time on protein adhesion to biomaterial surfaces. *Biomaterials*., **28**:3273-3283.

Yamaguchi, T., Hidaka, K. and Soper, A.K. (1999). The structure of liquid methanol revisited: A neutron diffraction experiment at -80^{o}C and +25^{o}C. *Mol. Phys*., **96**: 1159-1168 ;*erratum ibid*., **97**: 603-605.

Young, T. (1805). An Essay on the Cohesion of Fluids. *Phil. Trans. R. Soc. London*., **95**: 65-87.

Zhang, X. , Liu, C. and Wang, Z. (2008). Force spectroscopy of polymers: Studying on intramolecular and intermolecular interactions in single molecular level. *Polym*., **49**: 3353-3361.

Zhang, Z., Witham, S. and Alexov, E. (2011). On the role of electrostatics in protein-protein interactions. *Phys. Biol*., **8**: 035001.

Zhu, X.D., Fan, H.S., Chen, X.N., Li, D.X. and Zhang, X.D. (2007). Contribution of surface charge to bovine serum albumin adsorption on hydroxyapatite ceramic particles. *Key. Eng. Mater*., **330**: 861-864.

```
@article{majorekfirst,
  title={First Steps of Protein Structure Prediction},
  author={Majorek, K. and Koz{\l}owski, {\L}. and J{\k{a}}kalski, M. and
Bujnicki, J.M.},
  journal={Prediction of Protein Structures, Functions, and Interactions},
  pages={39--62},
  publisher={Wiley Online Library}
```